AFFDL-TR-65-73

AN ANALYTICAL STUDY OF V/STOL HANDLING QUALITIES IN HOVER AND TRANSITION

R. L. Stapleford
J. Wolkovitch
R. E. Magdaleno
C. P. Shortwell
W. A. Johnson

FOREWORD

The research reported here was sponsored by the Air Force Flight Dynamics Laboratory, Research and Technology Division, as part of Project No. 8219, Task No. 821909. It was conducted at Systems Technology, Inc., Hawthorne, California, under Contract No. AF 33(615)-1300.

The Air Force project monitor for the initial portion of the contract was Mr. Ralph H. Smith and for the final portion was Mr. Richard K. Wilson. The contractor's technical director was Mr. Irving L. Ashkenas and the project engineer was Mr. Robert L. Stapleford.

The authors gratefully acknowledge the considerable efforts of the STI publication department in the preparation of this report.

The contractor's internal report number is TR-140-1.

The manuscript was released by the authors in April 1965 for publication as an RTD Technical Report.

This technical report has been reviewed and is approved.

C. B. Westbrook

C. B. WESTBROOK
Chief, Control Criteria Branch
Flight Control Division
AF Flight Dynamics Laboratory

ABSTRACT

The pilot transfer-function model, and other analytical techniques, are used to study V/STOL handling qualities during hover and the transition to conventional flight. The hover analysis considers pilot attitude and position control tasks in the presence of horizontal gusts. The effects of each of the stability derivatives on the difficulty of the control tasks and on the closed-loop gust responses are determined. It is clearly shown that the handling qualities studies of control sensitivity and angular damping must consider the influences of M_u (or L'_v) and should include gust inputs. These conclusions are substantiated by previous variable-stability-helicopter experiments. The effects of vehicle size and geometry are investigated by several approaches. The key result of increasing size is found to be a reduction in M_u and L'_v which can, in turn, lower the requirements for control power and damping. The handling qualities during transition of two vehicles, a tilt duct and a tilt wing, which were previously tested on a simulator are analyzed. It is shown that both trim control and perturbations about the trim conditions must be considered. In fact, part of the increased difficulty in landing transitions, in comparison with takeoff transitions, is due to more difficult trim control; the much more stringent position control requirements in landing are also a contributing factor.

CONTENTS

		Page
I.	INTRODUCTION	1
II.	HOVER	3
	A. Equations of Motion and Pilot Model	3
	B. Airframe Open-Loop Characteristics	10
	C. Attitude Control	13
	D. Position Control	22
	E. Closed-Loop Gust Response	27
	F. Summary of Derivative Effects	43
III.	SIZE AND GEOMETRY	47
	A. Damping and Control Power Requirements	47
	B. Nondimensional Hover Equations of Motion	49
	C. Size Effects on Dimensional Hover Derivatives	54
	D. Geometry Effects on Dimensional Hover Derivatives	55
	E. Summary	56
IV.	TRANSITION	58
	A. Analysis Method	58
	B. Tilt-Duct Aircraft	62
	C. Tilt-Wing Aircraft	75
	D. General Comments	87
V.	SUMMARY	88
	A. Hover	88
	B. Size and Geometry	89
	C. Transition	90
REFERENCES		91
APPENDIX A.	APPROXIMATE FACTORS	97
APPENDIX B.	ESTIMATION OF HOVER DERIVATIVES BY MOMENTUM THEORY	111
APPENDIX C.	DERIVATION OF $h \rightarrow \delta_T$ METRIC	155
APPENDIX D.	GAIN IDENTITIES IN HOVER	157

ILLUSTRATIONS

		Page
1.	Attitude Loop	6
2.	Typical Bode Plot for $\theta \rightarrow \delta_e$ Closure	7
3.	Typical Root Locus for $\theta \rightarrow \delta_e$ Closure	8
4.	Position Loop	9
5.	Typical Bode Plot for $x \rightarrow \delta_e$ Closure	11
6.	Typical Root Loci for $x \rightarrow \delta_e$ Closure	12
7.	Hover Root Positions for Several V/STOL Vehicles	15
8.	Hover Attitude Loop Closures	18 – 21
9.	Hover Position Loop Closures	23 – 26
10.	Variations of Gust Responses with Pilot Gains	32 – 33
11.	Position Spectra	39
12.	Attitude Spectra	42
13.	Control Power Spectra	44
14.	Bell D-2064 Tilt Duct	60
15.	Tilt-Wing Configuration	61
16.	Tilt-Duct Trim, Takeoff	63
17.	Tilt-Duct Trim, Landing	64
18.	$\theta \rightarrow \delta_e$ Closures for Tilt Duct	66 – 68
19.	$h \rightarrow \delta_T$ Closures for Tilt Duct	70 – 72
20.	Tilt-Wing Trim, Takeoff	77
21.	Tilt-Wing Trim, Landing	78
22.	$\theta \rightarrow \delta_e$ Closures for Tilt Wing	80 – 82
23.	$h \rightarrow \delta_T$ Closures for Tilt Wing	83 – 85

		Page
B-1.	Configuration of Ref. 39 and Configuration of Ref. 35. .	120
B-2.	Power Versus $(rpm)^3$ at Two Forward Speeds for Ducted Fan of Ref. 35.	121
B-3.	Comparison of Experimental and Theoretical Lift, Drag, and Pitching Moment on Isolated Vertical Ducted Fan . .	123
B-4.	Scale Effect on Lift Coefficient.	126
B-5.	Scale Effect on Duct Drag Coefficient and Pitching Moment	127
B-6.	Lift, Drag, and Pitching Moment on Ducted Fan of Ref. 39 for Small u-Perturbations from Hover	128
B-7.	Rotor Working States in Axial Flow	132
B-8.	Typical Variation of C_T Versus J for Rigid and Flapping Propellers	135
B-9.	C_T Versus J for Three VTOL Propellers	140
B-10.	C_T Versus J for Doak VZ-4 Ducted Fan in Axial Flow. . .	144
B-11.	C_T Versus J for Duct with a 0.5" Lip Radius in Axial Flow	144

TABLES

		Page
I.	Survey of Longitudinal Hover Derivatives	14
II.	Survey of Lateral Hover Derivatives.	14
III.	Attitude Loop Closure Parameters.	16
IV.	Position Loop Closure Parameters.	22
V.	Effects of Gust Break Frequency	30
VI.	RMS Gust Responses	34
VII.	X_u Effects on Gust Responses	36
VIII.	Gust Response Numerator Zeros.	38
IX.	Parameter Variations with Weight.	54
X.	Summary of $h \rightarrow \delta_T$ Closure Parameters for Tilt Duct	73
XI.	$h \rightarrow \delta_T$ Metric for Tilt Duct	74
XII.	Summary of $h \rightarrow \delta_T$ Closure Parameters for Tilt Wing	79
XIII.	$h \rightarrow \delta_T$ Metric for Tilt Wing	86
A-I.	Conditions Used to Check Validity of Approximate Factors	99
A-II.	Transfer Function Forms.	100 – 101
A-III.	Availability and Key to Location of Approximate Factors	102
A-IV.	Approximate Factors Referred from Table A-III . .	103 – 110
B-I.	References Examined for Data on Ducted Fan Derivatives at Hover.	117 – 118

SYMBOLS

a_1	Lift curve slope for propeller blade section
A_e	Actuator disk area
b	Number of propeller blades
B	Propeller tip loss factor, $1 - \frac{\sqrt{2C_{T\Omega}}}{b}$
c	Propeller chord
C_T	Thrust coefficient, $T/\rho n^2 D^4$
$C_{T\Omega}$	Thrust coefficient, $T/\pi\rho\Omega^2 R^4$
d	Damping (or negative of open-loop pole)
D	Drag
D	Propeller diameter
E	Energy contained in the air flowing through a duct (per unit time
g	Acceleration due to gravity
G(s)	Loop transfer function
h	Altitude
h_D	Height of duct lip above vehicle c.g.
h_{DC}	Height of duct center above vehicle c.g.
i_y	$(k_y/l)^2$
I_x, I_y, I_z	Moments of inertia about x, y, and z axes
I_{xz}	Product of inertia
j	$\sqrt{-1}$
J	U_o/nD
J_i	$\pi V_i/\Omega R$
J_Ω	$U_o/\Omega D$

k_λ	Radius of gyration about subscript axis
K	Transfer function low frequency gain
l	Characteristic length
l_D	Duct length
L	Lift
L	Integral scale of turbulence
L	Rolling moment/I_x
L_p	$\partial L/\partial p$
L_r	$\partial L/\partial r$
L_v	$\partial L/\partial v$
L_δ	$\partial L/\partial \delta$
L'_λ	$\dfrac{L_\lambda + \dfrac{I_{xz}}{I_x} N_\lambda}{1 - \dfrac{I_{xz}^2}{I_x I_z}}$ where λ refers to any motion or input quantity
m	Mass of the airplane
m_q	$i_y \sqrt{\mu l/g}\, M_q$
m_u	$i_y \sqrt{\mu l^3/g}\, M_u$
m_δ	$i_y (l/g) M_\delta$
M	Pitching moment/I_y
M_q	$\partial M/\partial q$
M_u	$\partial M/\partial u$
M_w	$\partial M/\partial w$
$M_{\dot{w}}$	$\partial M/\partial \dot{w}$
M_δ	$\partial M/\partial \delta$
n	Rotational speed (rev/sec)
N	Number of rotors

N	Yawing moment/I_z
N_p	$\partial N/\partial p$
N_r	$\partial N/\partial r$
N_v	$\partial N/\partial v$
N_δ	$\partial N/\partial \delta$
N'_λ	$\dfrac{N_\lambda + (I_{xz}/I_z)L_\lambda}{1 - (I_{xz}^2/I_x I_z)}$ where λ refers to any motion or input quantity
$N(s)$	Transfer function numerator
p	Roll rate
p	Static pressure
p	Negative of a transfer function pole
P	Power absorbed by air flowing through a duct
q	Pitch rate
r	Yaw rate
r	Radial distance from propeller hub
R	Propeller radius
s	Laplace operator, $s = \sigma + j\omega$
S	Reference area
t	Time
t_c	Characteristic time
T	Thrust
T_λ	Time constant of λ zero or pole
u	Perturbation velocity along x-axis
u_g	Gust velocity along x-axis
$\hat{u}$	$\sqrt{\mu/gl}\, u$
U_o	Steady state velocity along x-axis
v	Perturbation velocity along y-axis

V	Total velocity
V_{as}	Steady state airspeed
V_e	Duct exit velocity
V_i	Velocity at actuator disk
V_∞	Velocity of fully developed slipstream
w	Perturbation velocity along z-axis
$\hat{w}$	$\sqrt{\mu/gl}\, w$
x	Horizontal displacement in direction of x-axis, $x = \int u\, dt$
x_u	$\sqrt{\mu l/g}\, X_u$
x_δ	X_δ/g
X	Force in x-direction divided by airplane mass
X_q	$\partial X/\partial q$
X_u	$\partial X/\partial u$
X_δ	$\partial X/\partial \delta$
Y	Force in y-direction divided by airplane mass
Y_p	$\partial Y/\partial p$
Y_r	$\partial Y/\partial r$
Y_v	$\partial Y/\partial v$
Y_δ	$\partial Y/\partial \delta$
$Y(s)$	Transfer function
z	Negative of transfer function zero
z_u	$\sqrt{\mu l/g}\, Z_u$
z_w	$\sqrt{\mu l/g}\, Z_w$
z_δ	Z_δ/g
Z	Force in z-direction divided by airplane mass
Z_q	$\partial Z/\partial q$

Z_u	$\partial Z/\partial u$
Z_w	$\partial Z/\partial w$
Z_δ	$\partial Z/\partial \delta$
α	Angle of attack
δ	Control deflection
$\hat{\delta}$	$\mu\delta$
$\Delta(s)$	Transfer function denominator
$\Delta\lambda$	Incremental change in λ
ζ_λ	Damping ratio of λ zero or pole
θ	Pitch angle
θ_o	Angle between (untwisted) blade no-lift chord line and plane of rotation
κ	Transfer function high frequency gain
λ	General variable
λ	$t_c s$
λ_i	Inflow factor, $V_i/\Omega R$
μ	$m/\rho l^3$
ρ	Density of air
σ	Real part of s
σ	Propeller solidity, (number of blades) x (average chord)/πR
σ_λ	Root-mean-squared value of λ
τ	Pilot transport lag
τ_e	Effective pilot transport lag, τ plus neuromuscular time constant
τ_{eff}	Effective transport lag in h $\rightarrow$ δ_T loop, τ_e plus thrust-lag time constant
φ	Roll angle
φ_M	Phase margin

Φ_λ	λ power spectrum
ψ	Angular position of propeller blades
ω	Imaginary part of s
ω_o	Frequency at which $h \rightarrow \delta_T$ closure goes unstable with no pilot lead
ω_λ	Undamped natural frequency of λ zero or pole
Ω	Rotational speed (rad/sec)

SECTION I

INTRODUCTION

While a great deal of effort has been spent studying the problems of V/STOL handling qualities, far too little of this research has been directed at closed-loop analyses using a pilot transfer function model. Since such analyses have been so successfully applied in the study of handling qualities for conventional aircraft, they should also prove highly useful in the study of V/STOL vehicles. The analyses summarized in this report apply the pilot transfer function model to an investigation of V/STOL handling qualities during hover and during the transition from hover to conventional flight. This is not to imply that the open-loop aspects of handling qualities are neglected here; rather, both open- and closed-loop analyses are utilized when appropriate.

The hover investigation of Section II considers the pilot tasks of attitude stabilization and of maintaining position over a fixed point. The effects of each stability derivative on the difficulty of the tasks and on the closed-loop pilot–vehicle responses to gusts are examined. The control deflection responses required to cope with gusts and the resulting attitude changes turn out to be important considerations.

The influences of vehicle size and geometry on the hover handling qualities are considered in Section III. This difficult problem is attacked by several different approaches. The roll requirements study for conventional aircraft of Ref. 7 is shown to have implications, which turn out to be independent of size and geometry, for the damping and control power of V/STOL craft. A new nondimensional form of the equations of motion is derived and sheds some light on size and geometry effects. The variations in dimensional stability derivatives with size are estimated and results examined in light of the Section II results. The key variation is shown to be in M_u (or L'_v), which also has implications on damping and control requirements. The most important geometric parameter for ducted-propeller vehicles is shown to be the height of the duct lips above the center of gravity.

The transition study of Section IV considers the effects of the time-varying dynamics and the differences between landing and takeoff transitions. A tilt-duct and a tilt-wing vehicle, which were tested in the simulator experiments of Ref. 4, are analyzed. The longitudinal control function during transition is divided into two tasks. The first task is maintaining vehicle trim during the transition; the second is controlling perturbations about the time-varying trim conditions. Both tasks are found to be important in the assessment of transition handling qualities.

The major results and conclusions of the study are summarized in Section V.

The appendices contain various technical details. Appendix A is a summary of approximate transfer function factors, which relate pole and zero locations to the stability derivatives. The relationships can provide useful understanding of the effects of the stability derivatives on vehicle dynamics and clues to stability augmentation methods to improve handling qualities.

Appendix B is the application of momentum theory to develop approximate expressions for ducted- and unducted-propeller vehicles in hover. The approximate expressions are used in the body of the report to estimate the effects of size and geometry on handling qualities.

Appendices C and D are detailed mathematical derivations of expressions used in the body of the report.

SECTION II

HOVER

This section examines the effects of the stability derivatives on vehicle handling qualities in hover. The basic objectives are to provide some physical understanding of the effects of each derivative and to establish the relative importance of the derivatives.

The equations of motion and the pilot model are briefly discussed in Subsection A. A key point of this discussion is that the longitudinal and the lateral equations of motion normally have identical forms. As a result the generalized study presented in the remainder of this section can be applied to either longitudinal or lateral control by simply changing symbols.

Subsection B discusses the effects of the derivatives on the vehicle open-loop characteristics.

The effects of the derivatives on the pilot's attitude control task are examined in Subsection C, and the effects on the pilot's ability to hover over a fixed point are considered in Subsection D.

Subsection E analyzes the closed-loop pilot–vehicle response to random horizontal gusts. The effects of the derivatives on the position, attitude, and control responses are examined.

The results of this section are summarized in Subsection F.

A. EQUATIONS OF MOTION AND PILOT MODEL

The similarity between the longitudinal and the lateral equations of motion is now discussed. This discussion is followed by a general description of the pilot model and pilot closure of an attitude stabilization loop and a position loop.

When terms which are usually negligibly small are omitted, the longitudinal equations of motion can be written (Ref. 2):

$$\begin{bmatrix} s - X_u & 0 & g \\ -Z_u & s - Z_w & 0 \\ -M_u & 0 & s^2 - M_q s \end{bmatrix} \begin{Bmatrix} u \\ w \\ \theta \end{Bmatrix} = \begin{Bmatrix} X_\delta \\ Z_\delta \\ M_\delta \end{Bmatrix} \delta - \begin{Bmatrix} X_u \\ Z_u \\ M_u \end{Bmatrix} u_g \qquad (1)$$

The control-fixed motion of the airplane consists of one mode, described by $s = Z_w$, which involves only the w-degree of freedom plus two other modes involving only u and θ.

The characteristic equation is:

$$\Delta(s) = (s - Z_w)\left[s^3 - (X_u + M_q)s^2 + X_u M_q s + g M_u\right] = 0 \qquad (2)$$

The $(s - Z_w)$ factor characterizes the plunging mode, which is controlled with the throttle or collective pitch. The other factor is called the "hovering cubic" and characterizes a motion which is controlled with the attitude control.

It is shown in Ref. 2 that the lateral equations are generally identical in form to Eq 1, with the following changes in symbols:

$u \rightarrow v$	$w \rightarrow r$	$\theta \rightarrow \varphi$
$X_u \rightarrow Y_v$	$g \rightarrow -g$	$Z_u \rightarrow N'_v$
$Z_w \rightarrow N'_r$	$M_u \rightarrow L'_v$	$M_q \rightarrow L'_p$
$X_\delta \rightarrow Y_\delta$	$Z_\delta \rightarrow N'_\delta$	$M_\delta \rightarrow L'_\delta$

That is, the lateral equations are:

$$\begin{bmatrix} s - Y_v & 0 & -g \\ -N'_v & s - N'_r & 0 \\ -L'_v & 0 & s^2 - L'_p s \end{bmatrix} \begin{Bmatrix} v \\ r \\ \varphi \end{Bmatrix} = \begin{Bmatrix} Y_\delta \\ N'_\delta \\ L'_\delta \end{Bmatrix} \delta - \begin{Bmatrix} Y_v \\ N'_v \\ L'_v \end{Bmatrix} v_g \qquad (3)$$

Because of this similarity of form the remainder of this section will use only the longitudinal terminology and symbols. The results apply

equally well to lateral control if the above changes in notation are made.

It should also be noted that the remainder of this section will only consider the motions characterized by the longitudinal and lateral hovering cubics. The two first-order modes ($s = Z_w$ and $s = N'_r$) represent situations which have been thoroughly analyzed. That is, pilot control of the transfer function form

$$Y_c = \frac{K}{s(s + d)} \tag{4}$$

which characterizes altitude and heading control in hover, has been studied extensively, especially as regards roll control of a conventional airplane, e.g., Refs. 2, 7, 13, and 14.

For control of the modes characterized by the hovering cubics, an attitude stabilization loop is of primary interest. The vehicle pitch-attitude-to-elevator transfer function can be written from Eq 1 as

$$\frac{\theta}{\delta_e}(s) = \frac{M_{\delta_e}\left(s - X_u + \frac{X_{\delta_e}}{M_{\delta_e}} M_u\right)}{\left(s + \frac{1}{T_{sp}}\right)\left(s^2 + 2\zeta_p\omega_p s + \omega_p^2\right)} \tag{5}$$

The hovering cubic is here assumed to take its conventional form of one first-order and one second-order mode. The first-order mode is referred to as the short-period mode because, as the vehicle speed is increased (from zero at hover), this mode couples with the plunging mode to form the conventional second-order short-period mode (Ref. 2).

The pilot transfer function model conventionally employed in handling qualities analyses consists of the general form

$$Y_p = \frac{K_p (T_L s + 1)e^{-\tau s}}{(T_I s + 1)(T_N s + 1)} \tag{6}$$

together with adjustment rules for the parameters K_p, T_L, and T_I. The fixed parameters τ and T_N represent reaction-time delay and neuromuscular

lag, which in this report are combined into an effective transport lag,

$$\tau_e = \tau + T_N \tag{7}$$

As details of this pilot model have been extensively documented, e.g., Ref. 3, they will not be repeated here.

Pilot closure of the $\theta \rightarrow \delta_e$ loop (Fig. 1) usually requires pilot lead, and never requires pilot lag, so the applicable pilot transfer

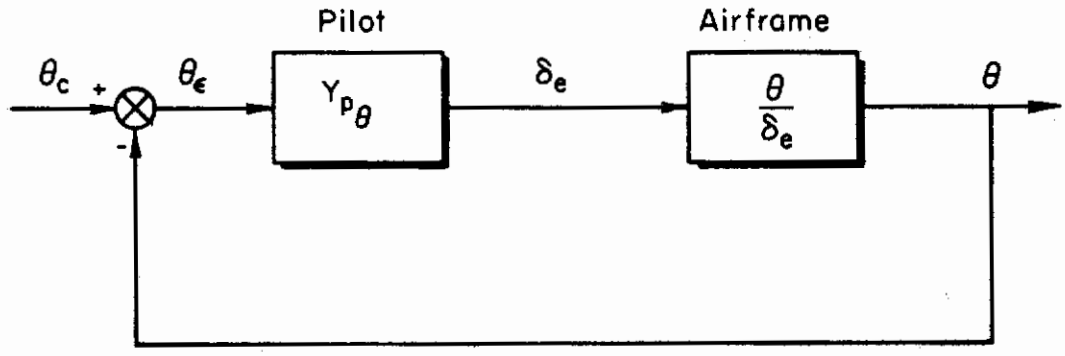

Figure 1. Attitude Loop

function is reduced to the simple form

$$Y_{p_\theta} = \frac{\delta_e}{\theta_\epsilon} = K_{p_\theta}(T_L s + 1)e^{-\tau_e s} \tag{8}$$

Combining Eqs 5 and 8 gives the total open-loop transfer function, which is sketched in Fig. 2 in Bode form and as a root locus plot in Fig. 3 [ω_c is the gain-crossover frequency, φ_M is the phase margin, and the transport lag has been approximated by $\left(-\frac{\tau_e s}{2} + 1\right)\Big/\left(\frac{\tau_e}{2} s + 1\right)$]. The phugoid mode is unstable open-loop, but can be stabilized with the $\theta \rightarrow \delta_e$ closure. For very high loop gains the phugoid mode again becomes unstable because of the pilot's transport lag.

Let us now consider the problem of controlling position, i.e., hovering over a spot. For the pilot to be able to control position with the elevator ($x \rightarrow \delta_e$ closure), it will normally be necessary for him to also maintain his $\theta \rightarrow \delta_e$ closure as an inner loop, Fig. 4. The x/δ_e transfer

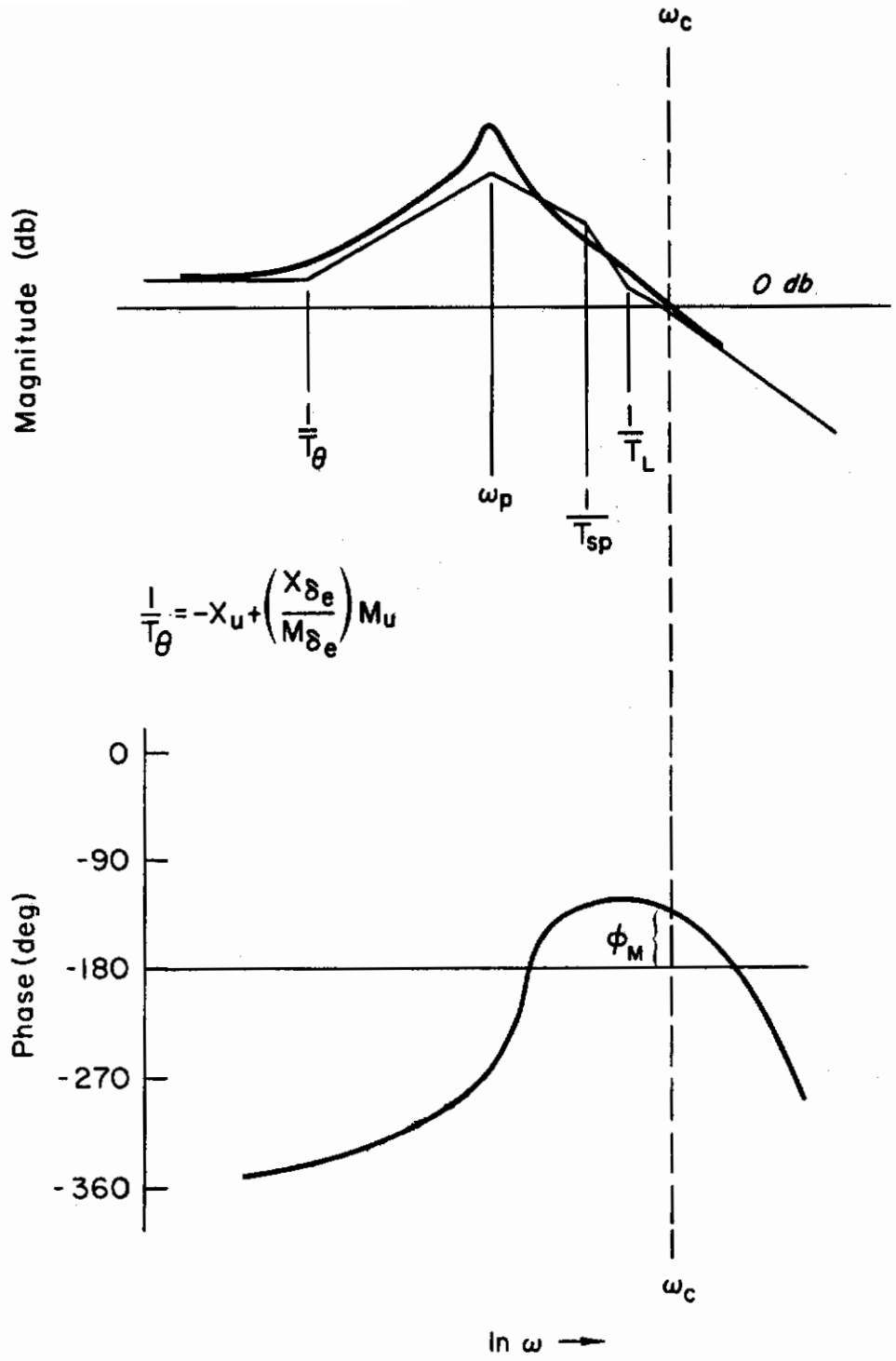

Figure 2. Typical Bode Plot for $\theta \rightarrow \delta_e$ Closure

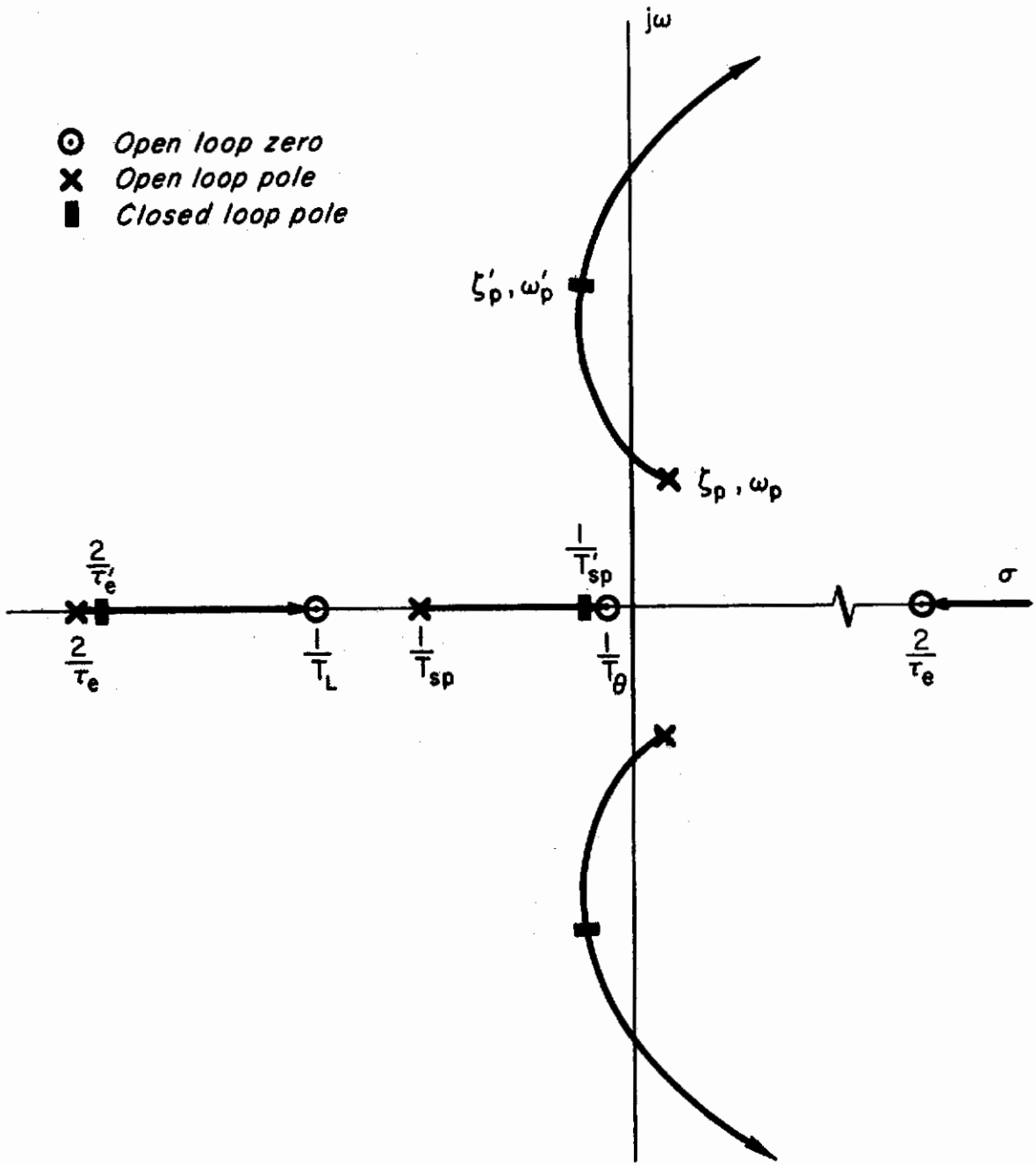

Figure 3. Typical Root Locus for $\theta \rightarrow \delta_e$ Closure

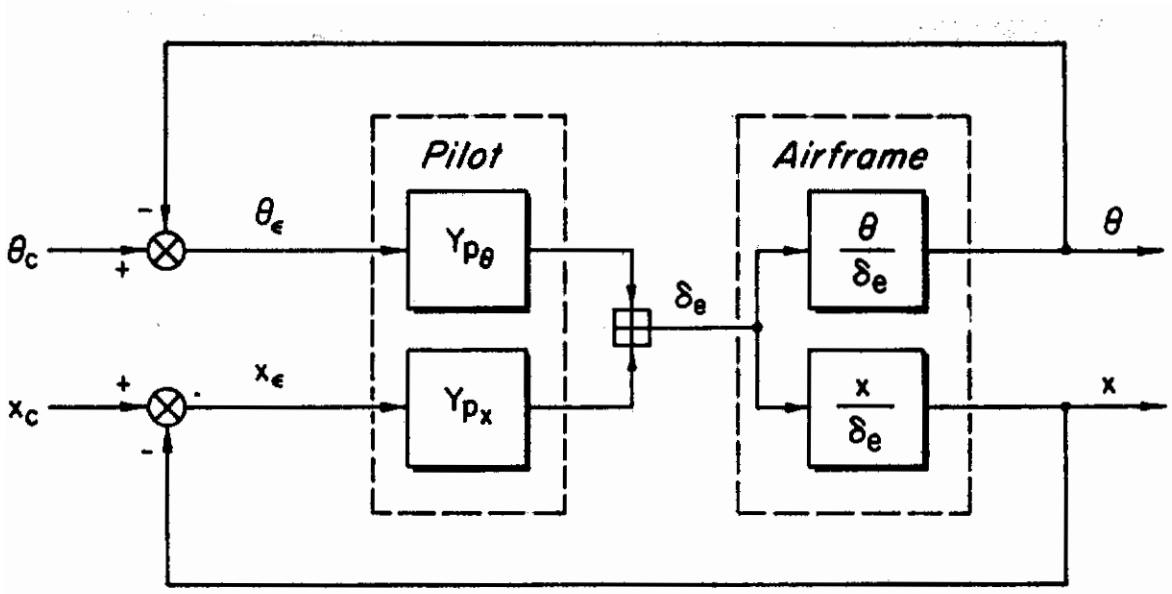

Figure 4. Position loop

function with a $\theta \rightarrow \delta_e$ inner loop is given by

$$\left(\frac{x}{\delta_e}\right)_{\theta \rightarrow \delta_e} = \frac{X_{\delta_e}\left(s^2 - M_q s - \frac{gM_{\delta_e}}{X_{\delta_e}}\right)\left(s + \frac{2}{\tau_e}\right)}{s\left(s + \frac{1}{T'_{sp}}\right)\left(s^2 + 2\zeta'_p\omega'_p s + \omega'^2_p\right)\left(s + \frac{2}{\tau'_e}\right)} \qquad (9)$$

where the primes denote the closed-loop value resulting from the $\theta \rightarrow \delta_e$ loop. Normally the crossover frequency for the $x \rightarrow \delta_e$ loop is very low (on the order of 0.2 – 0.5 rad/sec), so the only significant factors are the free-s and the modified phugoid and short period.

Since the x-loop can only be closed at relatively low frequencies, a pure gain pilot model is used. Pilot lag is not desirable; pilot lead and transport lag tend to cancel and neither is significant in the cross-over region of the $x \rightarrow \delta_e$ loop. The pilot transfer function is then

$$Y_{p_x} = \frac{\delta_e}{x_\epsilon} = K_{p_x} \qquad (10)$$

A typical Bode plot and root locus for the position loop are sketched in Figs. 5 and 6. With the $\theta \rightarrow \delta_e$ inner loop, the phugoid mode is well damped and the mode which goes unstable is the one formed from the $1/T'_{sp}$ and the free-s. Henceforth this latter mode will be referred to as the "x-mode."

The general forms of the open-loop airframe and pilot transfer functions have now been established. The next subsection shows how the airframe characteristic roots are affected by changes in the various stability derivatives.

B. AIRFRAME OPEN-LOOP CHARACTERISTICS

The longitudinal dynamics (excluding the plunging mode) of a hovering vehicle are completely specified by the five stability derivatives:

$$X_u \quad , \quad X_{\delta_e} \quad , \quad M_u \quad , \quad M_q \quad , \quad M_{\delta_e}$$

In the handling qualities analyses which follow, the effects of control sensitivity, M_{δ_e}, will not be considered. The analysis method considers only the pilot-vehicle transfer function pole-zero locations and total loop gain (product of pilot gain and control sensitivity). The resulting conclusions are therefore only valid for situations in which M_{δ_e} is adjusted to its optimum value for the selected values of the other terms. In other words, degradations in pilot rating due to too high or too low a control sensitivity are not considered here.

Eliminating M_{δ_e}, we will consider the four quantities:

$$X_u \quad , \quad X_{\delta_e}/M_{\delta_e} \quad , \quad M_u \quad , \quad M_q$$

Of these, M_u and M_q are generally recognized as the most important. Consequently, the major emphasis here will be on the effects of these two derivatives; that X_u and $X_{\delta_e}/M_{\delta_e}$ are of secondary importance will be demonstrated. The main point of the analysis is an examination of four combinations of derivatives; two values of both M_u and M_q for set values of X_u and $X_{\delta_e}/M_{\delta_e}$. These values of M_u and M_q were selected to bracket the majority of V/STOL aircraft.

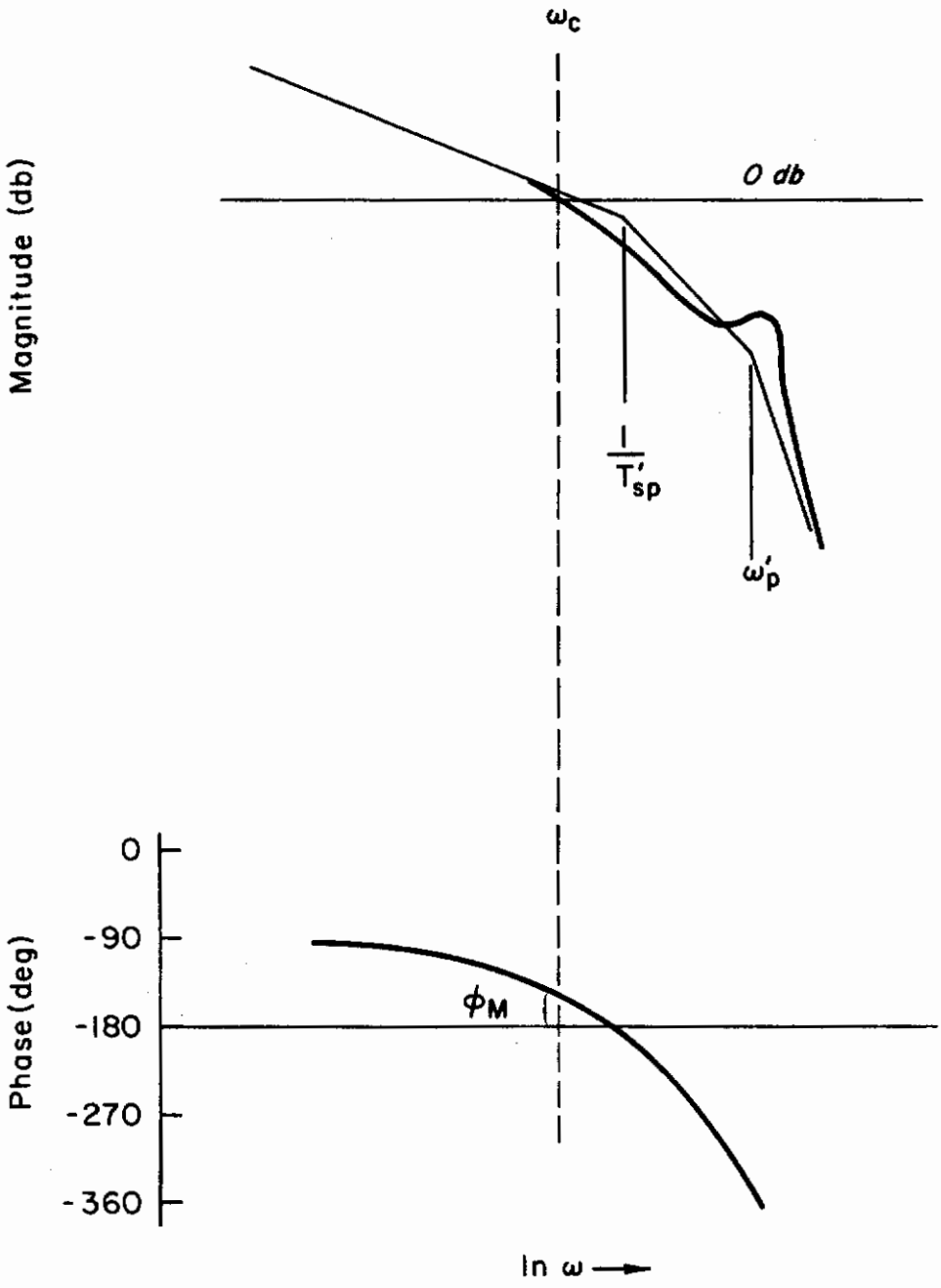

Figure 5. Typical Bode Plot for x ⟶ δ_e Closure

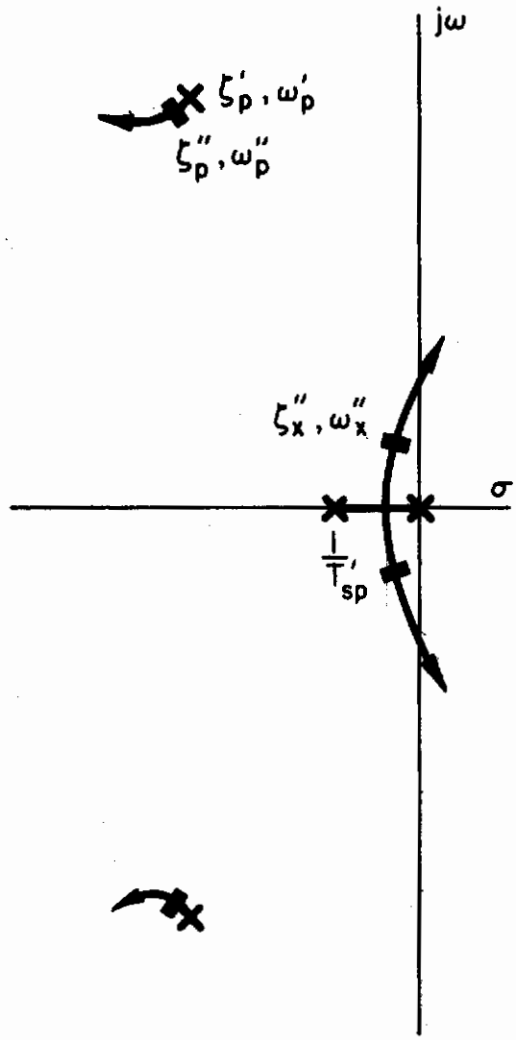

Figure 6. Typical Root Loci for x → δ_e Closure

The stability derivatives for a representative sampling of V/STOL vehicles are given in Tables I and II. From this survey the following values were selected:

$$X_u = -0.13 \text{ sec}^{-1}$$

$$X_{\delta_e}/M_{\delta_e} = 0$$

$$M_u = \begin{cases} 0.0088 \\ 0.088 \end{cases} \quad (\text{ft-sec})^{-1}$$

$$M_q = \begin{cases} -0.15 \\ -1.5 \end{cases} \quad \text{sec}^{-1}$$

The root positions are shown in Fig. 7, which also includes the root locations for the surveyed vehicles. It can be seen that the four values selected adequately cover the range of likely root positions.

Figure 7 also illustrates the effects of M_u and M_q on the characteristic roots. Increasing M_u increases the phugoid frequency at nearly constant damping ratio and increases $1/T_{sp}$. Increasing the pitch damping (M_q more negative) increases the phugoid damping at roughly constant frequency and also increases $1/T_{sp}$.

Making X_u more negative also increases phugoid damping at roughly constant damped frequency $\omega_p\sqrt{1-\zeta_p^2}$ and increases $1/T_{sp}$. The increases in $\zeta_p\omega_p$ and $1/T_{sp}$ are approximately equal to one-third the change in X_u (see Appendix A).

Of course $X_{\delta_e}/M_{\delta_e}$ has no effect on the characteristic roots, but does influence the θ/δ_e and x/δ_e numerators.

Additional information on the effects of the derivatives on the open-loop dynamics is readily obtained via the approximate factors of Appendix A.

C. ATTITUDE CONTROL

In this subsection the effects of the stability derivatives on pilot closure of an attitude stabilization loop are examined. The pilot model selected for this loop was a properly placed lead and an effective transport lag of 0.3 sec. The pilot lead and gain are generally adjusted for a crossover frequency of 2 – 3 rad/sec with roughly 30 deg phase margin.

TABLE I

SURVEY OF LONGITUDINAL HOVER DERIVATIVES

CLASS	VEHICLE	M_u	$-M_q$	$-X_u$	$-\frac{X_{\delta_e}}{M_{\delta_e}}$	SOURCE OF DERIVATIVE DATA
		$(ft\text{-}sec)^{-1}$	sec^{-1}	sec^{-1}	ft	
Helicopter	H-19 (single-rotor)	0.006	0.61	0.03	4.8	Ref. 2
	HUP-1 (tandem-rotor)	0.035	2.0	0.02	1.1	Ref. 2
Ducted Fan	VZ-4 (two ducts)	0.014	0.05	0.14	0	Ref. 2
	X-22 (four ducts)	0.016	0.13	0.23	0	Ref. 16
	Bell D-2064 (four ducts)	0.009	0.17	0.13	0	Ref. 4
Tilt Wing	VZ-2	0.068	0.43	0.29	0	Ref. 2
	XC-142 ①	0.010	0.20	0.15	0	Ref. 15
	XC-142 ②	0.017	0.19	0.43	0	Ref. 15
	AC-1 ③	0.047	0.65	0.35	5.3	Ref. 4
Tilt Rotor	Bell D-252	0.010	0.30	0.01	5.8	Ref. 4

① Aerodynamic data from Chance-Vought

② Aerodynamic data from Princeton Long Track

③ This is a scaled-up version of the Kaman K-16B, see Fig. 15

TABLE II

SURVEY OF LATERAL HOVER DERIVATIVES

CLASS	VEHICLE	$-L'_v$	$-L'_p$	$-Y_v$	$\frac{Y_{\delta_a}}{L'_{\delta_a}}$	SOURCE OF DERIVATIVE DATA
		$(ft\text{-}sec)^{-1}$	sec^{-1}	sec^{-1}	ft	
Helicopter	HUP-1 (tandem-rotor)	0.034	1.5	0.028	0.82	Ref. 2
Ducted Fan	VZ-4 (two ducts)	0.014	0.27	0.14	0	Ref. 2
	X-22 (four ducts)	0.032	0.29	0.22	0	Ref. 16
Tilt Wing	XC-142	0.007	0.22	0	0	Ref. 15

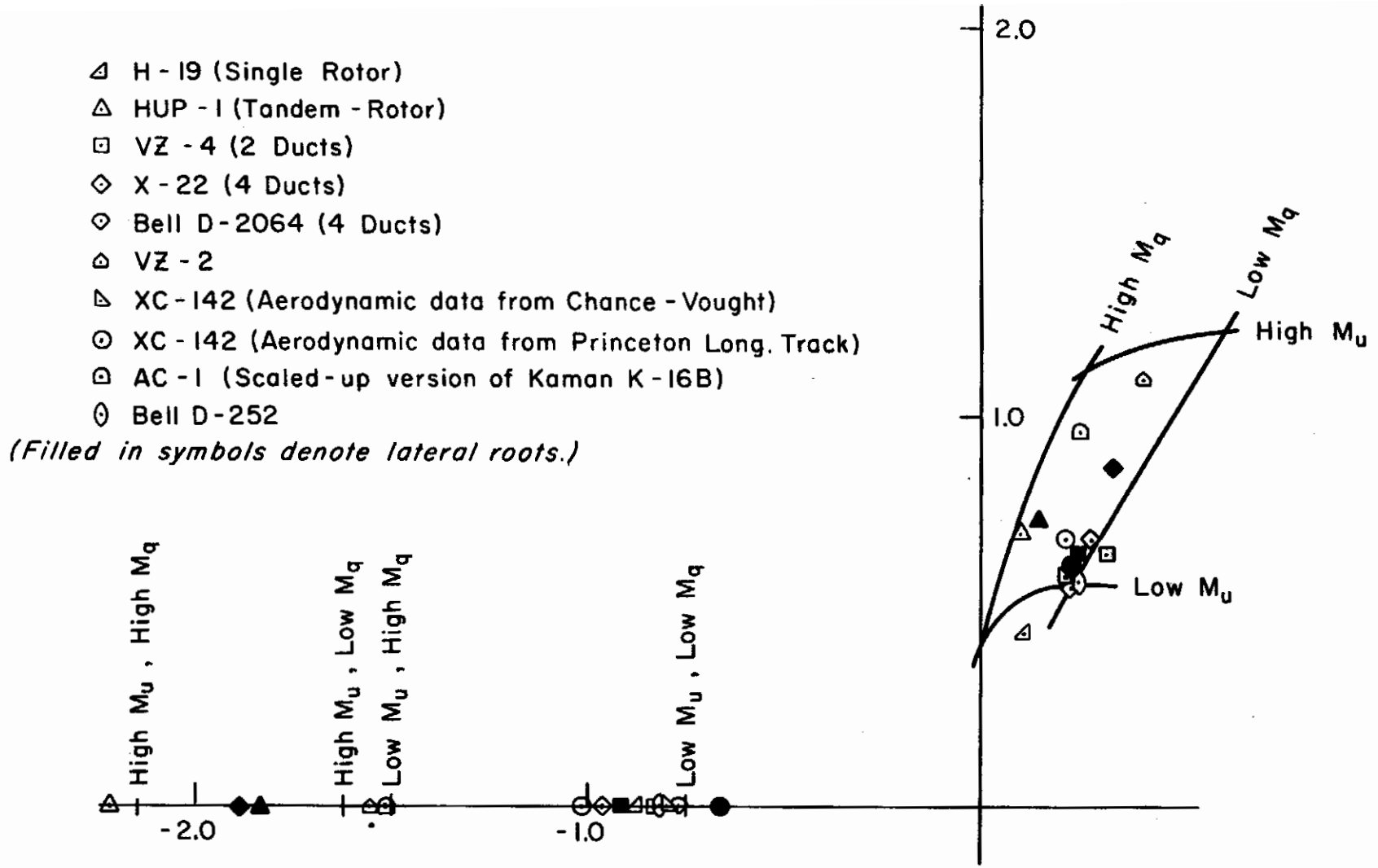

Figure 7. Hover Root Positions for Several V/STOL Vehicles

The $\theta \rightarrow \delta_e$ closures for the four combinations of M_u and M_q are illustrated in Fig. 8*; the key parameters are listed in Table III.

TABLE III

ATTITUDE LOOP CLOSURE PARAMETERS

CASE		PHASE MARGIN	GAIN MARGIN	CROSS-OVER FREQ.	PILOT LEAD, T_L	CLOSED-LOOP ROOTS				HIGH FREQ. LOOP GAIN, K_θ	D.C. LOOP GAIN, K_θ
M_u	M_q					ζ_p'	ω_p'	$\left(\frac{1}{T_{sp}}\right)'$	$\left(\frac{2}{\tau_e}\right)'$		
		deg	db	$\frac{\text{rad}}{\text{sec}}$	sec		$\frac{\text{rad}}{\text{sec}}$	sec^{-1}	sec^{-1}	$\frac{\text{rad}}{\text{sec}}$	
Low	Low	33	9	2.0	1.0	0.59	2.1	0.33	2.3	-1.80	0.825
High	Low	12	5	3.0	0.66	0.19	3.0	1.5	1.6	-2.66	0.184
Low	High	30	10	2.0	0.25	0.29	2.2	0.20	5.7	-1.10	2.02
High	High	26	6	3.2	0.46	0.33	3.8	0.77	2.2	-2.88	0.284

Note that for the high M_u, low M_q case the loop was closed at a lower phase margin than for the other cases. This was done after it was discovered that for this case a 30-deg phase margin closure, which required a pilot lead of 1.66 sec, resulted in gust responses which were very sensitive to the θ-loop gain. Any condition which places tight restrictions on pilot gain is bad because the pilot cannot maintain his gain within narrow limits for extended periods.

It can be seen from Table III that the most significant effect of increasing the pitch damping is to reduce the required pilot lead. This

*Throughout this report loop closures are analyzed by means of the USAM plot, which includes root locus, Bode, and Siggy plots (Ref. 68).

is as expected since the lead produces a pitching moment proportional to pitch rate (neglecting the lag introduced by the pilot's time delay). The reduction in pilot lead will be accompanied by an improvement in pilot ratings, as the ratings are a strong function of pilot lead (Ref. 3). A secondary effect of increasing the magnitude of M_q is to reduce the closed-loop short-period root, $1/T'_{sp}$. This result is surprising because increasing M_q increases the open-loop value; however, the increased d.c. gain which results from reduced pilot lead reverses this trend.

No serious effects of increasing M_u are noted for high M_q, although there is a substantial increase in $1/T'_{sp}$ (open-loop value was also increased). This is in complete accord with the variable-stability helicopter experiments of Ref. 8. In those tests a large increase in M_u (at $M_q = -1.98$ sec^{-1}) did not change the pilot rating for hover as long as the simulated gust input was reduced to keep the pitching moment disturbance constant, i.e., $M_u\sigma_{u_g}$ constant. The pilots noticed the degradation of open-loop phugoid stability, but did not consider it objectionable enough to change their ratings. The conclusion of the authors of Ref. 8, which will be substantiated here, is that increasing M_u has detrimental handling qualities effects, not because of the change in vehicle dynamics, but because of the increased pitching moment disturbances produced by gusts. Reference 8 also notes that a large M_u is objectionable at low speeds because of the resulting large trim deflections of the attitude control.

As noted earlier, changing X_u shifts the open-loop parameters, $\zeta_p\omega_p$ and $1/T_{sp}$, by approximately one-third the change in X_u. Thus, realistic variations in X_u have little effect on the open-loop poles, but more strongly influence the θ-numerator zero at $-X_u + M_uX_{\delta_e}/M_{\delta_e}$. As this zero is at a relatively low frequency it has little effect on the closed-loop phugoid roots. The effect on $1/T'_{sp}$ depends on the d.c. gain of the θ-loop. For high d.c. gain $1/T'_{sp}$ approaches the zero, so its change is nearly equal to the change in $-X_u$. For low d.c. gain $1/T'_{sp}$ is only slightly affected.

The θ-loop is affected by changes in $X_{\delta_e}/M_{\delta_e}$ only through the shift in the numerator zero at $-X_u + M_uX_{\delta_e}/M_{\delta_e}$. As the shift is proportional to M_u, the effect will be most important for large M_u cases. The high M_u,

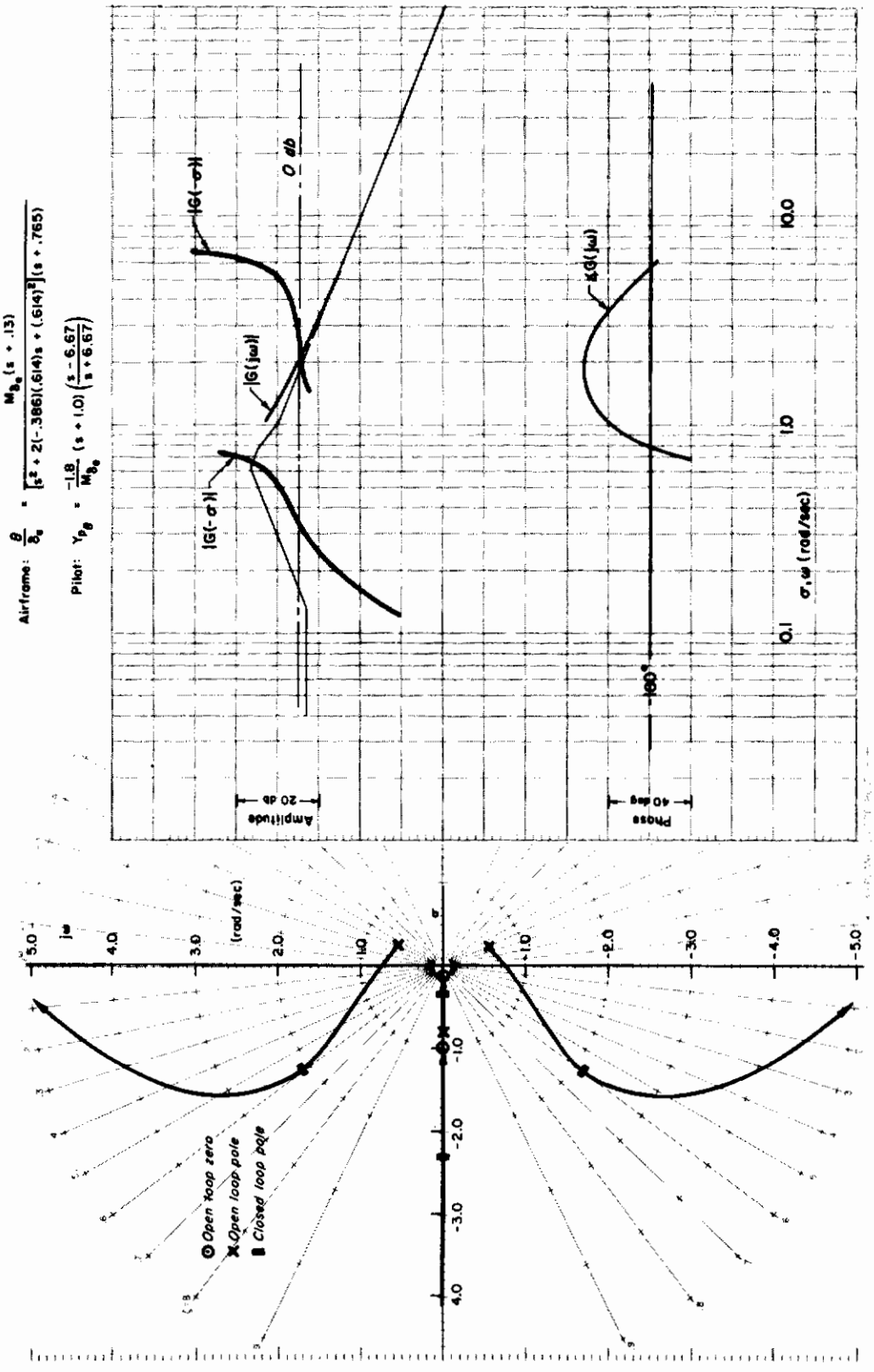

(a) Low $M_{\dot{u}}$, Low M_q

Figure 8. Hover Attitude Loop Closure

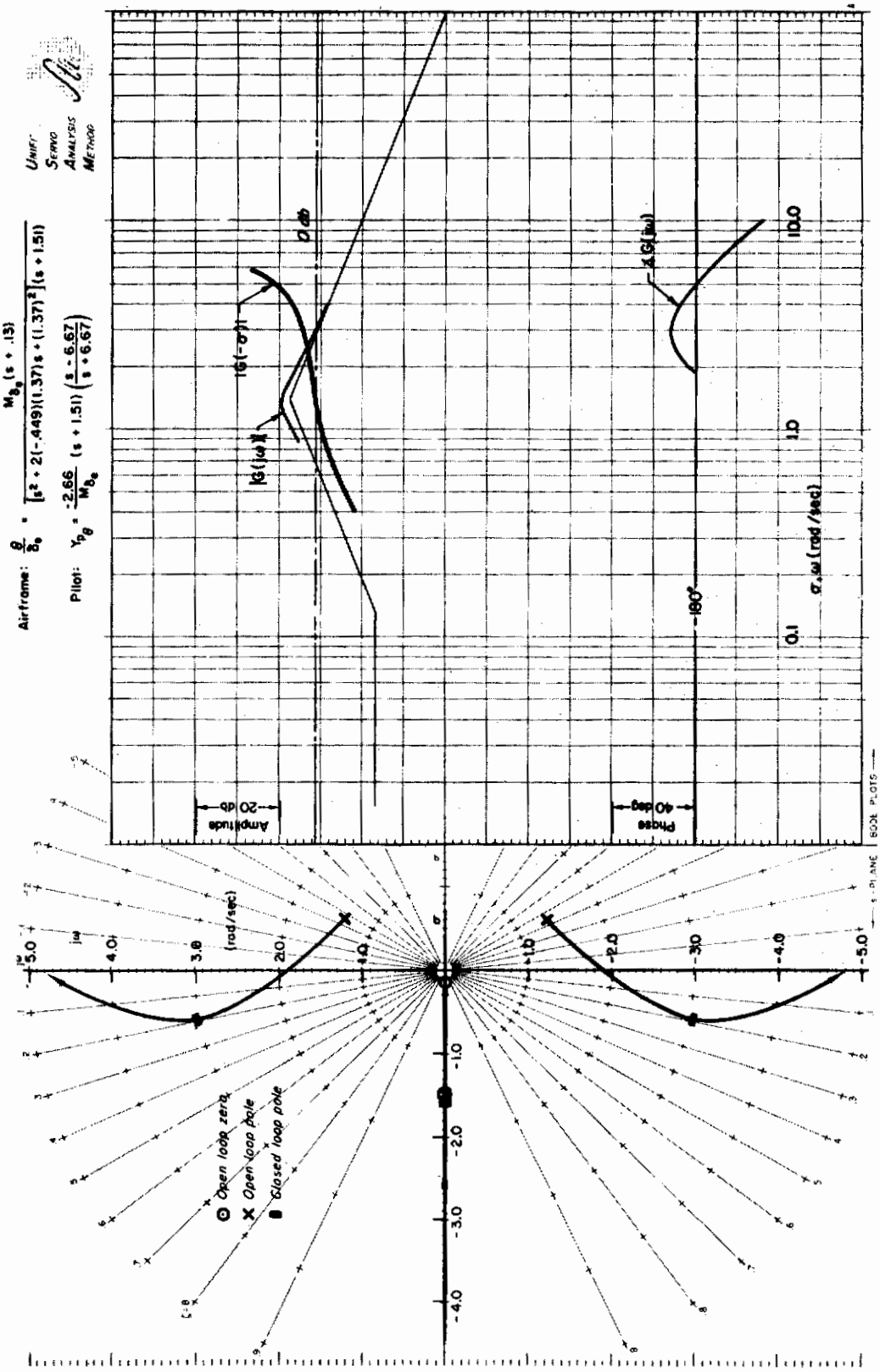

(b) High M_u, Low M_q

Figure 8 (Continued)

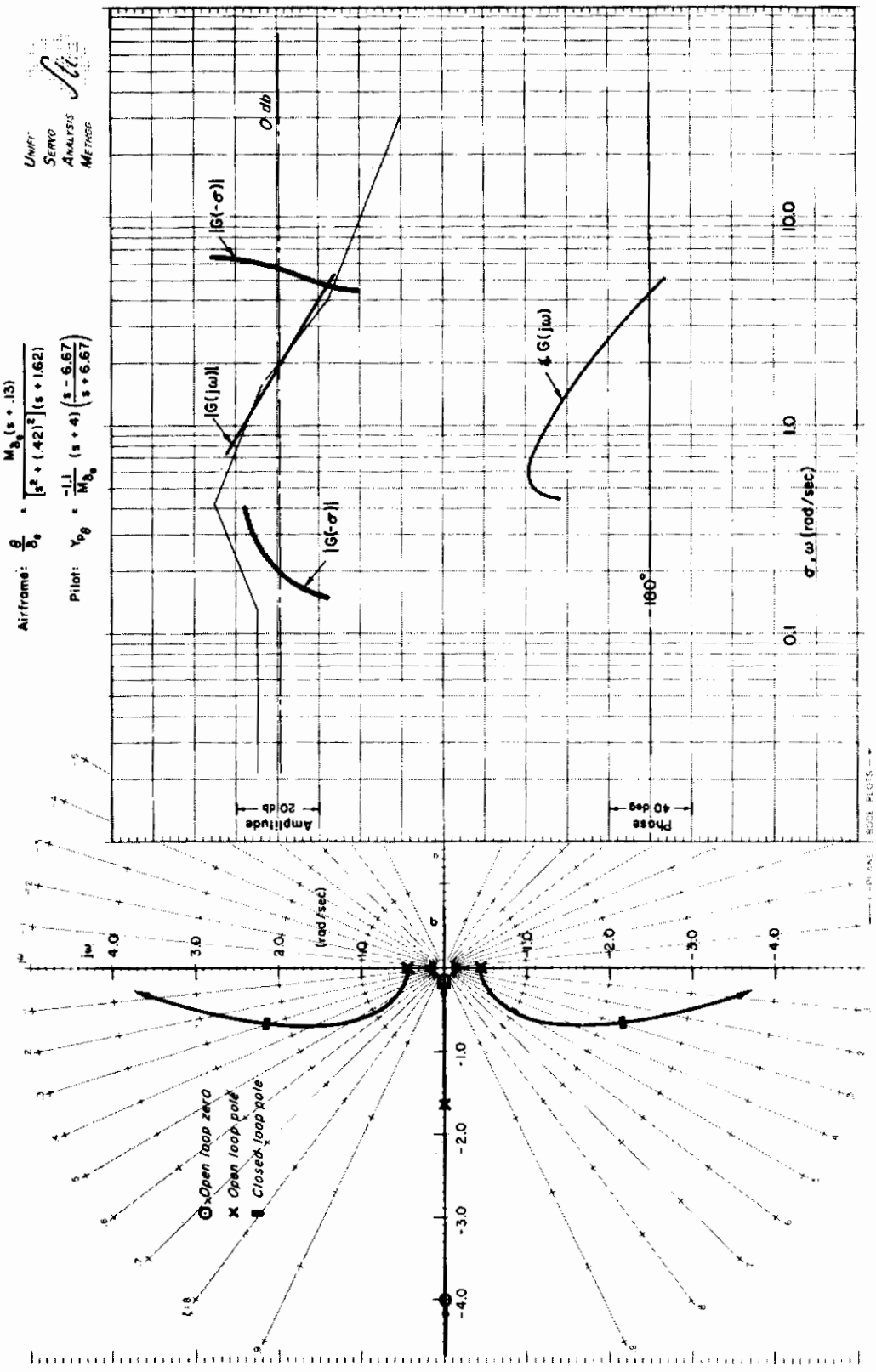

(c) Low M_u, High M_q

Figure 8 (Continued)

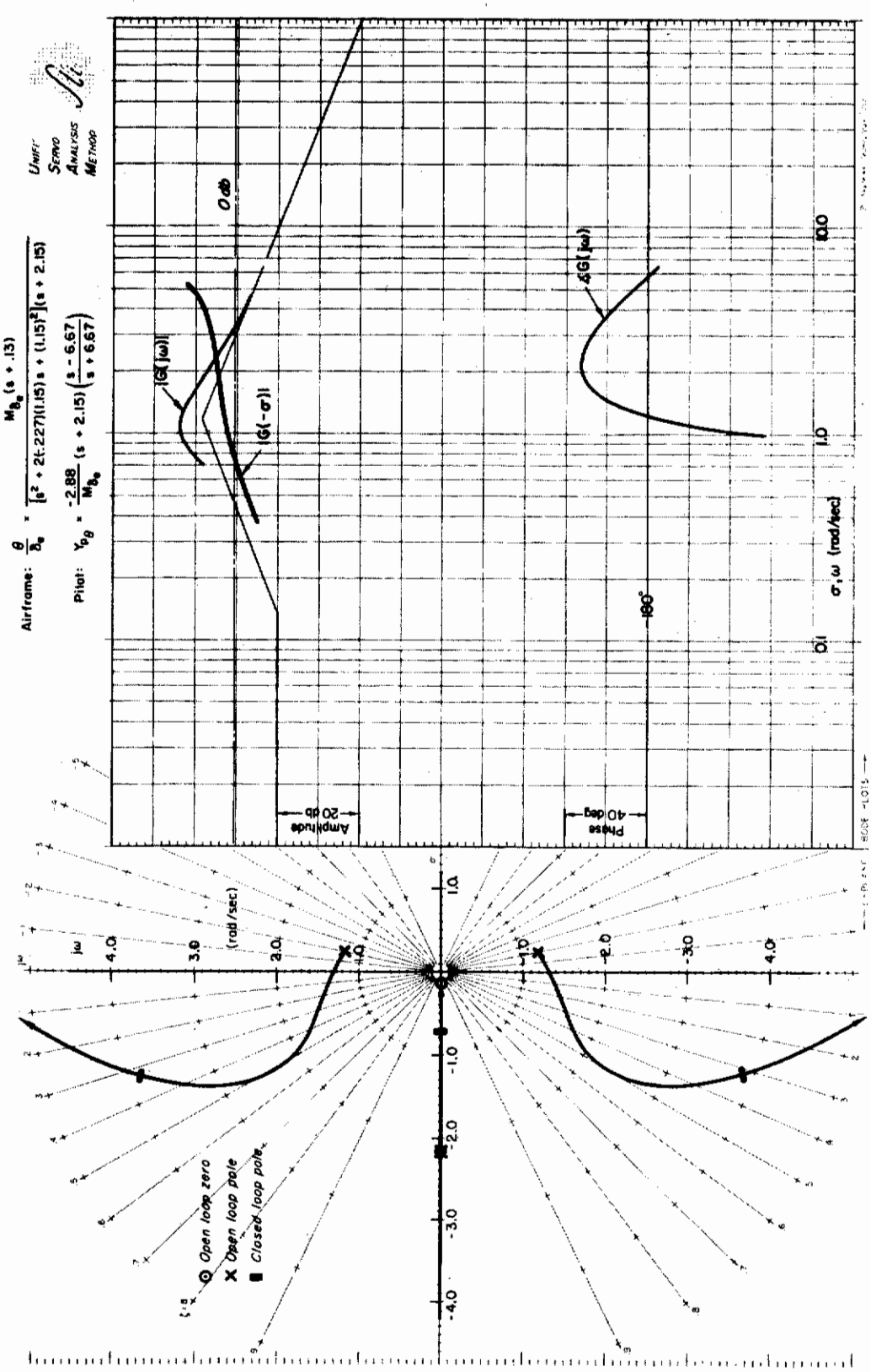

(d) High $M_{\dot{q}}$, High M_q

Figure 8 (Concluded)

low M_q case was recalculated with a relatively large $X_{\delta_e}/M_{\delta_e}$ of −5 ft. The phase margin was increased from 12 to 20 deg and $1/T'_{sp}$ was reduced from 1.5 to 0.65 sec^{-1}. Neither of these changes is very important and all others are negligible.

D. POSITION CONTROL

The analyses of the position control loops, $x \rightarrow \delta_e$, use the $\theta \rightarrow \delta_e$ closures of Subsection C as inner loops. As the x-loop can only be closed at relatively low frequencies, a pure gain pilot model is used. As previously explained, pilot lead and transport lag tend to cancel and neither is significant in the crossover region of the $x \rightarrow \delta_e$ loop.

The key parameters for the $x \rightarrow \delta_e$ closures for the four M_u, M_q combinations are summarized in Table IV and the closures are illustrated in Fig. 9. For ease of comparison a crossover frequency of roughly 0.3 rad/sec was used for all cases; this gives a minimum phase margin of about 30 deg.

TABLE IV

POSITION LOOP CLOSURE PARAMETERS

CASE		PHASE MARGIN	GAIN MARGIN	CROSS-OVER FREQ.	CLOSED-LOOP ROOTS					HIGH FREQ. LOOP GAIN, K_x	LOW FREQ. LOOP GAIN, K_x
					ζ''_x	ω''_x	ζ''_p	ω''_p	$\left(\frac{2}{\tau_e}\right)''$		
M_u	M_q	deg	db	$\frac{rad}{sec}$		$\frac{rad}{sec}$		$\frac{rad}{sec}$	sec^{-1}	$\left(\frac{rad}{sec}\right)^4$	$\frac{rad}{sec}$
Low	Low	34	8	0.30	0.29	0.36	0.60	2.2	2.4	0.210	0.406
High	Low	70	17	0.30	0.85	0.61	0.21	3.0	2.0	1.04	0.311
Low	High	28	14	0.30	0.26	0.33	0.30	2.2	5.7	0.458	0.536
High	High	66	20	0.25	0.73	0.44	0.33	3.8	2.2	0.960	0.263

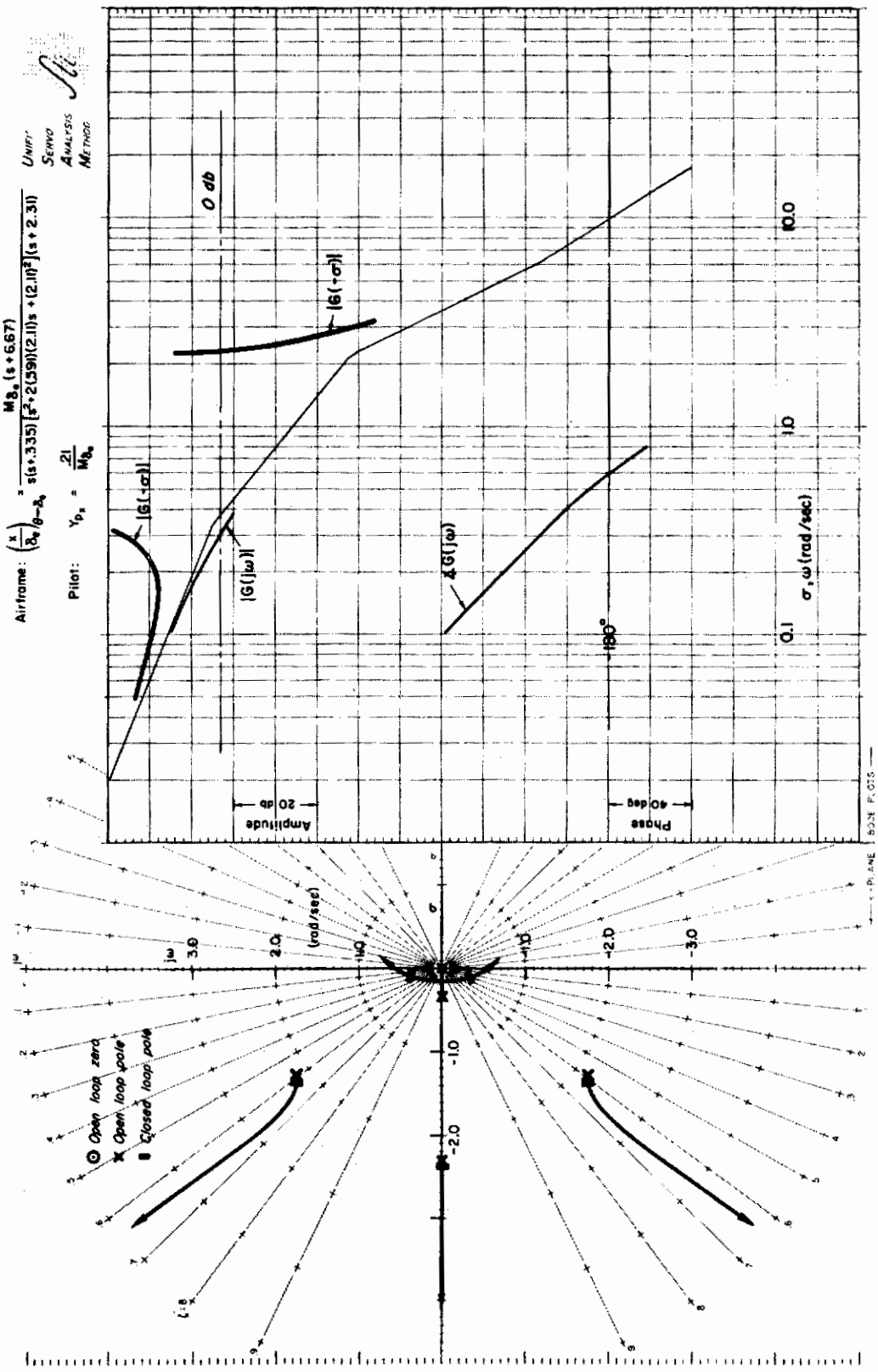

(a) Low M_{δ_1}, Low M_q

Figure 9. Hover Position Loop Closure

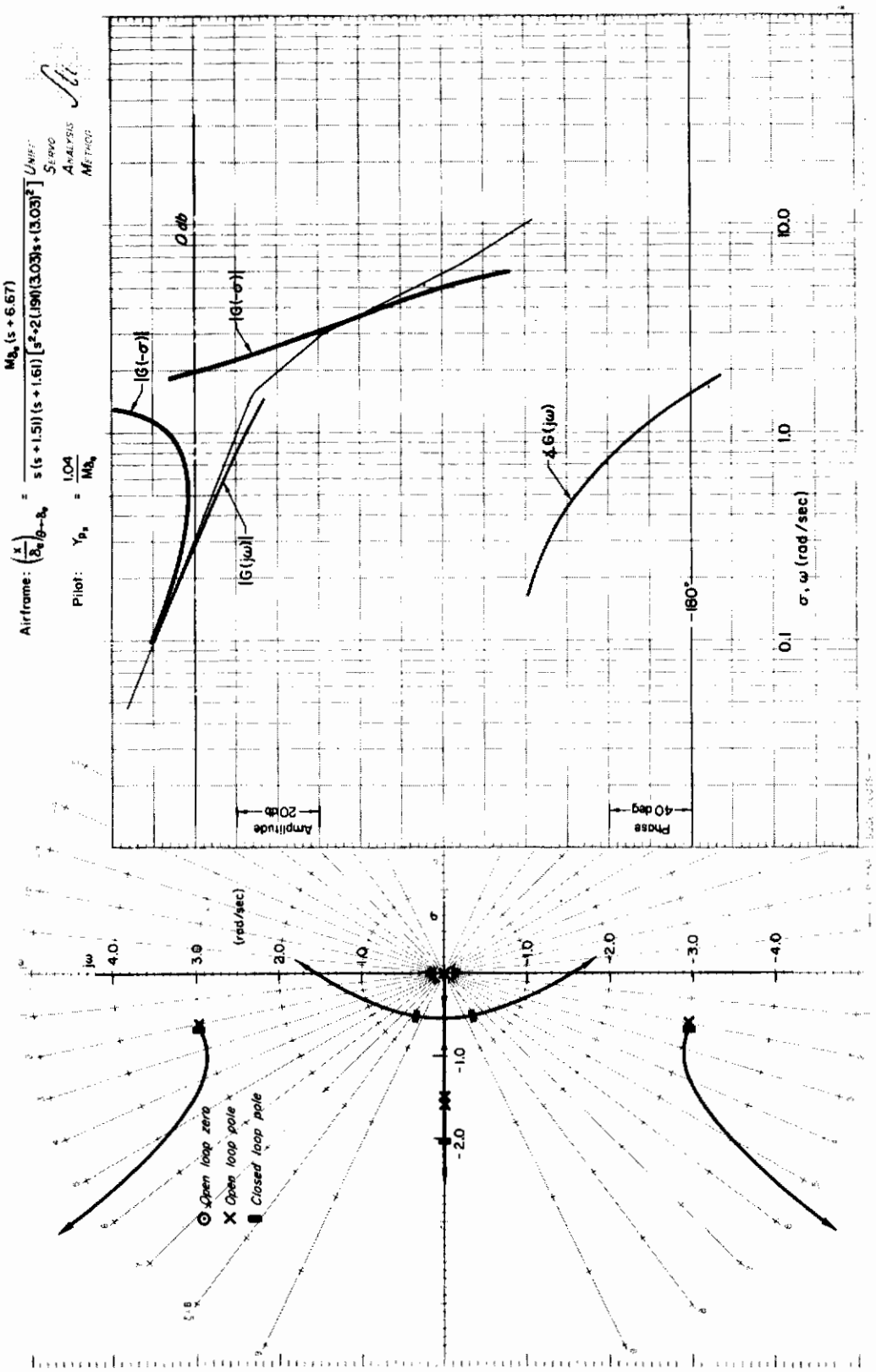

(b) High M_u, Low M_q

Figure 9 (Continued)

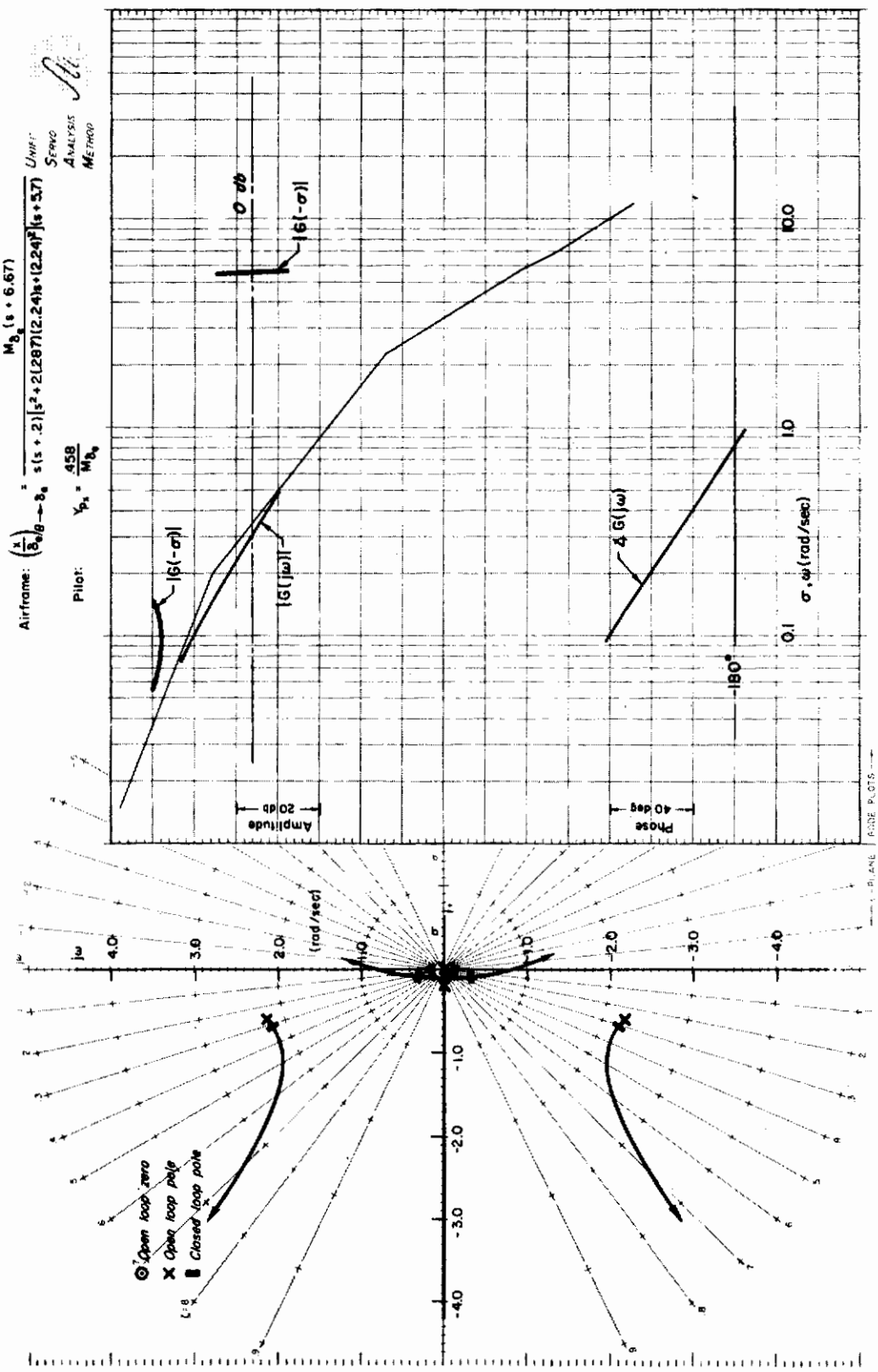

(c) Low M_u, High M_q

Figure 9 (Continued)

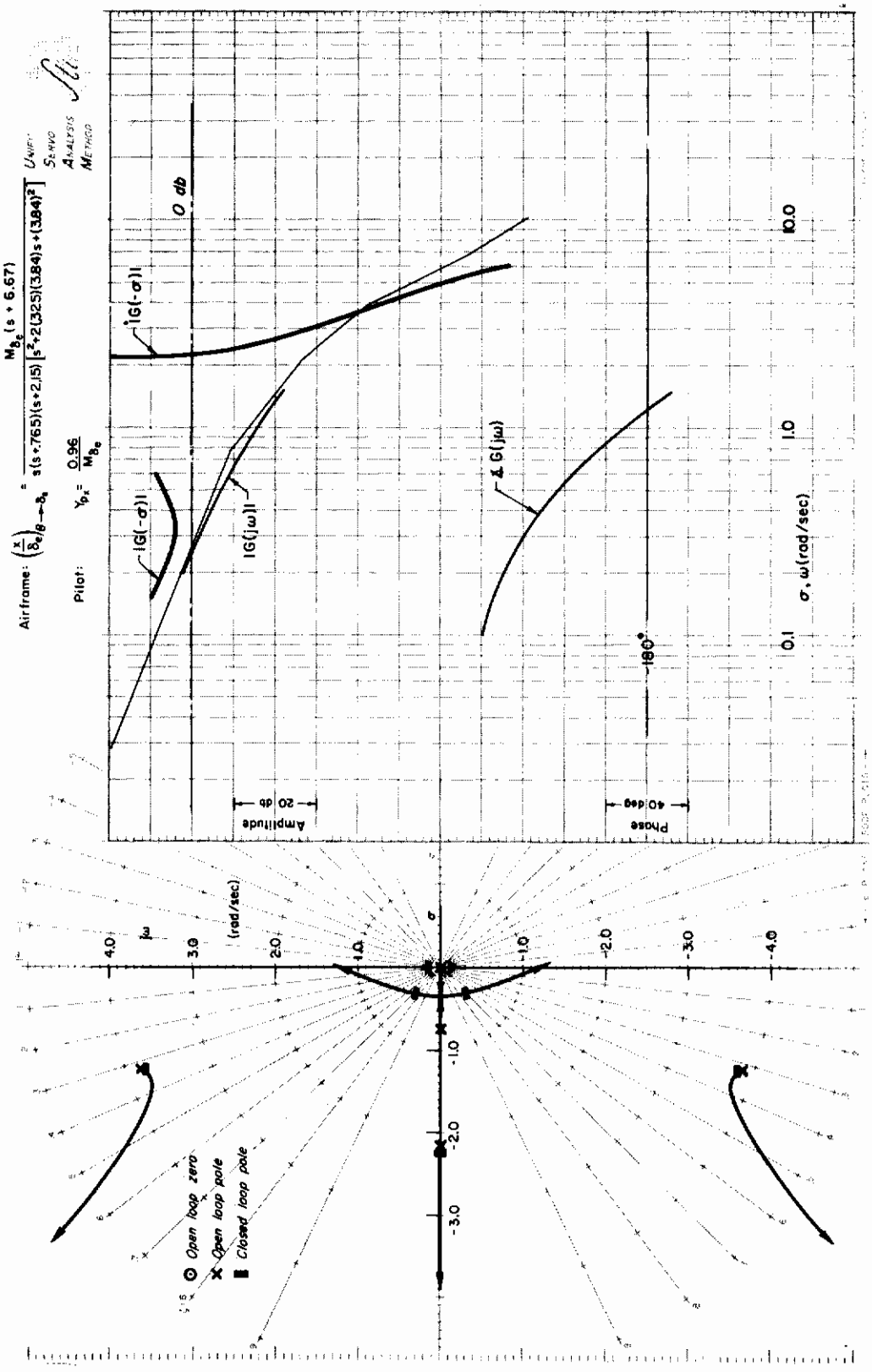

(d) High M_u, High M_q

Figure 9 (Concluded)

It can be seen from Table IV and Fig. 9 that changing M_q has unimportant effects on the position loop. The dominant x-mode (ω_x'') is only slightly influenced by M_q. On the other hand, increasing M_u has generally beneficial effects on the position loop. The crossover frequency could be increased or, for constant crossover frequency, the phase and gain margins (also ζ_x'' and ω_x'') are increased. The beneficial effects are largely due to the increase in $1/T_{sp}'$ which accompanies an increase in M_u.

Making X_u more negative has an advantageous effect on the position loop because of the increase in $1/T_{sp}'$. This allows a higher gain, higher bandwidth closure of the x-loop. For realistic variations in X_u the effect is rather unimportant.

A nonzero X_{δ_e} adds a second-order zero $\left[s^2 - M_q s - (gM_{\delta_e}/X_{\delta_e})\right]$ to the x/δ_e transfer function. For realistic values of $X_{\delta_e}/M_{\delta_e}$ this zero is at too high a frequency to be of significant benefit; even for the relatively large value of $X_{\delta_e}/M_{\delta_e} = -5$ ft the zero is at 2.54 rad/sec. For the high M_u, low M_q case the effects of this zero are more than offset by the lowered $1/T_{sp}'$ resulting from the shift in θ/δ_e zero (see Subsection C). For a crossover frequency of 0.3 rad/sec the net effect is to reduce the phase margin from 70 to 53 deg, reduce ζ_x'' from 0.85 to 0.51, and ω_x'' from 0.61 to 0.44 rad/sec. Thus, it appears that for realistic values, X_{δ_e} has a negligible effect on position control if M_u is small (because the shift in the θ/δ_e zero is small) and a detrimental effect if M_u is large.

E. CLOSED-LOOP GUST RESPONSE

When the pilot task is hovering in still air (or a steady wind), the parameter study of Subsections C and D is sufficient for the analysis of handling qualities. When the pilot task is that of hovering in gusty air, however, then the pilot is also concerned with the variations in position, attitude, and control deflection due to the gust disturbances. It is the purpose of this subsection to examine the effects of random u-gust inputs on pilot closure gains and to determine the effects of changes in the stability derivatives on the rms (root mean square) x, θ, and $M_{\delta_e}\delta_e$ responses with both the θ- and x-loops closed. In particular, variations in the pilot gains from the nominal values of Subsections C

and D will be considered. The nominal gains will be shown to be reasonable in terms of minimizing the "composite" rms x, θ, and $M_{\delta_e}\delta_e$ responses.

The effects of the various stability derivatives will be analyzed to determine those parameters which have the most influence on the attitude and position responses to u-gusts and on the control power requirements for hovering in gusty air.

The final part of this subsection will examine the shapes of response spectra to provide additional understanding of the effects of various parameters.

1. Gust Model

The gust response study will consider random u-gust inputs. For analytical purposes it is desirable to have an input spectrum that is simple in form but which adequately represents the gust phenomena. Such a model is given in Chapter 10 of Ref. 9. This gust spectrum is

Etkin, Dyn. of Airframe

$$\Phi_{u_g}(\omega) = \frac{\omega_{g_2}\left(3\omega^2 + \omega_{g_2}^2\right)\sigma_{u_g}^2}{\left(\omega^2 + \omega_{g_2}^2\right)^2} \qquad (11)$$

where

σ_{u_g} = rms gust velocity

ω_{g_2} = V_{as}/L

V_{as} = steady state airspeed (for hover, V_{as} = average wind speed)

L = integral scale of turbulence

The quantity L is generally considered proportional to altitude at low altitudes and equal to 1000 ft at altitudes greater than 1000 ft. In Ref. 12, L was taken as 30 ft at an altitude of 50 ft; in this report this value will be used as the nominal.

For analytical purposes it is desirable to represent the input spectra of Eq 11 as the output of a linear filter whose input is white noise. Such a filter has the transfer function:

$$Y_{f_2} = \frac{\sqrt{\omega_{g_2}}\left(\sqrt{3}\ s + \omega_{g_2}\right)\sigma_{u_g}}{\left(s + \omega_{g_2}\right)^2} \tag{12}$$

It was found that a simpler filter model of the form

$$Y_f = \frac{\sqrt{2\omega_g}\ \sigma_{u_g}}{s + \omega_g} \tag{13}$$

gave nearly identical rms responses when ω_g was chosen as

$$\omega_g = \frac{3}{2}\omega_{g_2} \tag{14}$$

The fact that the simpler model yields nearly the same rms results is not surprising when the Bode plots of the two filters are compared. The two are identical at high frequencies and very close at middle and low frequencies. The maximum difference between the two is 1.2 db and this occurs at low frequencies. Thus, for the work in this report the simpler filter model was used. The output spectrum corresponding to the passage of white noise through the filter of Eq 13 is

$$\Phi_{u_g} = \frac{2\omega_g \sigma_{u_g}^2}{\omega^2 + \omega_g^2} \tag{15}$$

For most of the work in this report, the gust break frequency, $\omega_g = (3/2)(V_{as}/L)$, was chosen as 1.0 rad/sec (this corresponds to an L of 30 ft and a mean wind speed of 20 ft/sec).

One other gust break frequency of 0.3 rad/sec was briefly considered to make sure the results of the analysis were not highly sensitive to this parameter. The effects of lowering ω_g from 1.0 rad/sec to 0.3 rad/sec at the nominal gains for the high M_u, high M_q case are presented in Table V. It may be seen that the rms gust responses are not strongly dependent on ω_g. Also, from other calculations, the slight differences between the σ's shown in Table V appear to be independent of pilot gain. That is, the differences between the σ's for $\omega_g = 1.0$ rad/sec and $\omega_g = 0.3$ rad/sec remain roughly constant despite pilot gain variations from the nominals.

TABLE V

EFFECTS OF GUST BREAK FREQUENCY

	ω_g = 1.0 rad/sec	ω_g = 0.3 rad/sec
σ_x/σ_{u_g} (sec)	2.0	2.9
$\sigma_\theta/\sigma_{u_g}$ (deg/ft/sec)	0.81	0.68
$M_{\delta_e}\sigma_{\delta_e}/\sigma_{u_g}$ (deg/ft/sec) ...	5.9	4.7

2. RMS Gust Responses

The significance of the rms x, θ, and $M_{\delta_e}\delta_e$ gust responses is discussed below. The x-response provides a measure of the pilot's success in the principal task of hovering over a given point. The θ-response describes the attitude deviations of the vehicle; if the pitching variations are large, the pilot will not like the aircraft even if he is able to satisfactorily maintain position. Finally, $M_{\delta_e}\sigma_{\delta_e}$ provides a measure of both the required control power and the control effort required of the pilot.

The mean-squared values of x, θ, and $M_{\delta_e}\delta_e$ were calculated from the response spectra

$$\varphi_\lambda = \left|\frac{\lambda}{u_g}(j\omega)\right|^2 \varphi_{u_g} \quad \text{for} \quad \lambda = x,\ \theta,\ \text{or}\ M_{\delta_e}\delta_e \tag{16}$$

φ_{u_g} is the gust spectrum of Eq 15, and $\frac{\lambda}{u_g}(j\omega)$ is the transfer function of λ to u-gust inputs with both the θ- and x-loops closed. Equation 16 can also be put into the form

$$\varphi_\lambda = |Y_\lambda(j\omega)|^2 \tag{17}$$

where

$$Y_\lambda(j\omega) = \frac{\lambda}{u_g}(j\omega)Y_f(j\omega)$$

and Y_f is given by Eq 13

The mean-squared values were computed by numerically integrating the spectra from Eq 17 by the method of Appendix E of Ref. 10.

3. Effects of Pilot Gains

The rms values of x, θ, and $M_{\delta_e}\delta_e$ were calculated for variations in pilot x- and θ-loop gains from those of Subsections C and D. The results for the two high M_q cases are shown in Figs. 10a – 10d. The trends shown in these figures also apply to the low M_q cases. In the regions of interest, increasing pilot x-loop gain increases σ_θ and $M_{\delta_e}\sigma_{\delta_e}$, while σ_x decreases. For gain increases beyond those shown in Fig. 10, σ_x reaches a minimum value, then increases. All three rms values go to infinity as the gain for neutral stability is approached. As the x-loop gain approaches zero, σ_x tends to infinity, and σ_θ and $M_{\delta_e}\sigma_{\delta_e}$ tend to minimum values.

In the gain regions of interest, as pilot θ-loop gain increases

a. σ_x varies slightly
b. σ_θ decreases
c. $M_{\delta_e}\sigma_{\delta_e}$ increases

At sufficiently low or high values of gain, the system becomes neutrally stable and all rms values go to infinity.

It can be seen in Figs. 10a – 10d that the nominal gains of Subsections C and D provide a reasonable compromise among the rms values of x, θ, and $M_{\delta_e}\delta_e$. The θ-gain gives a near minimum θ-response without greatly increasing x or $M_{\delta_e}\delta_e$. The x-gain gives near-minimum x-response with only modest increases in θ and $M_{\delta_e}\delta_e$.

4. Effects of Stability Derivatives

Having selected the values of pilot gains, the effects on the rms responses of changes in the stability derivatives can now be discussed. The results will generally be for the nominal pilot gains, so we are comparing the minimum composite gust responses for each set of derivatives. Because of the approximate nature of the nominal pilot parameters, small percentage changes in the gust responses should be ignored. Only gross variations can reliably be attributed as the effects of the stability derivatives.

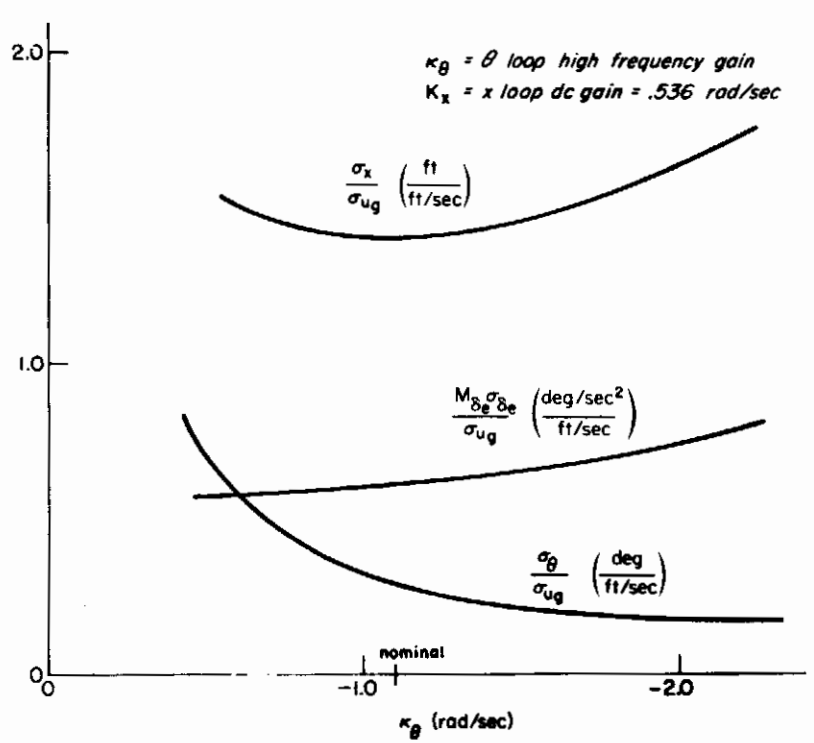

(a) Low M_u, High M_q; κ_θ variations

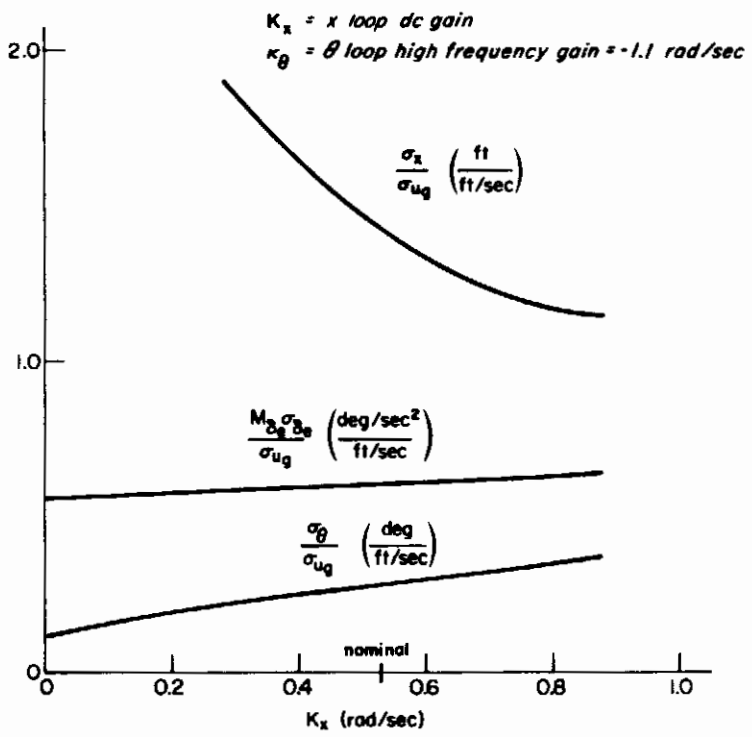

(b) Low M_u, High M_q; K_x variations

Figure 10. Variations of Gust Responses with Pilot Gains

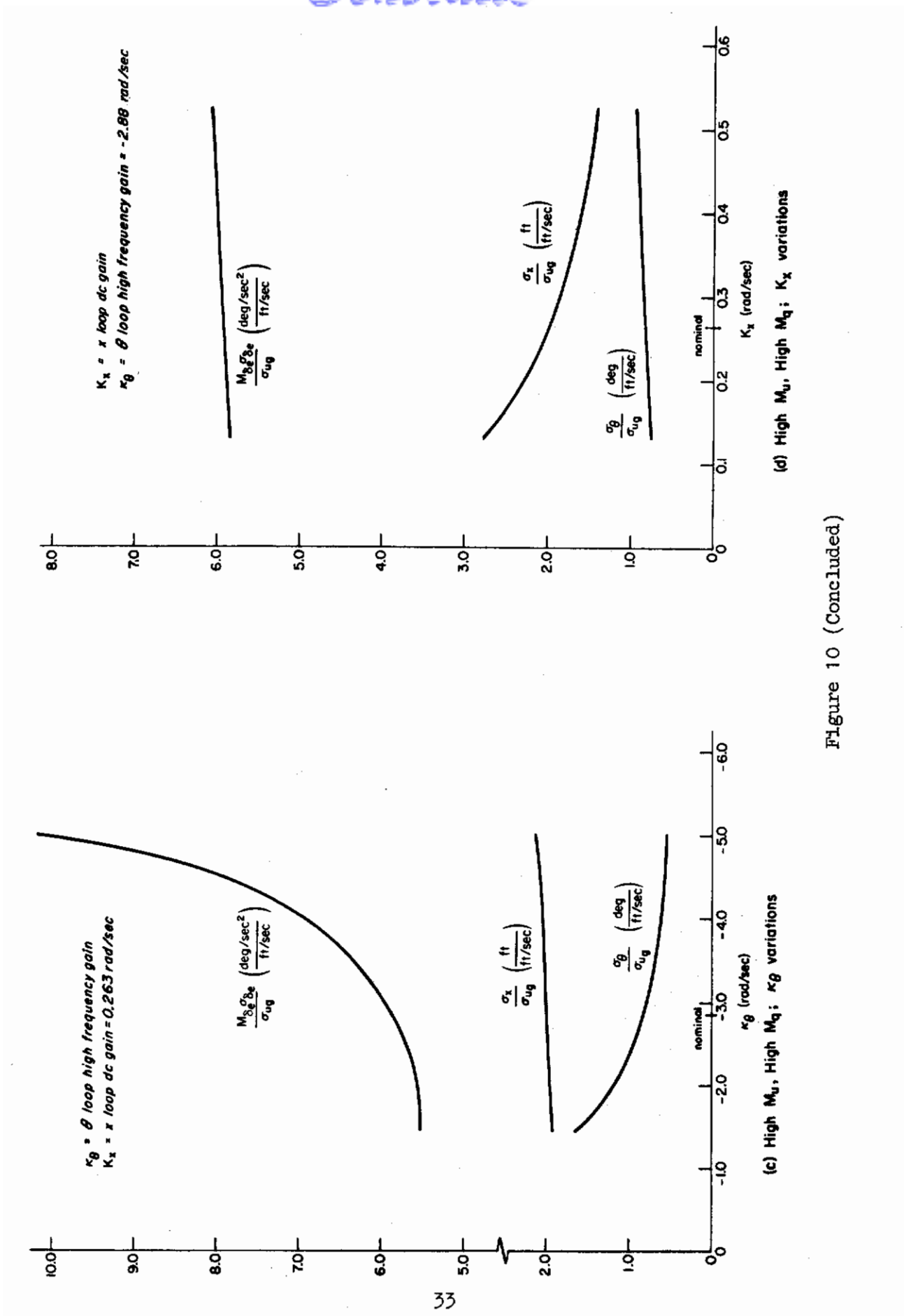

Figure 10 (Concluded)

The stability derivatives of most importance are M_u and M_q. The rms values for $\sigma_{u_g} = 5$ ft/sec for the four combinations of M_u and M_q are summarized in Table VI. The values all appear quite acceptable to a pilot except pitch attitude and control power variations for the high M_u cases.

TABLE VI

RMS GUST RESPONSES

	σ_x (ft)	σ_θ (deg)	$M_{\delta_e}\sigma_{\delta_e}$ (deg/sec^2)
Low M_u, Low M_q	9	2.0	3.2
High M_u, Low M_q	9	7.0	44
Low M_u, High M_q	7	1.4	3.0
High M_u, High M_q	10	4.0	29

$\sigma_{u_g} = 5$ ft/sec

An attempt was made to compare the above with the simulator results of Refs. 11 and 12. Unfortunately, a direct comparison could not be made because of numerous differences in some parameters; furthermore, the references do not specify the value of M_u. In the simulator tests the equivalent gust break frequency, ω_g, was 2.5 rad/sec and the pitch damping was $M_q = -2.2$ sec^{-1} (achieved by stability augmentation). The simulated vehicle was a 35,000 lb ducted-fan aircraft, and from the derivative survey of Table I it appears that M_u should be within a factor of 2 of the low M_u used in the analytical work here. Test data were given for $\sigma_{u_g} = 10$ ft/sec. Halving the rms responses for comparison with the $\sigma_{u_g} = 5$ ft/sec values of Table VI gives:

$$\sigma_x = 5.8 \text{ ft}$$
$$M_{\delta_e}\sigma_{\delta_e} = 3.2 \text{ deg/sec}^2$$

Compared to the low M_u, high M_q analytical values of

$$\sigma_x = 7.0 \text{ ft}$$
$$M_{\delta_e}\sigma_{\delta_e} = 3.0 \text{ deg/sec}^2$$

and considering the many differences in parameters, the results of the comparison are quite good, indicating at least that the analytical results are of the right order of magnitude.

From a comparison of the four cases of Table VI rough indications of the effects of M_u and M_q can be obtained. The effects of reducing M_q may be summarized as:

a. A negligible change in σ_x

b. A moderate increase in σ_θ

c. A moderate increase in $M_{\delta_e}\sigma_{\delta_e}$ when M_u is high, negligible change when M_u is low

The effects of increasing M_u by a factor of 10 may be summarized as:

a. A negligible effect on σ_x

b. A large increase (roughly a factor of 3) in σ_θ

c. A very large increase (roughly a factor of 10) in $M_{\delta_e}\sigma_{\delta_e}$

Thus, M_u emerges as the more significant parameter in determining the gust responses. M_q is less important because its variations can largely be offset by changes in pilot lead in the θ-loop. This does not mean that M_q is unimportant, as pilot ratings are strongly influenced by the lead he must use. In other words, M_q has a relatively minor effect on gust responses, but a major effect on pilot opinion.

A rather surprising result of this study is that lowering M_q, at low M_u, had very little effect on the rms control effort. Lowering M_q means that the pilot must generate more lead in the θ-loop, and this implies additional pilot control inputs. It was expected that the increased pilot input would show up as an increased $M_{\delta_e}\sigma_{\delta_e}$. The expected result did occur when M_u was large, but not when M_u was small.

In hindsight, it is noted that for very small M_u the gusts do not disturb the attitude directly. The attitude variations are largely the result of trying to offset the direct effect of the gusts on the fore-and-aft motion of the vehicle. Note the extreme percentage changes in σ_θ with x-loop gain in Fig. 10b. Consequently, it is reasonable to expect that for low M_u the gust responses are relatively insensitive to θ-loop parameters (Fig. 10a).

The effects of X_u on σ_x for the two high M_q cases and on σ_θ for the high M_u, high M_q case were evaluated by computing their partial derivatives with respect to X_u. The results appear in Table VII. None of the changes are very important, considering the extreme change in X_u that was used; the perturbed X_u equals the largest value in the survey of Table I.

TABLE VII

X_u EFFECTS ON GUST RESPONSES

	$\frac{\partial\left(\frac{\sigma_x}{\sigma_{ug}}\right)}{\partial(X_u)}$	$\Delta(X_u)$	$\Delta\sigma_x$* (ft)
Low M_u, High M_q	−1.53	−0.3	2.3
+High M_u, High M_q	−0.292	−0.3	0.44

	$\frac{\partial\left(\frac{\sigma_\theta}{\sigma_{ug}}\right)}{\partial(X_u)}$	$\Delta(X_u)$	$\Delta\sigma_\theta$* (deg)
+High M_u, High M_q	1.09	−0.3	−1.6

*These changes are for σ_{ug} = 5 ft/sec

+These were calculated at nominal K_x, but at κ_θ = 1.44 sec^{-1}

The above gust responses are all for X_{δ_e} = 0. The rms values of x, θ, and $M_{\delta_e}\delta_e$ were also calculated for the high M_u, low M_q case with $X_{\delta_e}/M_{\delta_e}$ = −5 ft. The results were quite close to the rms values for X_{δ_e} = 0; the maximum change was 10 percent. Thus, realistic values of X_{δ_e} appear to have little effect on the gust responses.

5. Gust Response Spectra

To provide additional insights to the numerical results, the forms of the gust response spectra will be examined. From Eqs 15-17 the response spectra can be written

$$\Phi_\lambda = |Y_\lambda(j\omega)|^2$$

$$= \frac{2\sigma_{u_g}^2}{\omega_g} \left| \frac{\lambda}{u_g}(s) \frac{\omega_g}{s + \omega_g} \right|^2_{s = j\omega} \tag{18}$$

where $\lambda = x, \theta,$ or $M_{\delta_e}\delta_e$.

The x/u_g transfer function with the θ- and x-loops closed is given by

$$\frac{x}{u_g}(s) = \frac{N''_{x_{u_g}}}{\Delta''} \tag{19}$$

where

$$N''_{x_{u_g}} = -X_u \left[\left(s + \frac{2}{\tau_e} \right) \left(s^2 - M_q s - \frac{gM_u}{X_u} \right) \right.$$

$$\left. - K_{p_\theta} T_L M_{\delta_e} \left(1 - \frac{X_{\delta_e} M_u}{X_u M_{\delta_e}} \right) \left(s + \frac{1}{T_L} \right) \left(s - \frac{2}{\tau_e} \right) \right] \tag{20}$$

$$\Delta'' = \left[s^2 + 2\zeta''_x \omega''_x s + (\omega''_x)^2 \right] \left[s^2 + 2\zeta''_p \omega''_p s + (\omega''_p)^2 \right] \left[s + \left(\frac{2}{\tau_e} \right)'' \right] \tag{21}$$

By employing some of the identities derived in Appendix D, we find that at low frequency the x/u_g transfer function approaches $1/K_x$. We also note that the zeros of x/u_g are considerably larger than ω''_x or ω_g (see Table VIII, so the general asymptotic shape of the x-spectrum is as sketched below. Actual logarithmic and linear plots of the x-spectrum for the high M_u, high M_q case are shown in Fig. 11

TABLE VIII

GUST RESPONSE NUMERATOR ZEROS

CASE		x-NUMERATOR			θ-NUMERATOR		$M_{\delta_e}\delta_e$ NUMERATOR			
		Complex Zeros		Real Zero*	Real Zeros*		Complex Zeros		Real Zeros*	
M_u	M_q	ζ	ω $\frac{rad}{sec}$	sec^{-1}	sec^{-1}		ζ	ω $\frac{rad}{sec}$	sec^{-1}	
Low	Low	0.29	2.8	3.4	±0.31	6.7	−0.09	0.32	1.1	−6.8
High	Low	−0.03	6.2	4.5	±0.22	6.7	−0.08	0.49	1.6	−6.7
Low	High	0.24	2.8	5.7	±0.46	6.7	0.12	0.32	4.0	−7.0
High	High	0.06	6.4	4.5	±0.21	6.7	−0.02	0.39	2.2	−6.7

*Positive in left-half plane

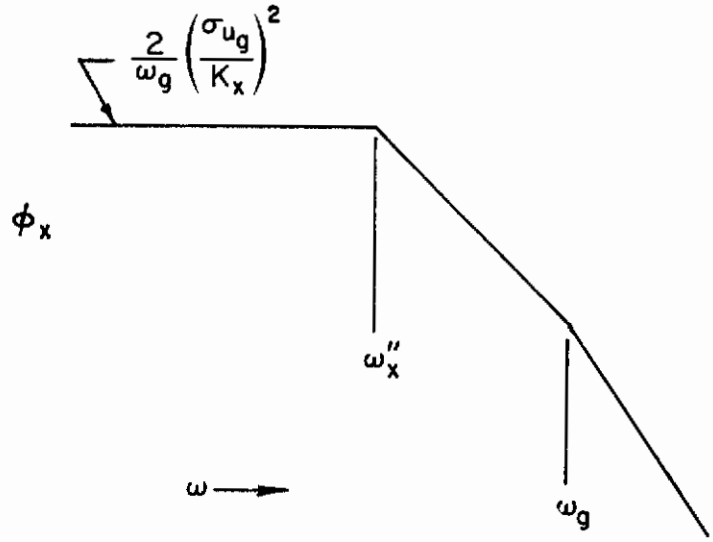

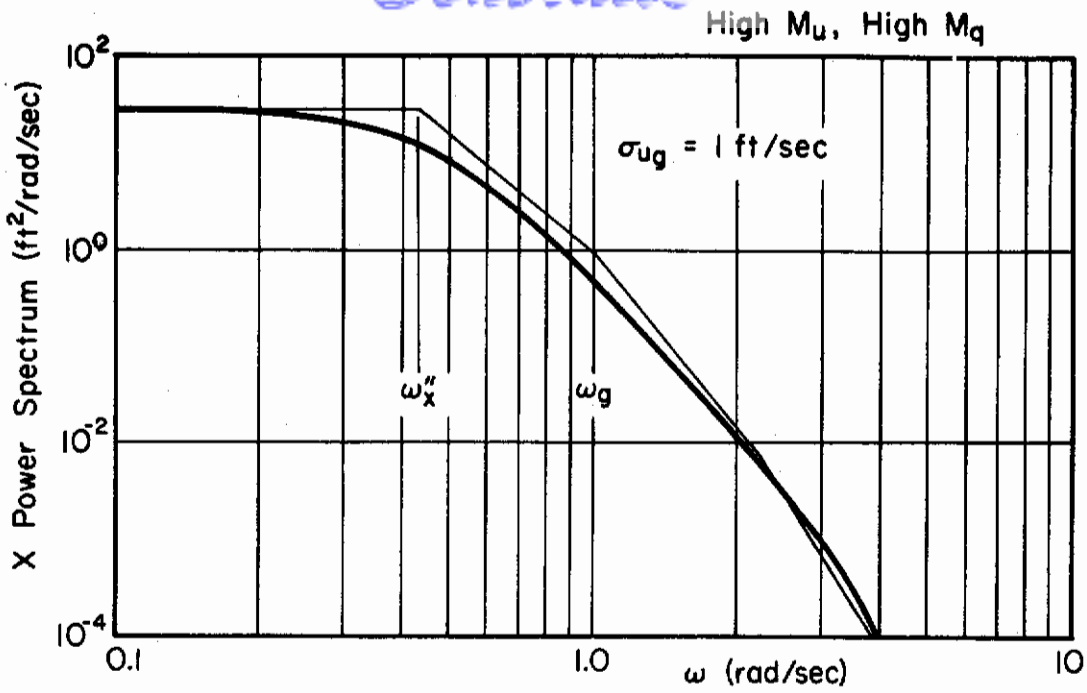

(a) Logarithmic Plot

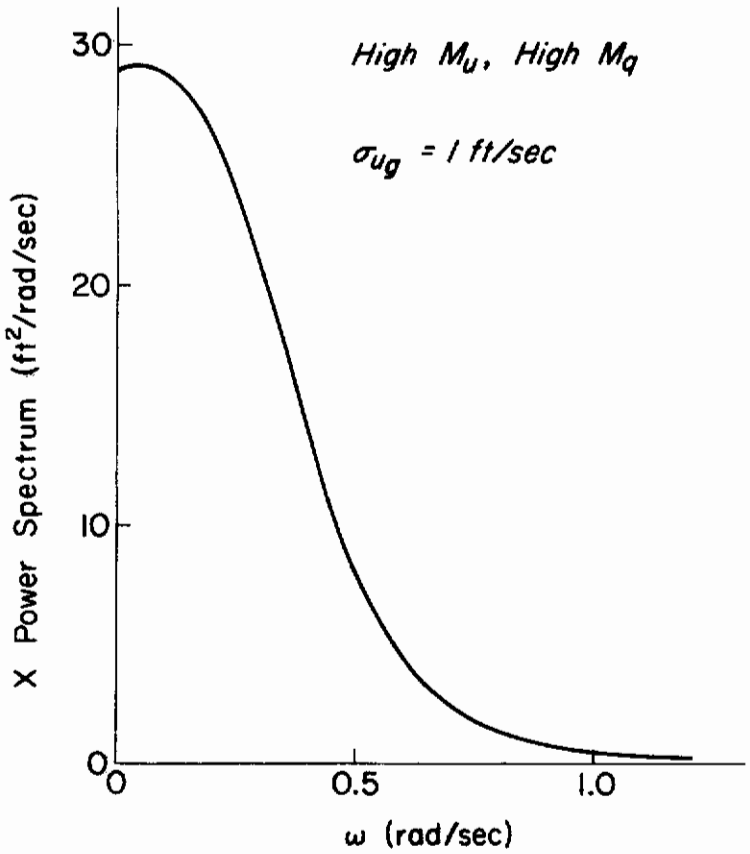

(b) Linear Plot

Figure 11. Position Spectrum

It is clear that the rms x-response is primarily influenced by K_x and the ω_x'' mode. A better appreciation for the numerical effects of these parameters is obtained by approximating the x-spectrum with only the ω_x'' break frequency, i.e.,

$$\varphi_x \doteq \frac{2}{\omega_g}\left(\frac{\sigma_{u_g}}{K_x}\right)^2 \left| \frac{(\omega_x'')^2}{s^2 + 2(\zeta_x\omega_x)''s + (\omega_x'')^2} \right|^2_{s = j\omega} \tag{22}$$

Then from the integration tables of Ref. 10,

$$\boxed{\left(\frac{\sigma_x}{\sigma_{u_g}}\right)^2 \doteq \frac{\omega_x''}{2\zeta_x''\omega_g} \frac{1}{(K_x)^2}} \tag{23}$$

Equation 23 has been found to approximate σ_x to within 20 percent.

The θ/u_g numerator with both the θ- and x-loops closed is

$$N''_{\theta u_g} = -M_u\left(s + \frac{2}{\tau_e}\right)\left[s^2 - K_x\left(1 + K_\theta\right)\left(-X_u + \frac{X_{\delta_e}}{M_{\delta_e}} M_u\right)\right] \tag{24}$$

The second-order term above gives a pair of real zeros which can be larger or smaller than ω_x'' (see Table VIII). The d.c. value of θ/u_g is

$$\frac{-X_u + (X_{\delta_e}/M_{\delta_e})M_u}{g}$$

Thus the θ-spectrum has the general asymptotic shape sketched below. An actual spectrum is plotted in Fig. 12.

It appears that the asymptotic value for the flat portion just below ω_g is a key parameter. This value is given by

$$\frac{2}{\omega_g}(\sigma_{u_g})^2 \frac{(\omega_x'')^4}{\left[gK_x(1 + K_\theta)\right]^2}$$

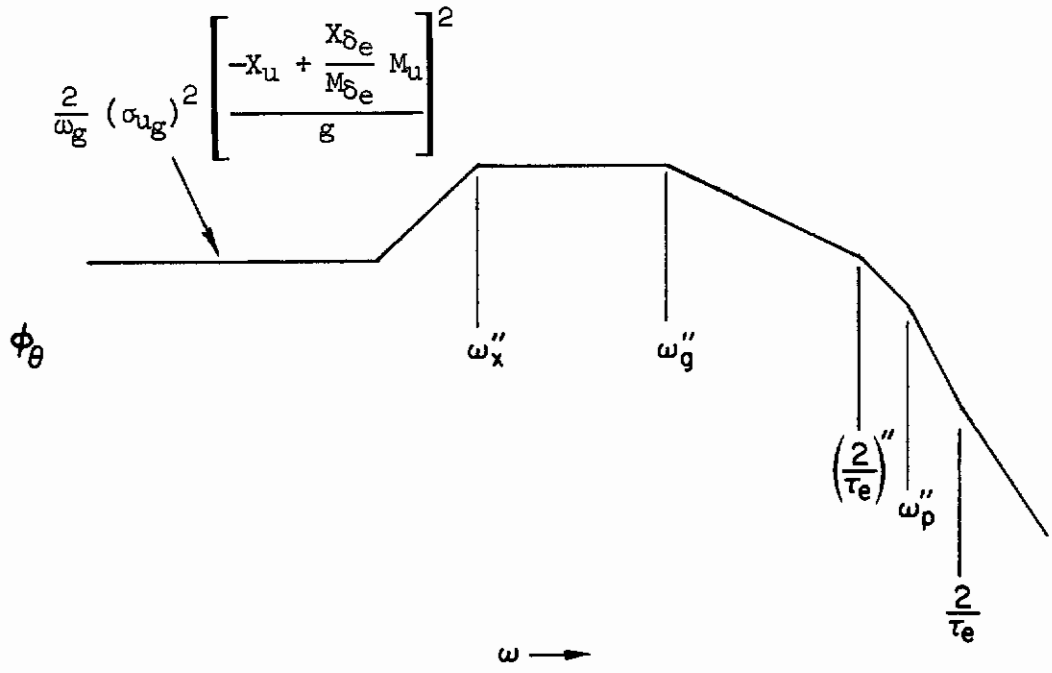

The increase in the rms θ due to increasing M_u can be seen to be primarily due to the reductions in K_x and K_θ and the increase in ω_x'' (this is partially offset by the increase in ζ_x'').

The reduction in the rms θ for increasing M_q has different causes for low and high M_u. For low M_u, the reduction is mainly due to increased K_θ, with the increase in K_x helping. For high M_u, the major cause is the reduction in ω_x''.

The numerator for $M_{\delta_e}\delta_e/u_g$ is given by

$$M_{\delta_e}N''_{\delta_e u_g} = \kappa_\theta M_u\left[s^2\left(s+\frac{1}{T_L}\right)\left(s-\frac{2}{\tau_e}\right) - \frac{X_u K_x(1+K_\theta)}{\kappa_\theta}\left(s+\frac{2}{\tau_e}\right)\left(s^2 - M_q s - \frac{gM_u}{X_u}\right)\right] \quad (25)$$

This quartic factors into a lightly damped, low frequency pair at a frequency which is approximately

$$\sqrt{\left(-X_u + \frac{X_{\delta_e}}{M_{\delta_e}} M_u\right)K_x\left(1 + \frac{1}{K_\theta}\right)}$$

plus one real zero slightly larger than $1/T_L$ and another in the right-half plane which is slightly greater than $2/\tau_e$ (see Table VIII). For all four cases the complex zeros are at a frequency slightly less than ω_x'', so the

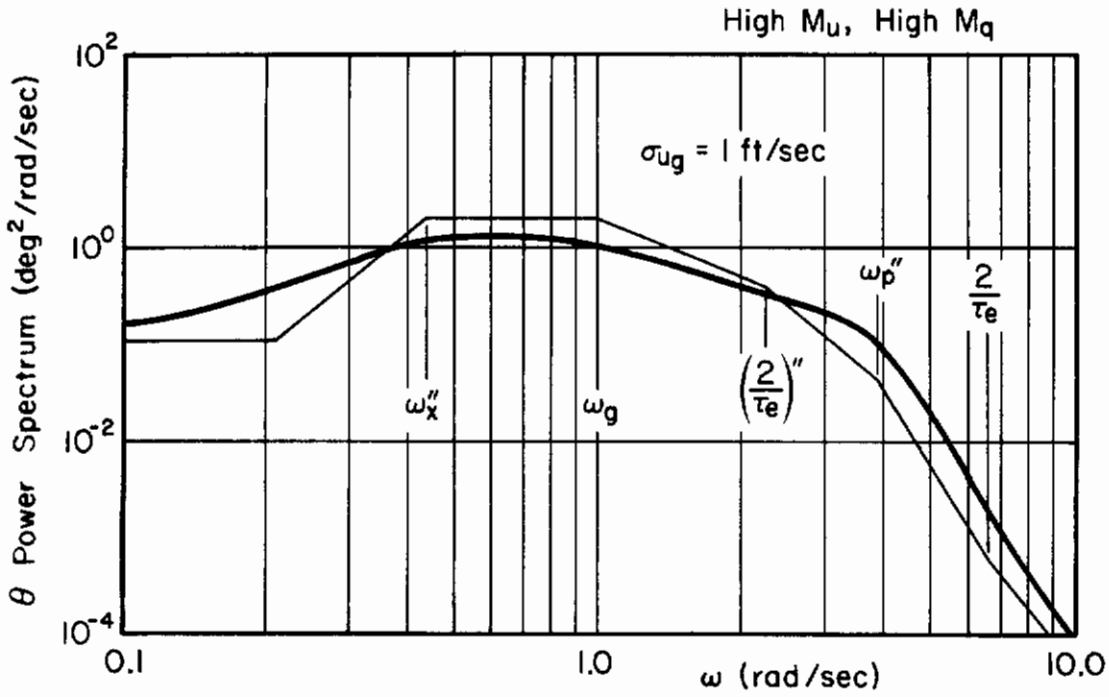

(a) Logarithmic Plot

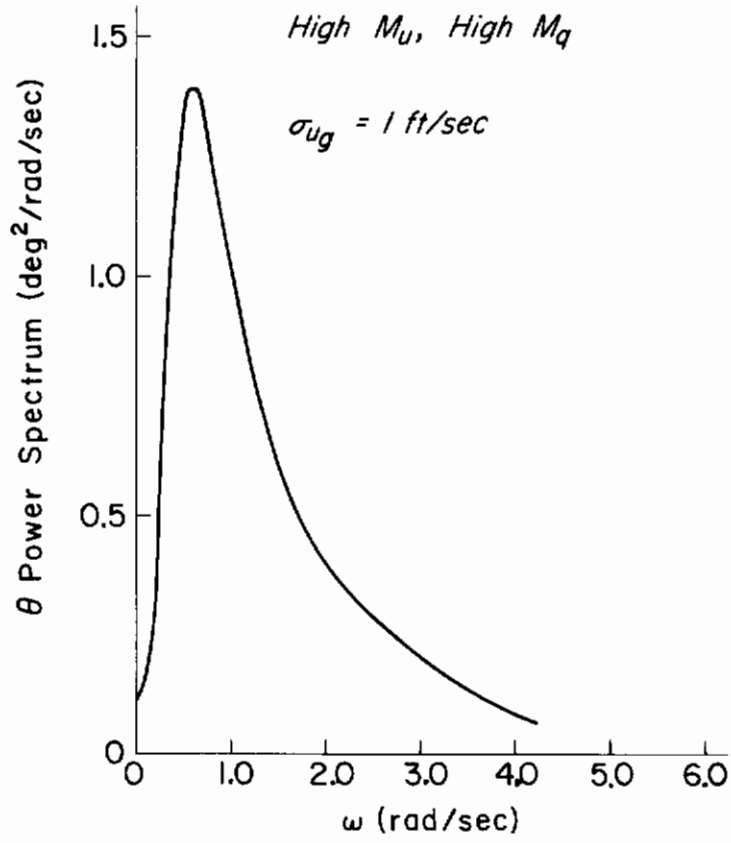

(b) Linear Plot

Figure 12. Attitude Spectrum

$M_{\delta_e}\delta_e$ spectrum takes the asymptotic form sketched here. A sample spectrum is plotted in Fig. 13.

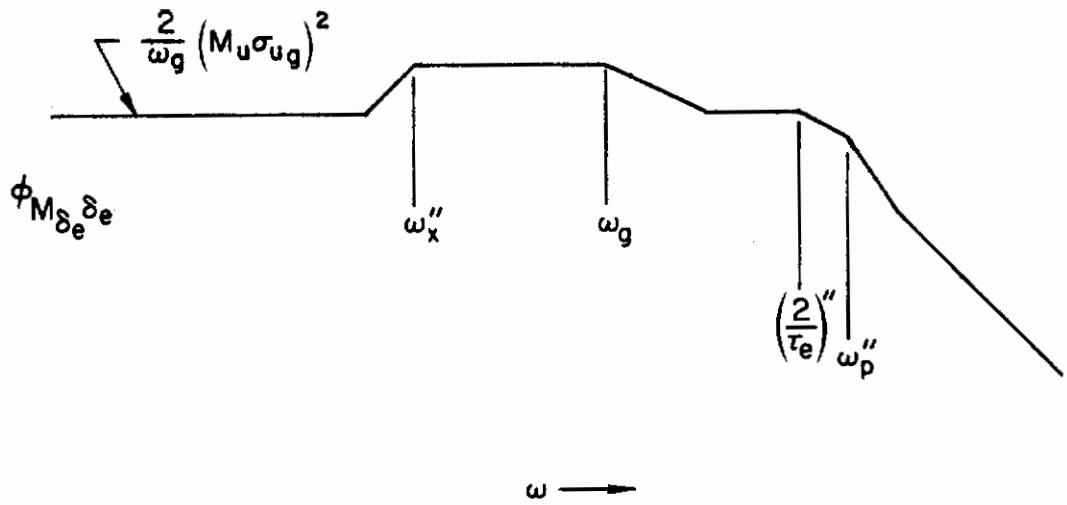

There is a general over-all scaling effect with M_u, so that the rms $M_{\delta_e}\delta_e$ is approximately proportional to M_u. Secondary effects of M_u come from changes in:

a. Spacing of complex zeros and ω_x''
b. Real zero which is approximately $1/T_L$
c. $(2/\tau_e)''$ and ω_p'' modes

Increasing M_q for low M_u does not change the response because of offsetting factors. The effects of increasing $1/T_L$ and the zero associated with it are offset by the effects of increasing $(2/\tau_e)''$ and decreasing ζ_p''.

No one factor can account for the change in the rms $M_{\delta_e}\delta_e$ with M_q for high M_u. It is apparently the combined result of a number of factors.

F. SUMMARY OF DERIVATIVE EFFECTS

The significant effects in hover of changes in the stability derivatives are summarized below. For each derivative the effects are listed in roughly their order of importance.

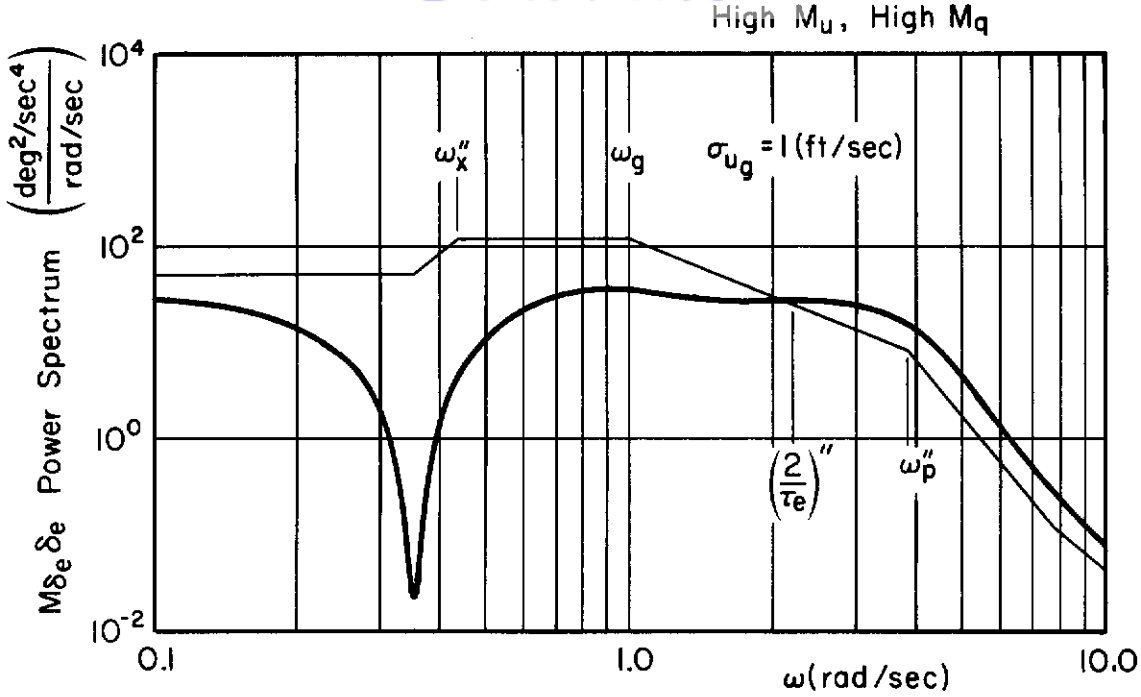

(a) Logarithmic Plot

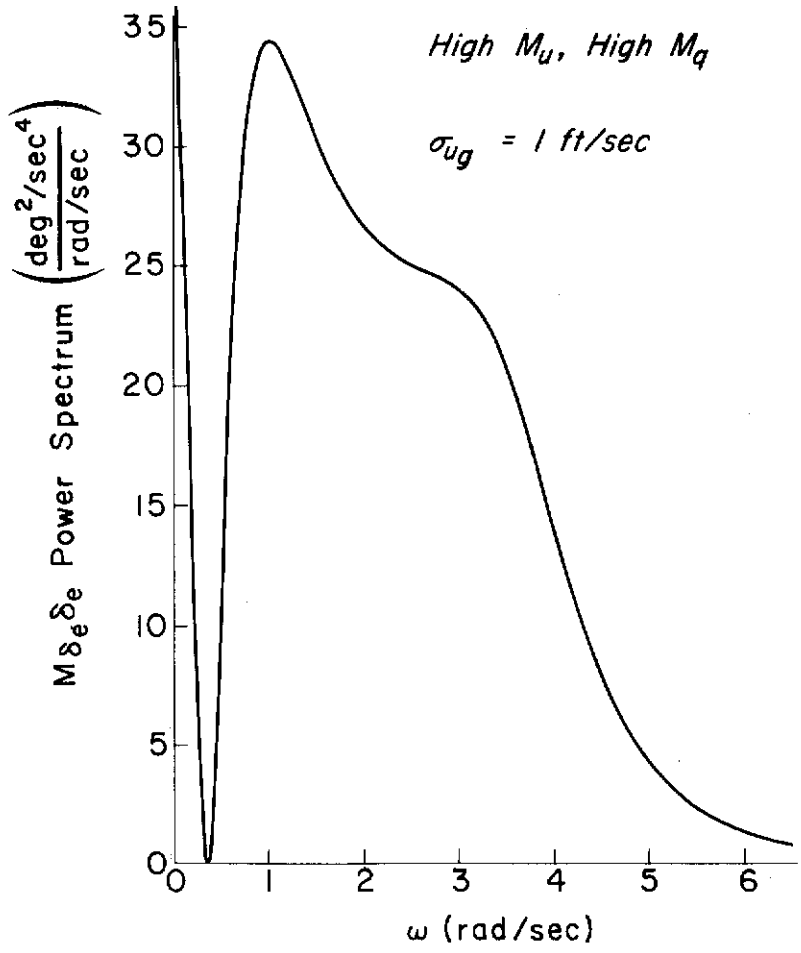

(b) Linear Plot

Figure 13. Control Power Spectrum

Increasing M_u:

1. Greatly increases control deflections in gusty air, $M_{\delta_e}\sigma_{\delta_e}$ is roughly proportional to M_u.

2. Increases closed-loop attitude response to gusts, σ_θ is roughly proportional to $\sqrt{M_u}$.

3. Destabilizes the open-loop phugoid and increases the frequency of all open-loop roots.

4. Improves the position loop closure; crossover frequency is increased.

5. Slightly degrades attitude loop; for high M_q pilot lead is increased, for low M_q closure becomes more sensitive to pilot parameters.

Making M_q more negative:

1. Improves the attitude loop by reducing pilot lead.

2. Increases the damping of all open-loop roots.

3. Slightly reduces the attitude responses to gusts.

4. Slightly reduces the control deflections in gusty air.

Making X_u more negative:

1. Increases the damping of all open-loop roots.

2. Increases the allowable gain and bandwidth of the position loop.

Making $X_{\delta_e}/M_{\delta_e}$ more negative has negligible effect if M_u is small. For large M_u the position loop is degraded by reductions in phase margin and the closed-loop damping ratio and natural frequency of the x-mode.

Two important conclusions are drawn from the above. First, the effects of M_u on open-loop roots and on the pilot's closure of attitude and position loops are of secondary importance; the major effect of M_u is that it determines the magnitude of the pitching moment disturbances produced by horizontal gusts. This conclusion is the same as one reached in Ref. 8; the analytical work reported here substantiates the experimental results of Ref. 8. This conclusion also shows the importance of

including gust inputs in experimental evaluations of hover handling qualities, particularly when evaluating the effects of M_u.

The second conclusion is that, contrary to the general notion, a nonzero X_{δ_e} of the magnitude available on typical V/STOL vehicles does <u>not</u> significantly improve the pilot's ability to hover over a spot.

All the foregoing conclusions can be applied to lateral control in hover by the equivalence relationships of Subsection A.

SECTION III

SIZE AND GEOMETRY

The objective of this section is to investigate the effects of vehicle size and geometry on handling qualities. This is an extremely complex problem and no one approach yields all the desired information. Consequently, the problem is attacked from several aspects in the following subsections. Taken collectively the various approaches yield a considerable amount of information on the variations of handling qualities with vehicle size and geometry.

Subsection A discusses the applicability of the roll requirements study for conventional aircraft of Ref. 7. Some general conclusions concerning the damping and control power requirements for V/STOL vehicles can be inferred from that work.

The use of a new form of nondimensionalized equations of motion for hovering vehicles sheds some light on size and geometry effects. This approach to the problem is considered in Subsection B.

The variations of the hover dimensional derivatives with size and the implications of these changes are discussed in Subsection C, while Subsection D considers the effects of vehicle geometry on the derivatives. Subsection E summarizes the results.

A. DAMPING AND CONTROL POWER REQUIREMENTS

Although Ref. 7 is primarily concerned with roll control for conventional aircraft, some of the results can be applied to V/STOL vehicles. In fact, some of the handling qualities data analyzed in Ref. 7 were for V/STOL craft.

Reference 7 presents an analysis of the damping requirements for controlled elements of the form $K/s(s+d)$. Controlled elements of this form represent:

1. The idealized roll control of a conventional airplane

2. The altitude, heading, pitch (for $M_u = 0$), and roll (for $L'_v = 0$) control of a hovering V/STOL

An analysis was made of the variations in pilot ratings with damping (or d) for conditions in which the gain was optimized for each level of damping. Data from several sources, including conventional and V/STOL aircraft, showed a remarkable consistency. In closed-loop tracking situations pilot ratings improved as damping was increased up to $d \doteq 1$ sec^{-1}. Further increases in damping did not improve pilot ratings as long as adequate control power was maintained. It was concluded that the minimum damping for satisfactory ratings (3-1/2 on the Cooper scale) is about 0.8 sec^{-1}. These results were independent of vehicle size, type, or mission, or the axis being controlled.

Roll power requirements were also analyzed in Ref. 7. Paraphrasing that report, the pilot must have sufficient control power to:

1. Balance the aircraft under all conditions of aerodynamic, inertial, or power plant asymmetries
2. Maintain attitude in steady side winds or deliberate sideslips
3. Maintain or quickly recover attitude in gusty air
4. Permit rapid recovery from stalls and spins
5. Permit crosswind takeoff and landing
6. Perform required maneuvers consistent with the aircraft's effective utilization

For a given vehicle the evaluation of the control power to satisfy Items 1, 2, 4, and 5 is a relatively simple, straightforward task. Items 3 and 6 are much more difficult to evaluate and are frequently the critical requirements.

While the hover study presented here (Section II) is some help in evaluating Item 3, Item 6 remains an elusive requirement. The basic problem is defining the required maneuvers for a given mission. The roll power requirements for several combat and landing maneuvers are analyzed in Ref. 7 and correlated with pilot comments on numerous operational aircraft. The result of interest here is that the control power requirements (measured in terms of maximum roll rate, maximum bank angle in a specified time, or minimum time to reach a specified bank angle) appear to depend on mission rather than vehicle size or geometry.

This almost intuitive result says that, for a given mission, control power (to satisfy Item 6) can be specified regardless of vehicle size and geometry. Subsections C and D will consider the requirements of Item 3 by examining the variations in gust response with size and weight.

B. NONDIMENSIONAL HOVER EQUATIONS OF MOTION

The value of dimensional analysis in aerodynamics is beyond dispute. One would hardly think of attempting to analyze lift data without expressing them in the form

$$C_L = f\left[\begin{matrix}\text{geometry (including } \alpha\text{),} \\ \text{Reynolds No. and Mach No.}\end{matrix}\right] \tag{26}$$

Dimensionless relations of this kind are so useful that even for VTOL aircraft, where C_L becomes meaningless at hover, it is usual to employ an alternative dimensionless group. Several alternatives have been suggested, e.g., the definition of

$$C_{L,s} = \frac{\text{Lift}}{\frac{1}{2}\rho S V^2_{\text{slipstream}}} \tag{27}$$

used by McKinney (Ref. 18), Kuhn (Ref. 19), and in other NASA publications.

Neglecting Mach number effects, $C_{L,s}$ is a function only of vehicle geometry and through-flow Reynolds number, $V_i l/\nu$, where V_i is the through-flow velocity at the actuator disk, l is a characteristic length, and ν is the kinematic viscosity. For the remainder of this discussion we shall assume that viscosity effects do not significantly change with scale, and therefore they will not be mentioned explicitly. This assumption is made only to simplify the presentation; in applying experimental data or in refined theoretical calculations one should, of course, correct for through-flow Reynolds number as far as possible.

Applications of dimensional analysis have also been directed at problems of airplane dynamics to develop nondimensional equations of motion, e.g., Refs. 9, 20–23. In all these works the characteristic unit of time is inversely proportional to airplane steady state forward

speed, U_o. It is clear that none of the schemes can be applied directly to hover conditions where $U_o = 0$. It is therefore necessary to devise a new* set of nondimensionalizing parameters. The required dimensional analysis is given below.

We assume that the period, or the time to half amplitude, or some other characteristic time, t_c, of a hovering vehicle depends on

l	some characteristic length, a measure of scale
ρ	air density
m	the mass of the vehicle
g	gravity
k	the radius of gyration about the appropriate axis

Following the usual procedures of dimensional analysis (e.g., Ref. 25), we put

$$t_c = \text{Constant} \cdot l^a \rho^b m^c g^d k^e \tag{28}$$

In dimensional terms,

$$[T] \equiv [L]^a \left[\frac{M}{L^3}\right]^b [M]^c \left[\frac{L}{T^2}\right]^d [L]^e \tag{29}$$

This equation must be satisfied for M, L, and T, i.e., we must solve the set of equations:

$$\begin{aligned} T: \quad & 1 = -2d \\ L: \quad & 0 = a - 3b + d + e \\ M: \quad & 0 = b + c \end{aligned} \tag{30}$$

This set of three equations has five unknowns. We choose to allow b and e to remain the unsolved quantities for now, but will ultimately

*References 26 and 27 present a nondimensionalization scheme employing rotor tip speed as a divisor, yielding hovering equations of motion for helicopters. The method presented here is preferred as being more general, because the divisors are simple functions of vehicle mass and size.

set them to give the most useful form of the nondimensional equations. Thus, in terms of b and e, Eq 28 reduces to

$$t_c = \text{Constant} \sqrt{\frac{l}{g}} \left(\frac{\rho l^3}{m}\right)^b \left(\frac{k}{l}\right)^e \tag{31}$$

It is shown in Appendix B that for ducted-fan vehicles the derivatives X_u, Z_u, and Z_w are proportional to $\sqrt{\rho g A_e/m}$, where A_e is the total actuator disk area. The constants of proportionality are dimensionless and depend only on vehicle geometry. Since the parameter $\sqrt{\rho g A_e/m}$ has the dimensions of t^{-1}, it is appropriate to choose $b = -1/2$, $e = 0$ in Eq 31, giving the following characteristic parameters:

$$\text{Unit of length, } l = \sqrt{A_e} \tag{32}$$

$$\text{Unit of mass, } m = \text{mass of airplane} \tag{33}$$

$$\text{Unit of time, } t_c = \sqrt{\frac{m}{\rho g A_e}} = \sqrt{\frac{\mu l}{g}} \tag{34}$$

$$\text{where } \mu = \frac{m}{\rho l^3} \tag{35}$$

For the pitch derivatives* it is desirable to introduce an additional parameter defined by

$$i_y = \left(\frac{k_y}{l}\right)^2 \tag{36}$$

Then M_u is proportional to $\frac{1}{i_y}\sqrt{\frac{g}{\mu l^3}}$ and M_q is proportional to $\frac{1}{i_y}\sqrt{\frac{g}{\mu l}}$

We are now ready to nondimensionalize the equations of motion, which are (omitting terms usually negligibly small):

*The derivation here will use only the longitudinal notation and symbols, but the results can also be applied to the lateral equations by changing the symbols as discussed in Subsection II-A.

$$\begin{bmatrix} s - X_u & 0 & g \\ -Z_u & s - Z_w & 0 \\ -M_u & 0 & s(s - M_q) \end{bmatrix} \begin{Bmatrix} u \\ w \\ \theta \end{Bmatrix} = \begin{Bmatrix} X_\delta \\ Z_\delta \\ M_\delta \end{Bmatrix} \delta \tag{37}$$

The X- and Z-equations are divided by the unit of linear acceleration,

$$\frac{1}{t_c^2} = \frac{g}{\mu} \tag{38}$$

and the M-equation by the unit of angular acceleration,

$$\frac{1}{t_c^2} = \frac{g}{\mu l} \tag{39}$$

With the nondimensional differential operator λ defined by

$$\lambda = \frac{d}{dt/t_c} = t_c s = \sqrt{\frac{\mu l}{g}}\, s \tag{40}$$

the nondimensional equations of motion become

$$\begin{bmatrix} \lambda - x_u & 0 & \mu \\ -z_u & \lambda - z_w & 0 \\ -\frac{m_u}{i_y} & 0 & \lambda\left(\lambda - \frac{m_q}{i_y}\right) \end{bmatrix} \begin{Bmatrix} \hat{u} \\ \hat{w} \\ \theta \end{Bmatrix} = \begin{Bmatrix} x_\delta \\ z_\delta \\ \frac{m_\delta}{i_y} \end{Bmatrix} \hat{\delta} \tag{41}$$

where

$$\begin{aligned} x_u &= \sqrt{\frac{\mu l}{g}}\, X_u & m_u &= i_y \sqrt{\frac{\mu l^3}{g}}\, M_u & \hat{u} &= \sqrt{\frac{\mu}{gl}}\, u & x_\delta &= \frac{X_\delta}{g} & \hat{\delta} &= \mu\delta \\ z_u &= \sqrt{\frac{\mu l}{g}}\, Z_u & m_q &= i_y \sqrt{\frac{\mu l}{g}}\, M_q & \hat{w} &= \sqrt{\frac{\mu}{gl}}\, w & z_\delta &= \frac{Z_\delta}{g} & & \\ z_w &= \sqrt{\frac{\mu l}{g}}\, Z_w & & & & & m_\delta &= i_y \frac{l M_\delta}{g} & & \end{aligned} \tag{42}$$

To show how the nondimensional forms are useful in expressing directly the effects of geometric parameters, radius of gyration, etc., consider the characteristic equation of the hovering oscillation. This can be expressed as

$$s(s - X_u)(s - M_q) + gM_u = 0 \qquad (43)$$

or, in nondimensional terms,

$$\lambda\left(\lambda - x_u\right)\left(\lambda - \frac{m_q}{i_y}\right) + \frac{\mu m_u}{i_y} = 0 \qquad (44)$$

Now conventional (Refs. 20–23) nondimensional derivatives can be expressed in terms of airplane geometry, at least for low Mach numbers. Similarly, we can express our nondimensional hover derivatives in terms of airplane geometry. In other words, just as C_{m_q} depends only on "what the vehicle looks like," so too the hover derivatives m_q, m_u, x_u, etc., are completely independent of vehicle size, disk loading,* mass, mass distribution, etc.

To illustrate the usefulness of Eq 44 we will consider two examples. First, we will examine the effects of changing vehicle size with μ and i_y held constant, i.e., m proportional to l^3 and radius of gyration proportional to l. Equation 44 is not changed so the nondimensional roots are not affected, but the time scale changes. Doubling the linear dimensions increases the weight by a factor of 8, doubles the disk loading, and increases the characteristic time by a factor of $\sqrt{2}$. Hence, the phugoid damping ratio is unchanged, but the frequency of the characteristic roots is reduced by a factor of $1/\sqrt{2}$.

As a second example let us consider the effects of changing mass at constant disk loading and i_y, i.e., m proportional to l^2, radius of gyration proportional to l, and μ proportional to l^{-1}. Now, doubling the linear dimensions will quadruple the mass, halve μ, and not change the characteristic time. The nondimensional roots are changed due to the halving of the $\mu m_u/i_y$ term in Eq 44. From the approximate factors of Appendix A

*Disk loading equals mg/A_e or $\rho g \mu l$.

or the numerical example of Section II, we see that this change will generally have little effect on the phugoid damping ratio, but will reduce the magnitudes of the dimensionless roots by roughly a factor of $2^{-1/3}$. Since the characteristic time is not changed, the actual values of the roots change proportionately to the dimensionless roots.

Whether the effects of changing vehicle size can best be analyzed by the nondimensional equations of Eq 44 or the material in the next subsection depends on which parameters are held constant. In general, it will probably be best to use both approaches to fully understand all the effects.

C. SIZE EFFECTS ON DIMENSIONAL HOVER DERIVATIVES

Another approach to size effects on handling qualities is to estimate the variations in the dimensional derivatives. These variations, considered in the light of the analyses of Section II, can then provide some insight into the effects of size. An important point is what type of weight variations with size to use. A realistic weight variation with size seems to be somewhere between constant disk loading (m proportional to l^2) and constant aircraft density, μ, (m proportional to l^3). Accordingly, both cases will be considered below.

The variation of several parameters with weight were determined from relationships of the previous subsection. For the moment derivatives the additional assumption of constant i_y was made. The results are given in Table IX.

TABLE IX

PARAMETER VARIATIONS WITH WEIGHT

PARAMETER	EXPONENT*	
	Constant Disk Loading	Constant μ
l	1/2	1/3
Disk loading.....	0	1/3
μ	-1/2	0
X_u or Z_w	0	-1/6
M_u	-1/2	-1/2
M_q	0	-1/6
$X_{\delta_e}/M_{\delta_e}$	1/2	1/3

*Parameter proportional to (weight)$^{\text{exponent}}$

The derivatives X_u, Z_w, and M_q are relatively unaffected by size, while M_u is inversely proportional to the square root of weight in both cases. Thus, from the Section II analyses we know that large vehicles will have smaller attitude responses to horizontal gusts and will require much less control power for hovering in gusty air. With a reduced M_u it seems that larger vehicles may have a lower pitch damping requirement because, as shown in Section II, M_u and M_q effects are somewhat canceling as regards gust responses. This argument is somewhat offset by the necessary increase in pilot lead in the $\theta \rightarrow \delta_e$ loop as M_q is reduced.

As M_u becomes very small, the pitch response of the airplane can be approximated by

$$\frac{\theta}{\delta_e} \doteq \frac{M_{\delta_e}}{s(s - M_q)} \tag{45}$$

This is the transfer function form analyzed in Ref. 7 and discussed in Subsection A above, where the conclusion was reached that the minimum damping for satisfactory pilot rating is approximately 0.8 sec^{-1}. This suggests that the requirements for damping as a function of size (e.g., Ref. 24) should have an absolute lower limit for normal operation on the order of 0.8 sec^{-1}. In other words, the required damping for normal operation might decrease with increasing size only until the absolute limit is reached.

Another parameter variation worth noting is the significant increase of $X_{\delta_e}/M_{\delta_e}$ with increasing size. Although $X_{\delta_e}/M_{\delta_e}$ is not big enough on current vehicles to offer any important benefits, future very large vehicles, which use cyclic pitch to provide pitching moments in hover, may have values of $X_{\delta_e}/M_{\delta_e}$ large enough to significantly improve their ability to hover over a spot. The large $X_{\delta_e}/M_{\delta_e}$ will not affect pitch control ($\theta \rightarrow \delta_e$ loop) as the product $M_u X_{\delta_e}/M_{\delta_e}$ does not increase appreciably with size.

D. GEOMETRY EFFECTS ON DIMENSIONAL HOVER DERIVATIVES

The approximate expressions for dimensional hover derivatives given in Appendix B indicate one geometric parameter of particular significance.

For ducted-fan vehicles M_u is proportional to the height of the duct lip above the vehicle c.g., h_D. For configurations such as the Doak VZ-4, in which the ducts are located close to the pitching axis (in plan view), the dominant M_q contribution is due to the change of momentum at the duct inlets and is proportional to h_D^2. Thus, the pitch damping can be increased by raising the duct positions, but there will be an attendant increase in M_u and a corresponding increased gust response and increased pitch trim moment at forward speeds. Since the damping increases as h_D^2 and M_u varies only linearly with h_D, there may be situations where raising the ducts gives an over-all improvement in handling qualities.

E. SUMMARY

Control power requirements are set by a number of factors, such as maintaining attitude in gusty air. Section II showed that the control power required to hover in gusty air is nearly proportional to M_u. This section indicates that M_u is roughly inversely proportional to the square root of vehicle weight; therefore the required control power for this one factor should also vary inversely with the square root of weight.

The variation of required control power with size in Ref. 24 is slightly slower than the analytical variation; the specification requirement is inversely proportional to the cube root of vehicle weight plus 1000 lb. This slower variation is quite compatible with the analytic results when the other factors in the control power requirements are considered. For example, the control power to perform the maneuvers associated with the vehicle's mission appears to be independent of size or geometry.

The variation in M_u also supports the lowering of pitch damping requirements with increasing size, as M_u and M_q effects are somewhat canceling in regard to gust responses. There should, however, be an absolute lower limit on pitching damping independent of size. For normal operation this limit should be on the order of 0.8 sec^{-1}.

For ducted-propeller vehicles the most significant geometric parameter is the height of the duct lips above the center of gravity, h_D, as M_u is directly proportional to h_D. Reductions in M_u by decreasing h_D are at

least partially offset by decreases in pitch damping. Whether the changes in M_q are significant or not depends on other geometric parameters, such as the number and locations of the ducts.

SECTION IV

TRANSITION

A. ANALYSIS METHOD

To understand piloting techniques during V/STOL transitions let us first consider how this maneuver might be performed with an ideal programmed controller in the absence of any external disturbances. If the complete time histories of the vehicle motions during transition were specified, the control deflections required could be determined and programmed into an ideal controller. Since an ideal controller could perfectly duplicate these control motions, henceforth referred to as trim deflections, it could perform the desired transition without any feedbacks.

When a pilot first performs transitions in a new vehicle, his control will be entirely closed-loop unless he has some prior information on the transition behavior of the aircraft. He will try various transition techniques to find the one that is easiest. His selection of what he considers to be the best technique will be influenced by the trim deflections required. After the pilot has selected the best technique, he can make some open-loop or precognitive control inputs for trim, but must also exercise closed-loop control because he cannot perfectly match the trim deflections and because of external disturbances, such as gusts.

From the above it should be clear that the trim deflections are an important handling qualities factor. Simple, easily repeated trim deflection time histories are desirable, while complicated ones with rapid changes are bad because more pilot effort is required and the disturbances introduced by the pilot's not matching the trim deflections will be larger.

The other important factor is the vehicle dynamic characteristics when perturbed from the trim conditions. Control of these perturbations in a closed-loop fashion may be an easy or a difficult task for the pilot.

Both the trim and the perturbation problems will be considered here. The major emphasis in the analyses will be on determining

1. The differences in the trim and perturbation problems between accelerating (takeoff), constant velocity, and decelerating (landing) flight conditions
2. The effects on the perturbation problem of the time-varying dynamics caused by the changing trim conditions in landing or takeoff

To obtain a preliminary evaluation of both problems — trim and perturbations about trim — the transition characteristics of two aircraft simulated in Ref. 4 were studied. The two aircraft were the Bell D-2064 (Fig. 14) and a scaled-up version of the Kaman K-16B tilt wing (Fig. 15). The primary reason for studying simulator rather than flight tests is that the simulated aerodynamic characteristics are known exactly, whereas the actual flight characteristics may be uncertain. Although Ref. 4 was the best simulator data available at the time, it has two shortcomings: no gust inputs were included and only the longitudinal dynamics were simulated (the pilot did not have to divert any of his attention to lateral control and could concentrate on the longitudinal task). Nevertheless, it was felt that a handling qualities analysis of these simulated transitions could provide at least a preliminary indication of the possible longitudinal problems.

The analysis for each airplane began with a calculation of the trim time histories for landing and takeoff, as well as the trim for constant speed flight. For each condition there are an infinity of possible trim variations. The trim time histories for the analysis were computed on the basis of the gross flight path features (e.g., constant altitude, deceleration, etc.) used in Ref. 4 and on an estimation of the easiest way to make the transitions.

The study of the dynamics of perturbations about the trim conditions was based on the frozen system concept. In this approach the conventional linearized equations of motion are used with the coefficients assumed constant but evaluated at various times or trim conditions. Although this method is not mathematically rigorous, it is a commonly used technique and a more exact, usable method does not currently exist.

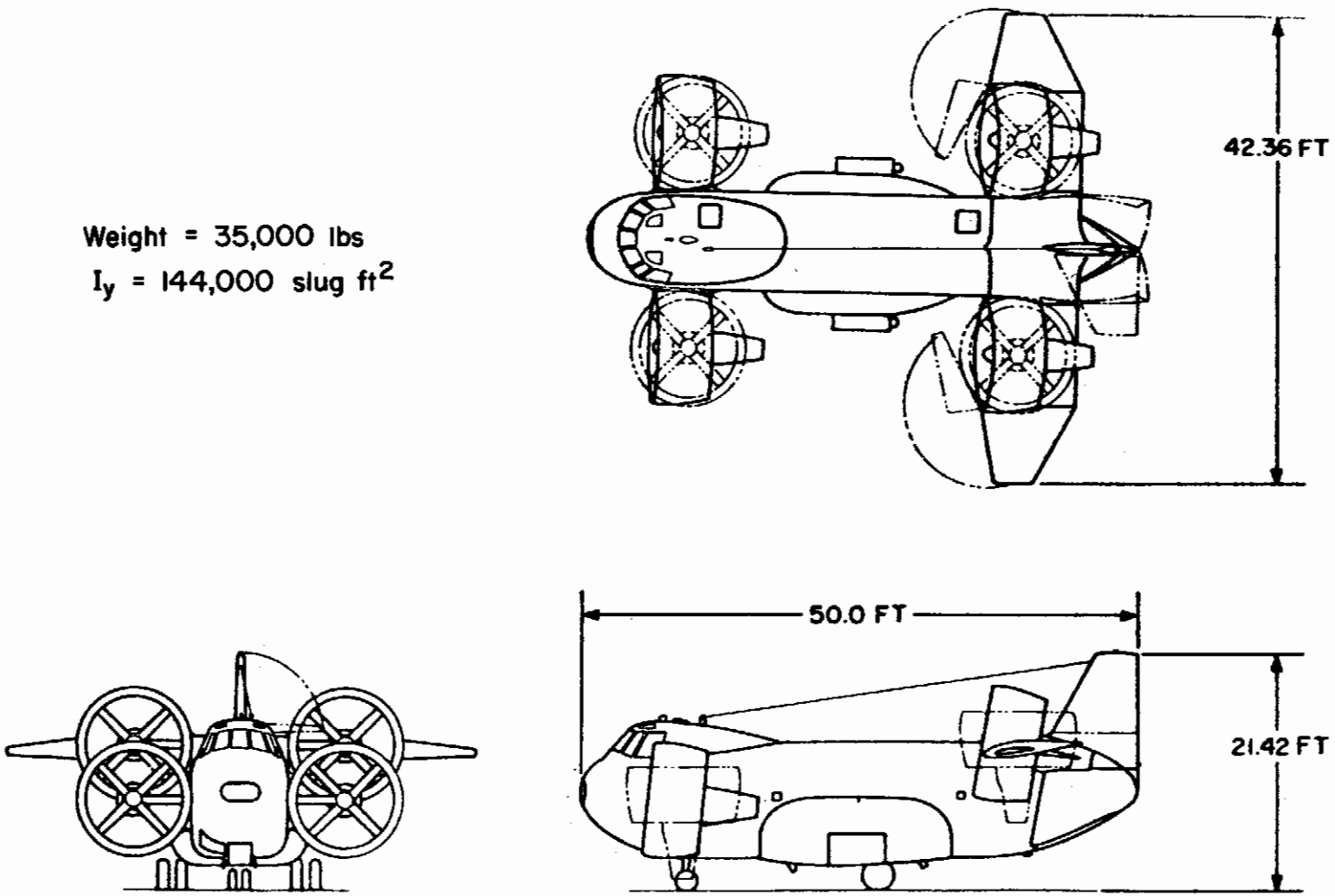

Figure 14. Bell D-2064 Tilt Duct

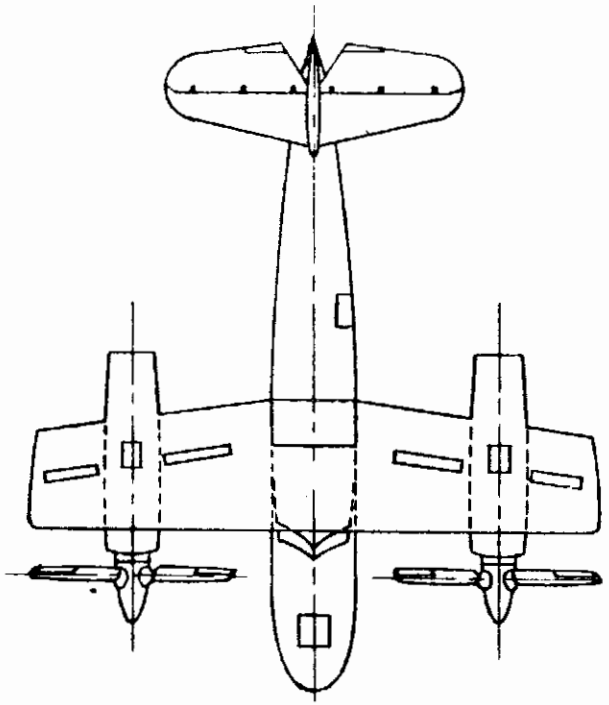

Weight = 35,000 lbs

I_y = 76,000 slug ft^2

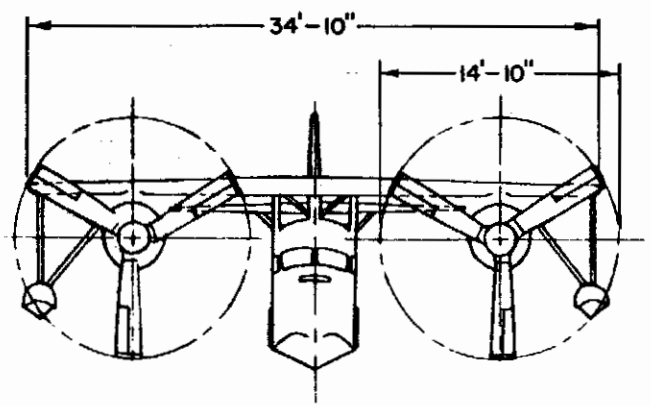

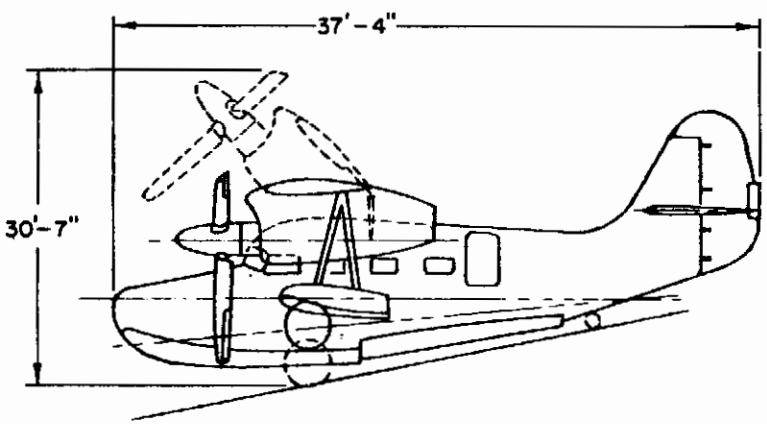

Figure 15. Tilt-Wing Configuration

Furthermore, if the key parameters are only slowly time-varying with respect to the characteristic frequencies, then the frozen system analysis is essentially correct (Ref. 28). Fortunately, this occurred in the cases of interest here, so the results presented in the remainder of this section may be regarded with confidence.

The (perturbed) transfer functions for both aircraft were calculated for nine flight conditions (three velocities for accelerating, constant speed, and decelerating flight), based on stability derivatives computed from the formulas of Ref. 4. The next step was to examine the variations in the pilot's "frozen" attitude stabilization task as a function of velocity and acceleration. This gave a set of nominal pilot closures for the $\theta \rightarrow \delta_e$ loop. These closures were then used as inner loops in an investigation of the altitude control task.

B. TILT-DUCT AIRCRAFT

A trim time history for a takeoff (accelerating) transition is shown in Fig. 16. (The minimum simulator speed was approximately 20 knots.) This is a constant altitude acceleration at the maximum value used in the simulation, 0.4g. The trim requirements of this case are particularly simple:

1. Constant attitude
2. Constant throttle setting
3. Constant duct rotation rate
4. Elevator deflections between 16 and 41 percent* of maximum available

A trim time history for a landing (decelerating) transition is shown in Fig. 17. The trim requirements are much more severe than for takeoff because of:

1. Large throttle movements
2. Larger duct rotations
3. Elevator deflections between 29 and 64 percent of maximum

*Elevator control power was varied during the simulator study. The numbers used here are based on the basic airplane values.

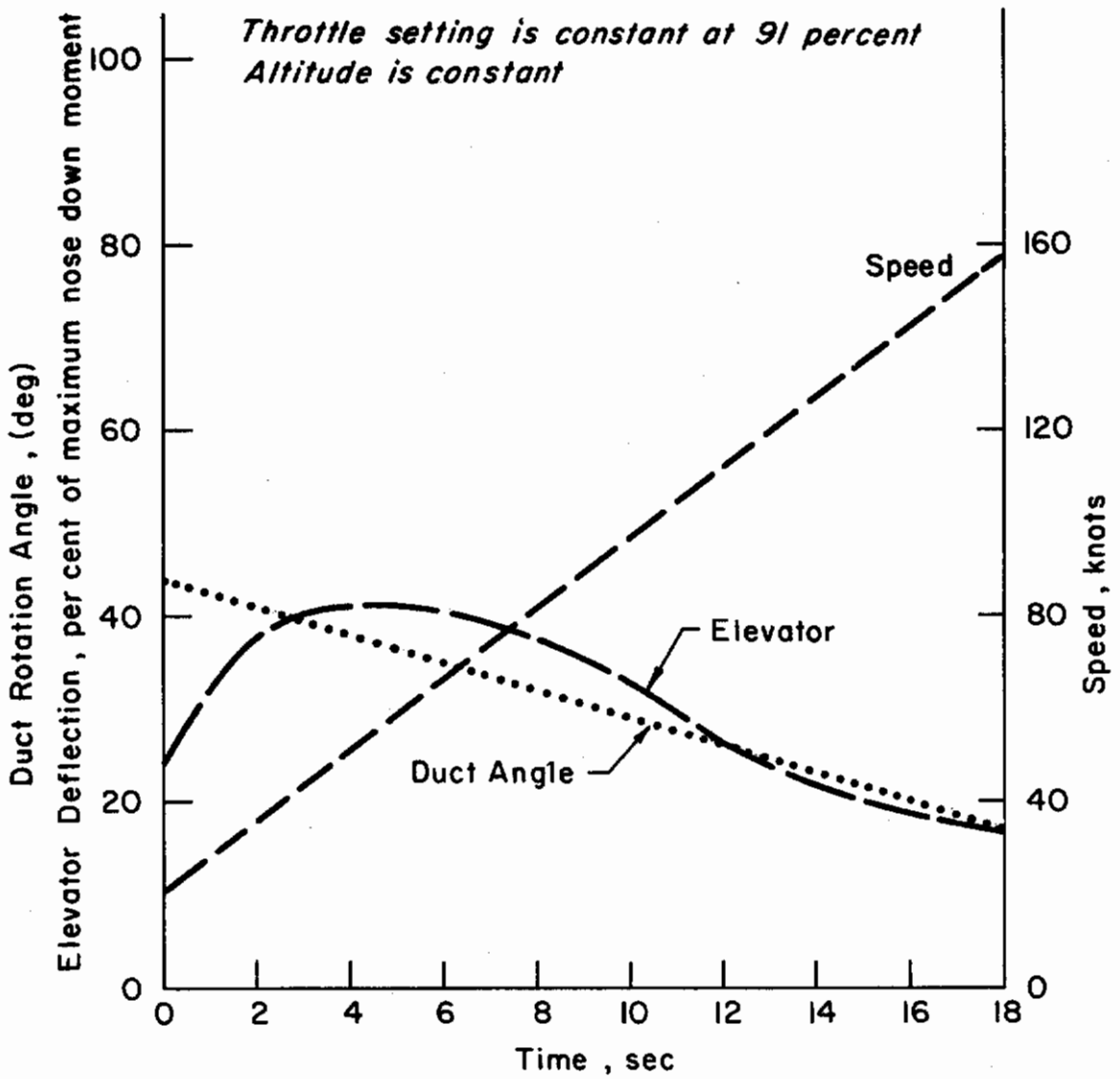

Figure 16. Tilt-Duct Trim, Takeoff

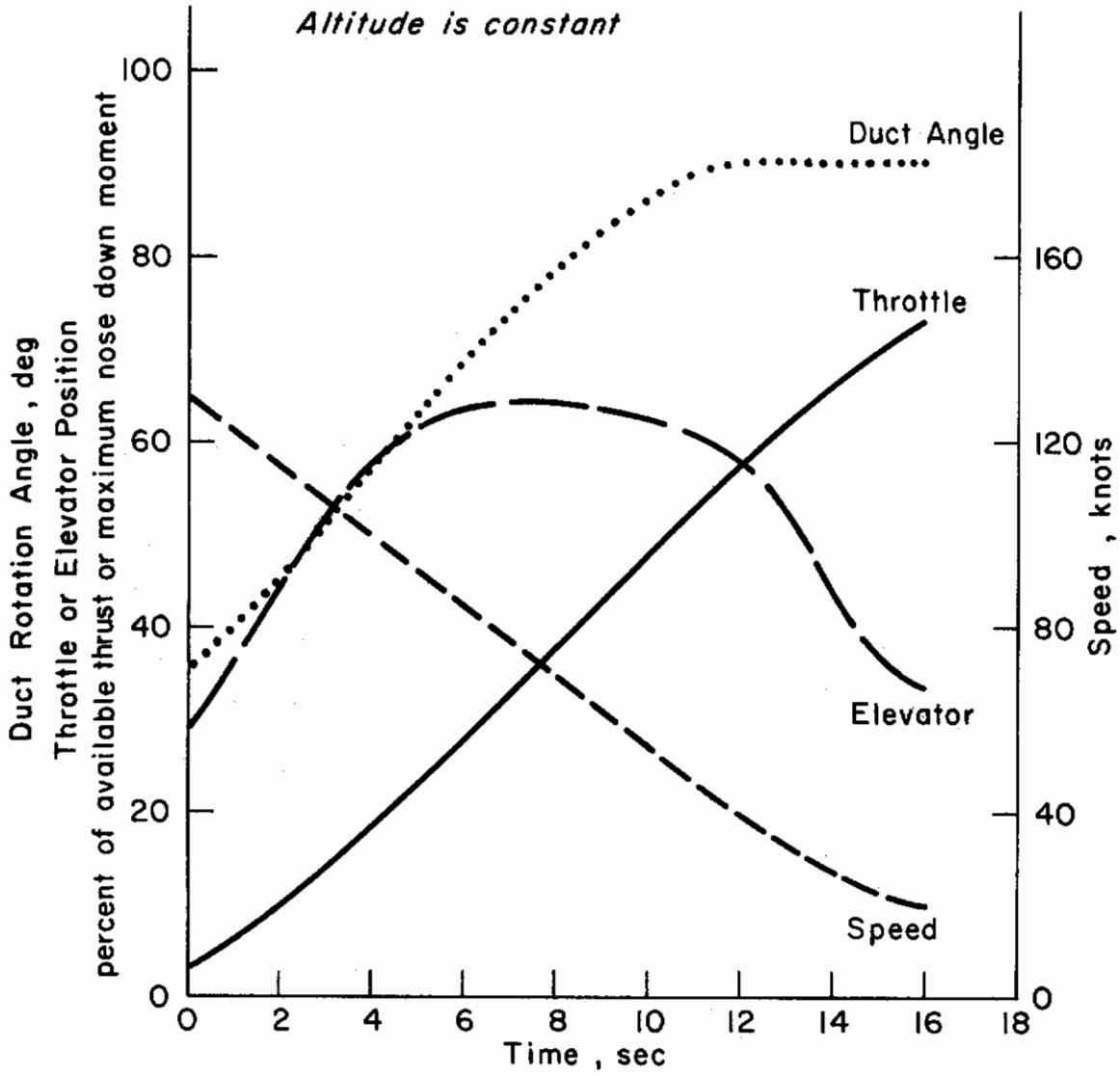

Figure 17. Tilt-Duct Trim, Landing

As noted in Ref. 4, the larger elevator deflections during landing are due to the increased nose-up moment on the ducts. For a given speed the duct angle of attack is larger in landing (decelerating) than takeoff (accelerating) transitions.

Whereas the trim task for takeoff is quite easy, the pilot has his hands full during landing. He has to use large throttle and elevator motions, as well as large and rapid duct rotations. Furthermore, although not revealed in the comparisons cited above, the terminal control aspects of landing demand more precision than do the essentially free end conditions of takeoff.

Turning now to the question of controlling the perturbed motions about the trim point, three speeds — 30, 80, and 130 knots — were selected for the computation of "frozen" transfer functions. For the accelerating and decelerating cases the trim angle of attack, duct angle, throttle setting, and elevator deflection are those given in Figs. 16 and 17. For the zero acceleration cases the trim conditions corresponding to level flight at zero angle of attack were used.

The basic damping of the airplane was so low ($M_q = -0.17$ sec^{-1} at hover) that it was rated unacceptable. Consequently, the simulated augmented damping which gave an M_q of -1.5 at hover was used in the analysis. This improved pilot ratings into the unsatisfactory but acceptable category. It was felt that with higher or lower damping the pilot's task might be so easy or so difficult as to mask the effects of variations in velocity and acceleration.

A detailed analysis was made of pilot closure of the $\theta \rightarrow \delta_e$ loop for seven of nine flight conditions. It was found that in all cases the pilot could, by using a lead of only 0.5 sec, obtain a crossover frequency of approximately 2 rad/sec with a phase margin of 45 deg and more than 10 db gain margin. Three sample closures are shown in Fig. 18. In all cases the only differences occur at low frequency and in the region of crossover they are nearly identical; consequently, the closed-loop characteristics are nearly the same. The net conclusion is that neither velocity nor acceleration has an appreciable effect on pilot closure of the θ-loop.

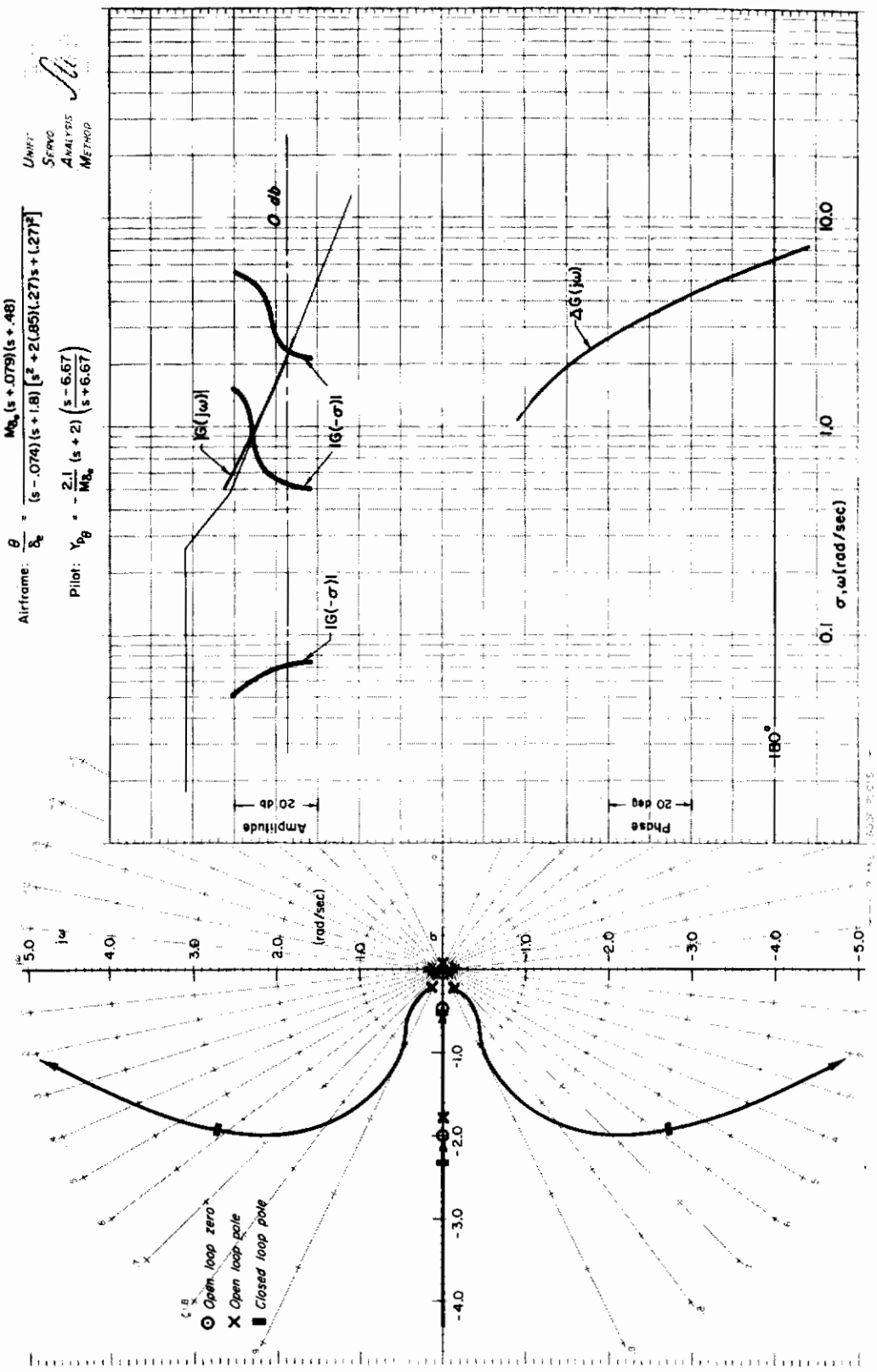

(a) V = 30 Kt, $\dot{V} = -0.3g$

Figure 18. $\theta \rightarrow \delta_e$ Closure for Tilt Duct

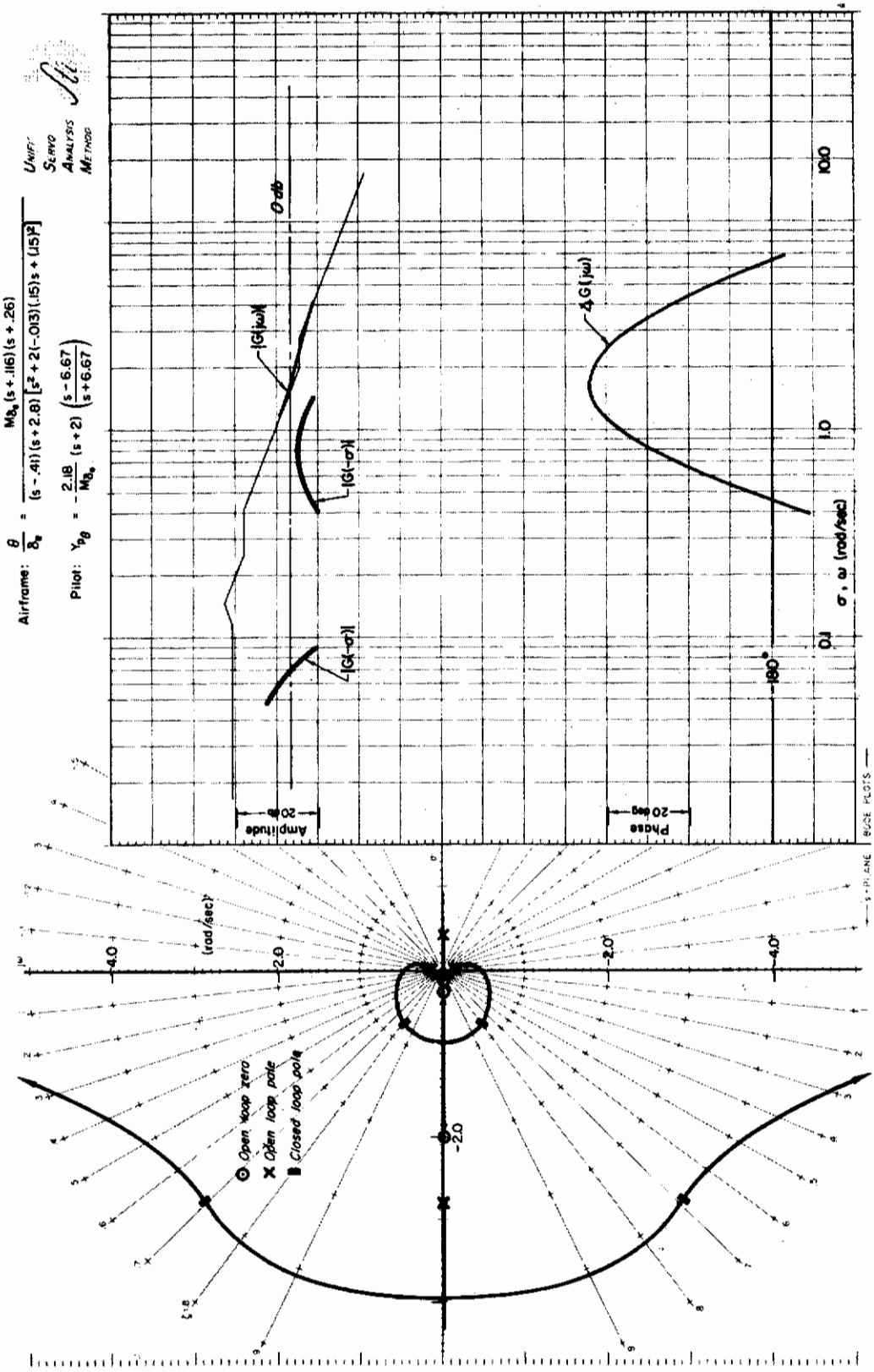

(b) V = 130 Kt, $\dot{V}$ = −0.4g

Figure 18 (Continued)

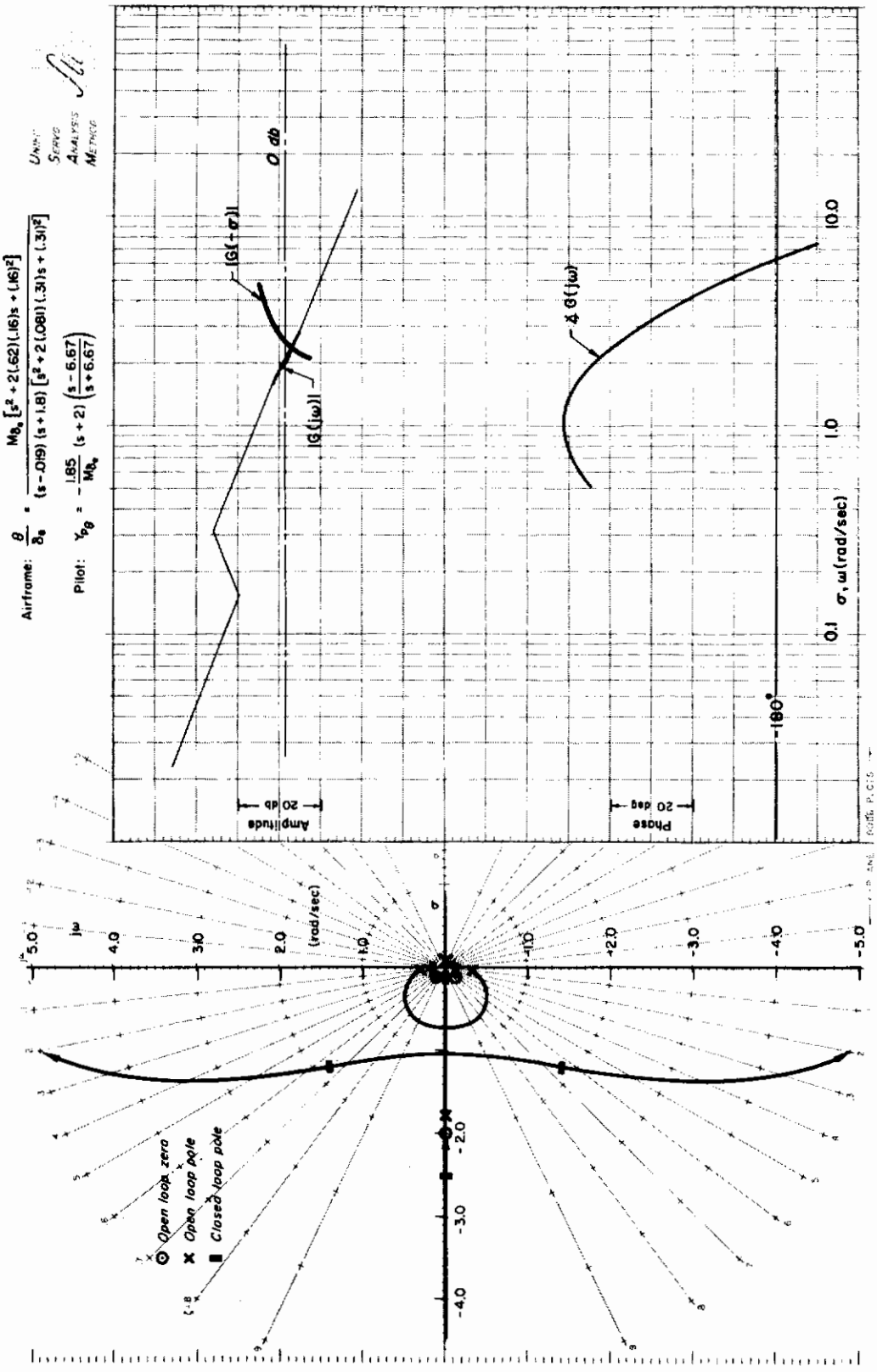

(a) V = 30 Kt, $\dot{V}$ = 0.4g

Figure 18 (Concluded)

The next phase of the analysis was a study of the altitude control task with the previously described $\theta \rightarrow \delta_e$ inner loops closed. The major portion of the analysis was devoted to altitude control with the throttle, because the altitude response to elevator is very poor at slow speeds. However, at high speeds, when the aircraft behaves like a conventional airplane, the pilot can effectively use the elevator for altitude control. Nevertheless, arguing that it would be preferable to use the same control technique throughout the transition, the variations of the $h \rightarrow \delta_T$ closure were studied over the entire speed and acceleration spectrum.

Closure criteria for flight path control loops (which are invariably limited to lower bandwidth) are not as well defined as those for attitude loops; however, prior handling qualities studies of path control during landing approach, Refs. 5 and 6, indicate that bandwidths on the order of 0.3 rad/sec are acceptable. It was therefore decided to use closure criteria of 45 deg phase margin for a crossover frequency of roughly 0.3 rad/sec.

Examination of the closures for seven of the nine combinations of speed and acceleration showed that the pilot lead required to meet the closure criteria increased with increased speed or acceleration. Sample closures are shown in Fig. 19* and Table X summarizes the important closure parameters. It was found that the speed and acceleration effects can be explained by considering their influence on the parameter $\left[-Z_w - (X_{\delta_T}/Z_{\delta_T})Z_u\right]$.

This parameter is a measure of the bandwidth available without pilot lead. That is, zero damping frequency for a closure without lead is approximated by (see Appendix C for derivation)

$$\omega_o \doteq \sqrt{\left(-Z_w - \frac{X_{\delta_T}}{Z_{\delta_T}} Z_u\right) \frac{1}{\tau_{eff}}} \qquad (46)$$

where τ_{eff} = effective lag (pilot lag plus any thrust lags)

*These closures include a first-order thrust lag of 0.2 sec as used in the simulator. Canceling high frequency poles-zeros are not indicated.

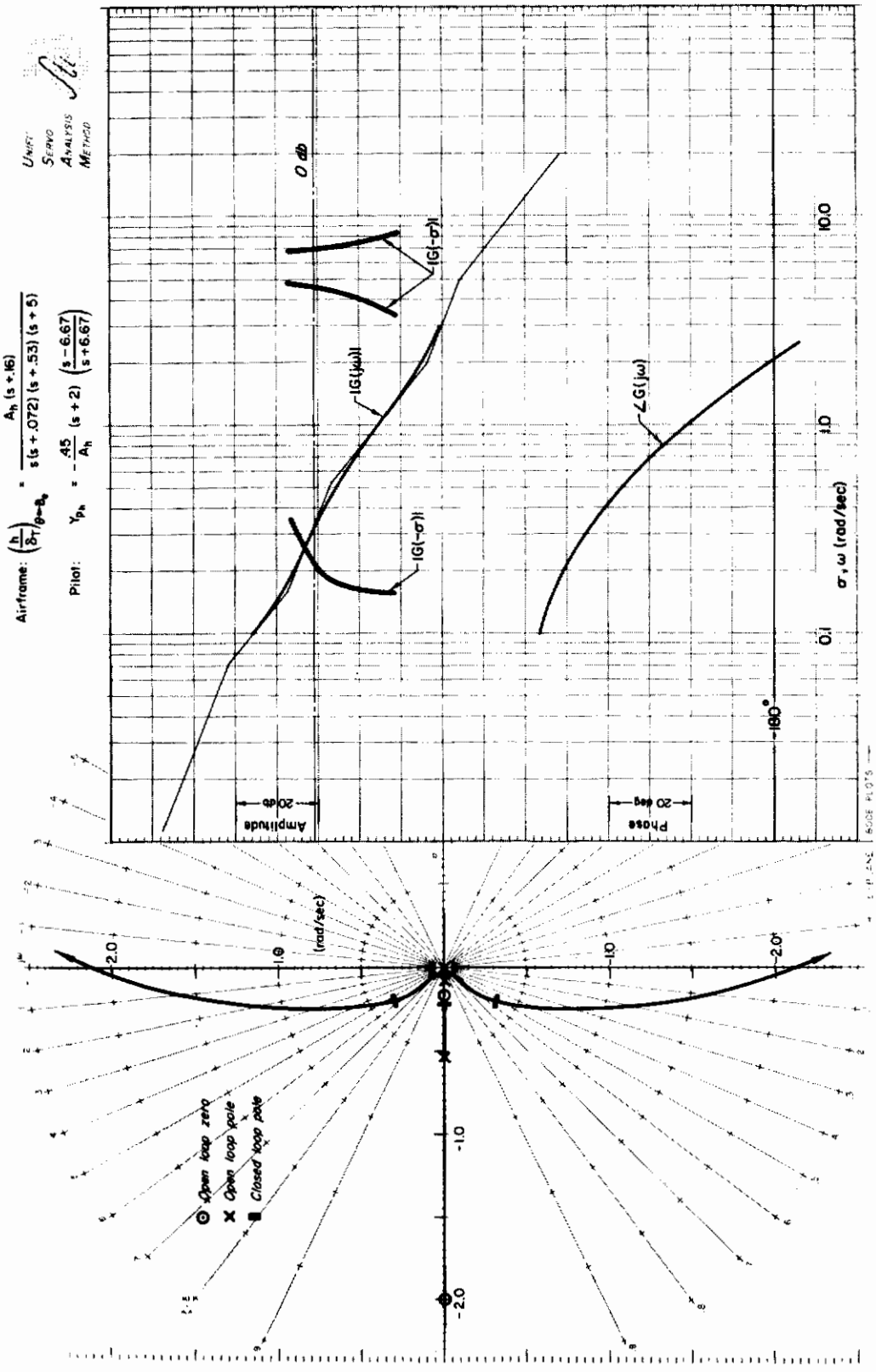

(a) V = 30 Kt, $\dot{V}$ = −0.3g

Figure 19. h ⟶ δ_T Closure for Tilt Duct

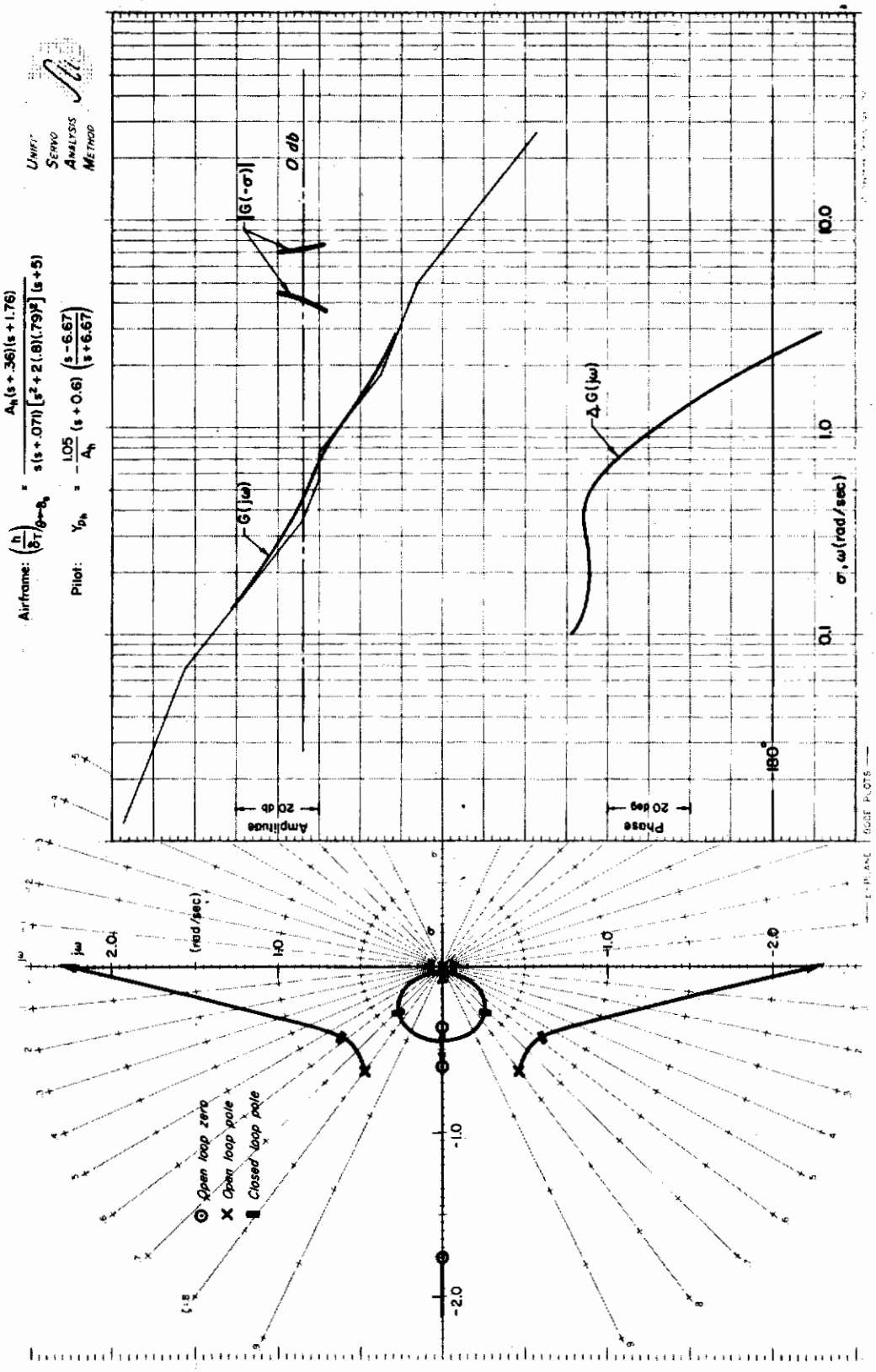

(b) V = 130 Kt, $\dot{V}$ = −0.4g

Figure 19 (Continued)

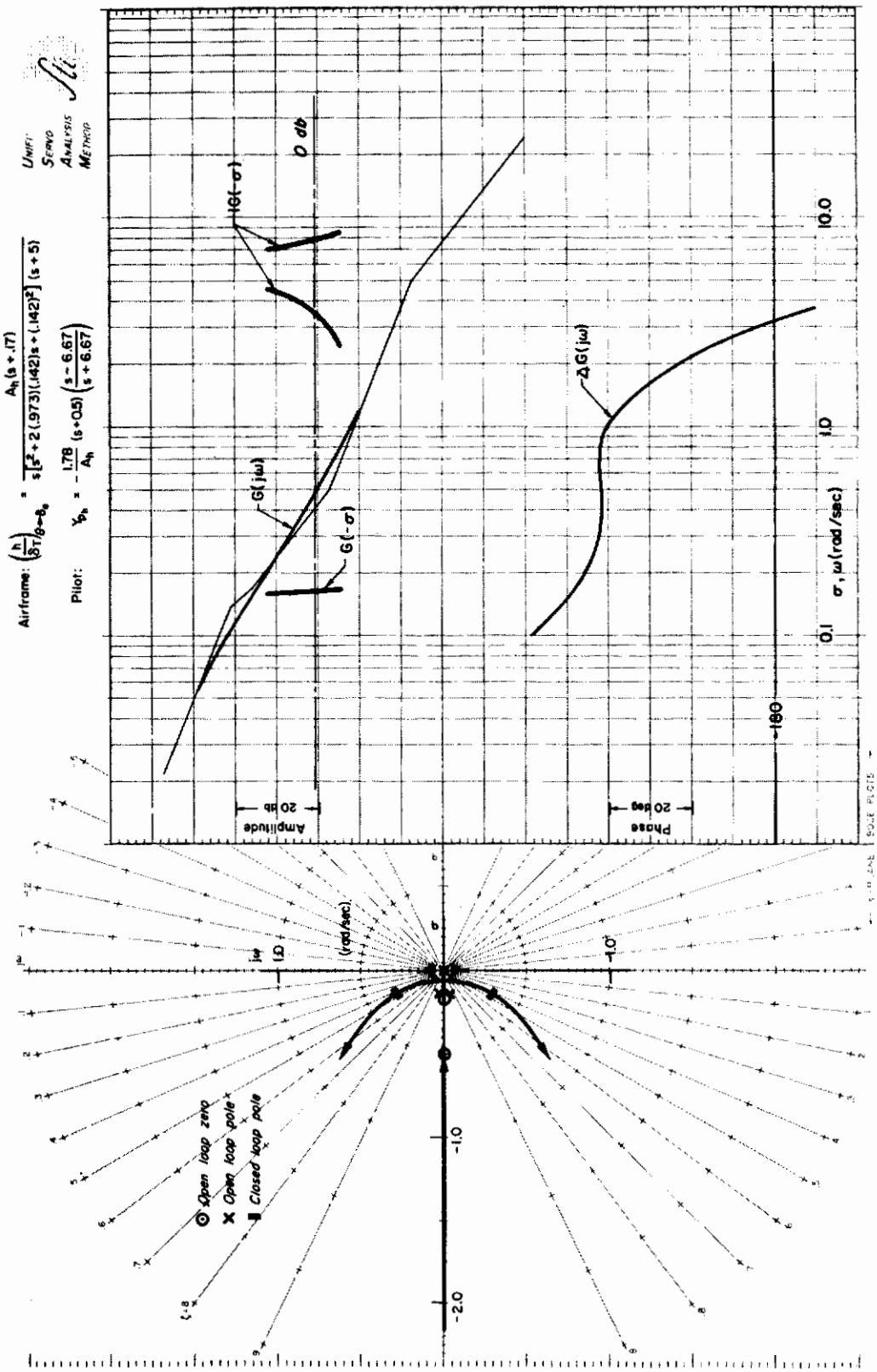

(c) V = 30 Kt, $\dot{V}$ = 0.4g

Figure 19 (Concluded)

TABLE X

SUMMARY OF h → δ_T CLOSURE PARAMETERS FOR TILT DUCT

VELOCITY	ACCELERATION	PILOT D.C. GAIN	PILOT LEAD	CROSSOVER FREQUENCY	GAIN MARGIN
knots		lb/ft	sec	rad/sec	db
30	+	970	2.0	0.50*	20
30	0	760	1.0	0.32	26
30	−	980	0.5	0.32	25
80	0	500	1.0	0.26	30
80	−	710	0.5	0.30	23
130	0	840	2.0	0.42*	21
130	−	1060	1.7	0.50*	19

*These crossover frequencies are unusually large because the phase margin is very flat between frequencies of 0.2 and 0.5 rad/sec.

The parameter ω_o is indicative of how well the pilot can do without lead or, conversely, the amount of lead he must use to obtain a given bandwidth. Table XI compares the ω_o predicted by Eq 46 with the actual values obtained from closures without pilot lead.

Table XI shows that with the simulated dynamics the primary effect of increasing acceleration is to lower the vertical damping ($-Z_w$ decreases) as the ducts are rotated down. In real flight there would also be an additional detrimental effect from the increase in $-X_{\delta_T}/Z_{\delta_T}$ with acceleration due to decreased duct angles, which was not simulated. However, the major effect of increasing speed for the simulated dynamics is the increase in $-X_{\delta_T}/Z_{\delta_T}$. (The lift and drag increments due to throttle deflection were assumed to be functions of speed only.)

TABLE XI

$h \rightarrow \delta_T$ METRIC FOR TILT DUCT

VELOCITY	ACCELERATION	$-Z_w$	$-\frac{X_{\delta_T}}{Z_{\delta_T}}$	$-Z_u$	PREDICTED* ω_o	ACTUAL ω_o
knots		sec^{-1}		sec^{-1}	rad/sec	rad/sec
30	+	0.0728	0.1148	0.134	0.34	0.47
30	0	0.274	0.1148	0.166	0.71	0.72
30	−	0.417	0.1148	0.160	0.89	0.88
80	+	0.210	0.531	0.198	0.46	NA
80	0	0.259	0.531	0.202	0.55	0.65
80	−	0.307	0.531	0.170	0.66	0.77
130	+	0.229	1.115	0.260	IM	NA
130	0	0.265	1.115	0.267	IM	0.47
130	−	0.299	1.115	0.272	IM	0.55

*Predicted ω_o from Eq 45 with τ_{eff} = 0.5 sec, 0.3 from pilot, and 0.2 from thrust lag

IM Predicted ω_o imaginary because $-Z_w - (X_{\delta_T}/Z_{\delta_T})Z_u < 0$

NA Not available

The physical importance of Z_w is clear; it supplies the vertical damping. The detrimental effects of the $(X_{\delta_T}/Z_{\delta_T})Z_u$ term can be explained as follows. Increasing the thrust to increase altitude provides a vertical acceleration through the Z_{δ_T} term and a forward acceleration through X_{δ_T}. The forward acceleration increases forward speed and produces an additional altitude acceleration through the Z_u term; however, this latter acceleration lags the initial thrust acceleration (by one integration) and is therefore a destabilizing influence.

It may appear that the above analysis concludes that the takeoff task is more difficult than landing—a conclusion contrary to all previous

studies in this area. Actually, the analysis merely shows that it is harder (requires more lead) for the pilot to maintain a given bandwidth in his h → δ_T closure during takeoff than landing. This factor is more than offset by two important additional considerations:

1. The altitude control requirements during takeoff are less stringent than during landing, so that a smaller bandwidth and less precision are acceptable.
2. The trim task is much more difficult during landing than takeoff.

The proper conclusion to be drawn from the above analysis is that the key problem in landing is not that the control of perturbations about trim is any more difficult than for takeoff, but that the trim task becomes more difficult and more precise control is required.

The analysis also shows that the h → δ_T task becomes more difficult as speed increases. However, at higher speeds altitude control requirements are generally less stringent and, also, the pilot has the option of switching to altitude control with elevator. A sample closure for the latter technique was made for a speed of 130 knots and zero acceleration. It was found that a crossover of 0.38 rad/sec could be obtained without any pilot lead, but that a low frequency instability would result because the airplane is still on the backside of the drag curve.* For the constant-velocity case this mode is easily stabilized with a low frequency airspeed-to-throttle closure. For accelerating or decelerating flight the existence of this instability is questionable because the frozen system technique is not applicable for the very low frequency modes; even if this instability exists, it is of too low a frequency to be of concern.

C. TILT-WING AIRCRAFT

In Ref. 4 two tilt-wing aircraft with deflected slipstreams were studied. These were identical except that pitch control in one was obtained with cyclic propeller pitch and in the other by using a tail fan. At the basic value of M_u it was found that there was no essential

*A nose-up elevator deflection gives a steady state descent.

difference between these two aircraft, and cyclic pitch control was arbitrarily chosen for the handling qualities study of this report.

A trim time history for takeoff transition is shown in Fig. 20. To provide a 30 percent control margin, and to allow for the control of possible dynamic variations, the acceleration must be less than the 0.4g used for the tilt-duct configuration. The trim conditions for this case are

1. Constant attitude
2. Acceleration between 0.04g and 0.14g
3. Constant throttle setting
4. Wing tilt angles between 2 and 42 deg (the tilt rate is higher at low speeds)
5. Elevator deflections between 45 and 69 percent of maximum available

A trim time history for landing is shown in Fig. 21. As with the tilt-duct vehicle, the trim requirements are more severe for landing than for takeoff. For the tilt wing the extra difficulties in landing are due to

1. Large throttle movements
2. Larger elevator deflections (the elevator deflection varies between 15 and 49 percent)

The foregoing indicates that for this tilt-wing vehicle in both landing and takeoff the pilot must make large variations in elevator and rotate the wings through large angles. The principal differences between landing and takeoff control techniques are the large throttle variations and elevator motions required in landing.

The pilot's attitude stabilization task was studied for "frozen" velocities of 30, 65, and 100 knots. The trim characteristics for accelerating and decelerating flight were the same as those given in Figs. 20 and 21. For constant speed cases the trim conditions corresponding to level flight at zero angle of attack were used.

As in the case of the tilt-duct aircraft, the augmented damping which gave an M_q of -1.5 at hover was used. This gave pilot ratings in the unsatisfactory but acceptable category.

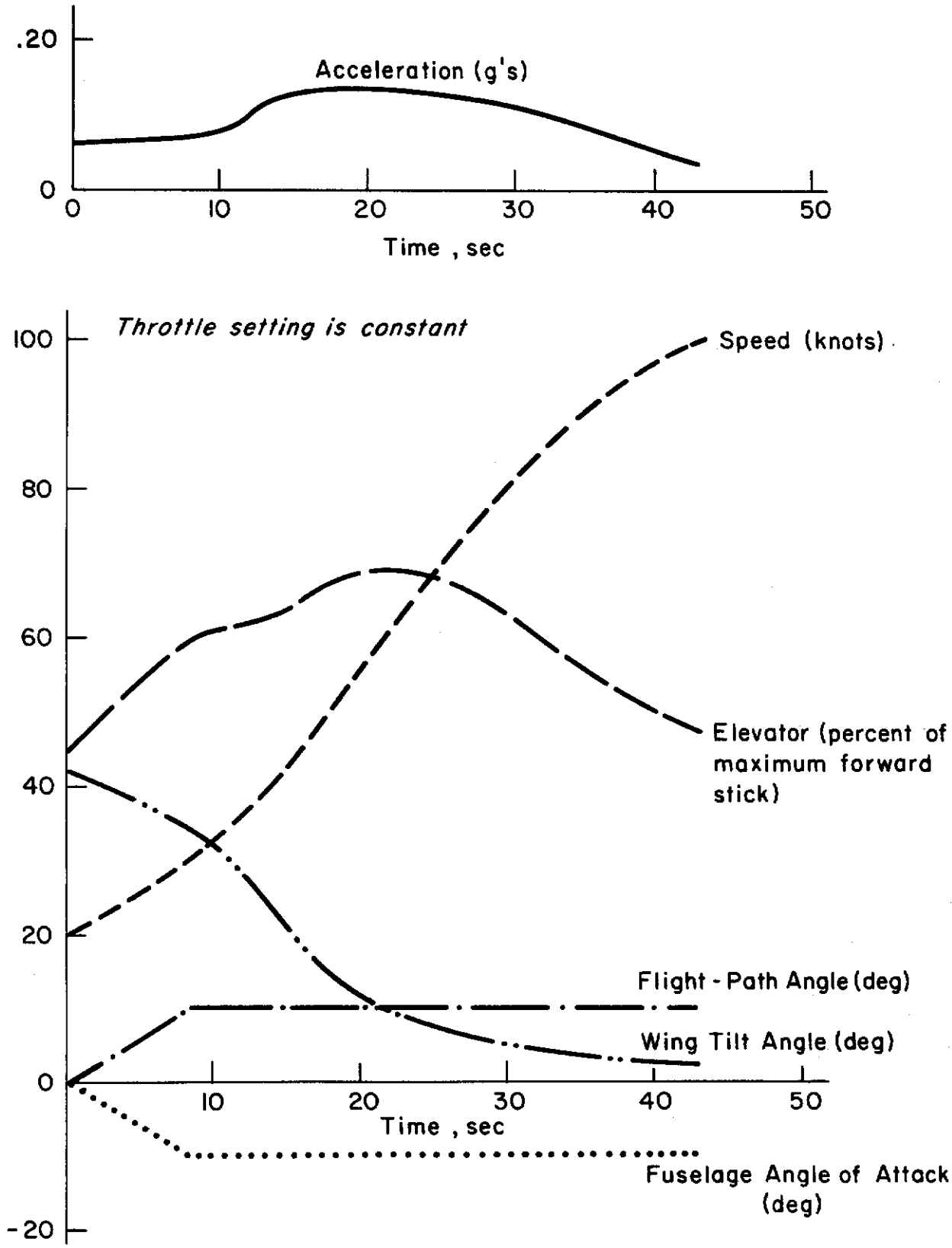

Figure 20. Tilt-Wing Trim, Takeoff

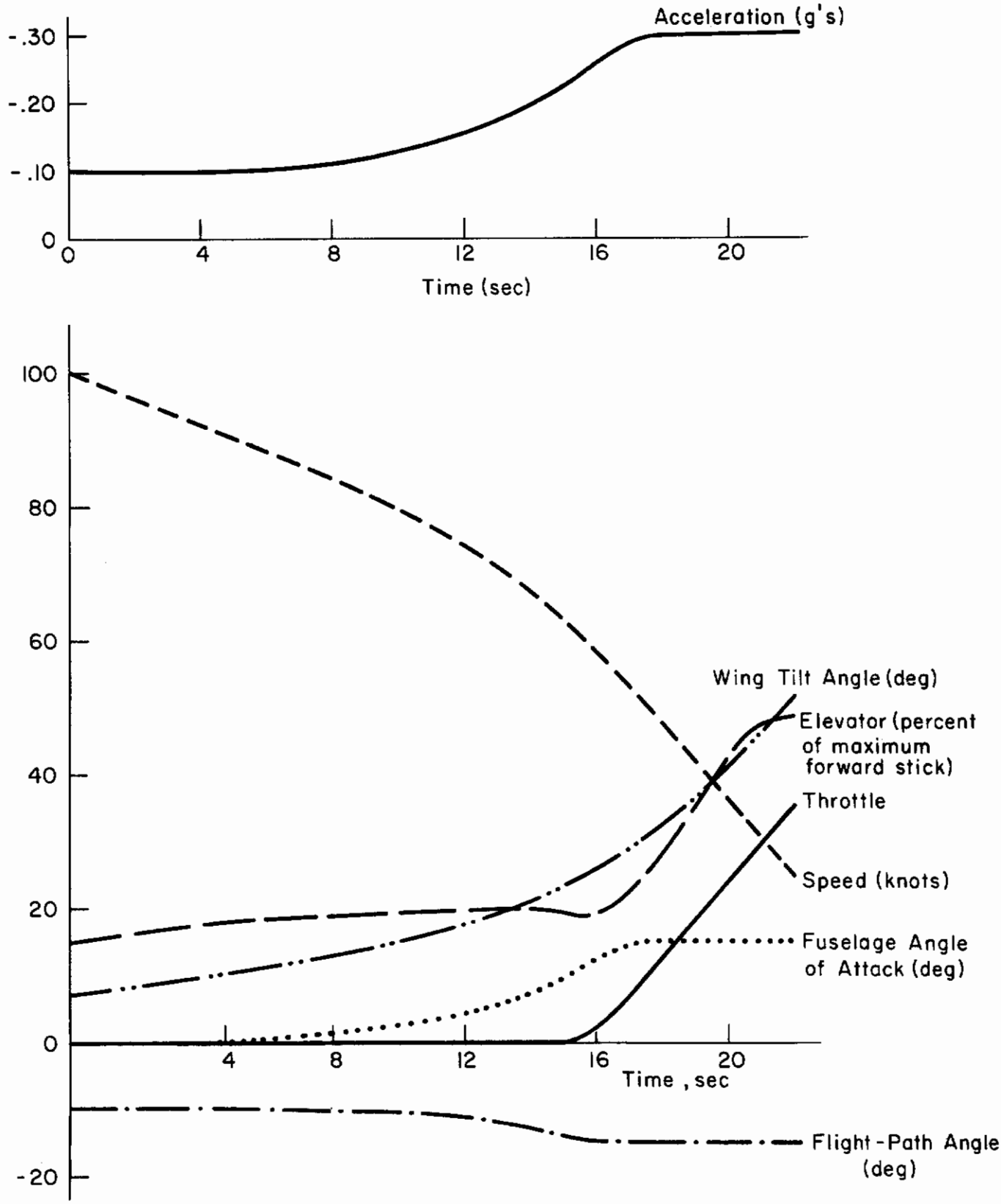

Figure 21. Tilt-Wing Trim, Landing

A detailed analysis was made of pilot closure of the $\theta \rightarrow \delta_e$ loop for seven out of the nine combinations of acceleration and velocity. It was found that in all cases the pilot could, by using small leads in the range of 0.5 to 0.25 sec, obtain a crossover frequency of approximately 2 rad/sec with a phase margin of 45 deg and a gain margin of more than 9 db. Three sample closures are shown in Fig. 22. As in the case of the ducted vehicle, the Bode plots are nearly identical in the region of crossover; the principal differences occur at low frequencies. Consequently, the closed-loop characteristics are nearly identical. The net conclusion for the tilt wing is that neither velocity nor acceleration has an appreciable effect on pilot closure of the attitude loop.

Detailed analyses of pilot control of altitude with throttle with the $\theta \rightarrow \delta_e$ inner loop closed showed that in all cases the pilot, without using any lead, could obtain a crossover frequency of approximately 0.35 rad/sec with phase and gain margins, respectively, of 45 deg and more than 10 db. Three sample closures are shown in Fig. 23 and key parameters are summarized in Table XII.

TABLE XII

SUMMARY OF $h \rightarrow \delta_T$ CLOSURE PARAMETERS FOR TILT WING

VELOCITY	ACCELERATION	PILOT GAIN	CROSSOVER FREQUENCY	GAIN MARGIN
knots		lb/ft	rad/sec	db
30	+	130	0.31	13
30	0	190	0.35	13
30	-	370	0.45	12
65	0	140	0.41	10
65	-	130	0.40	10
100	0	64	0.37	12
100	-	77	0.39	11

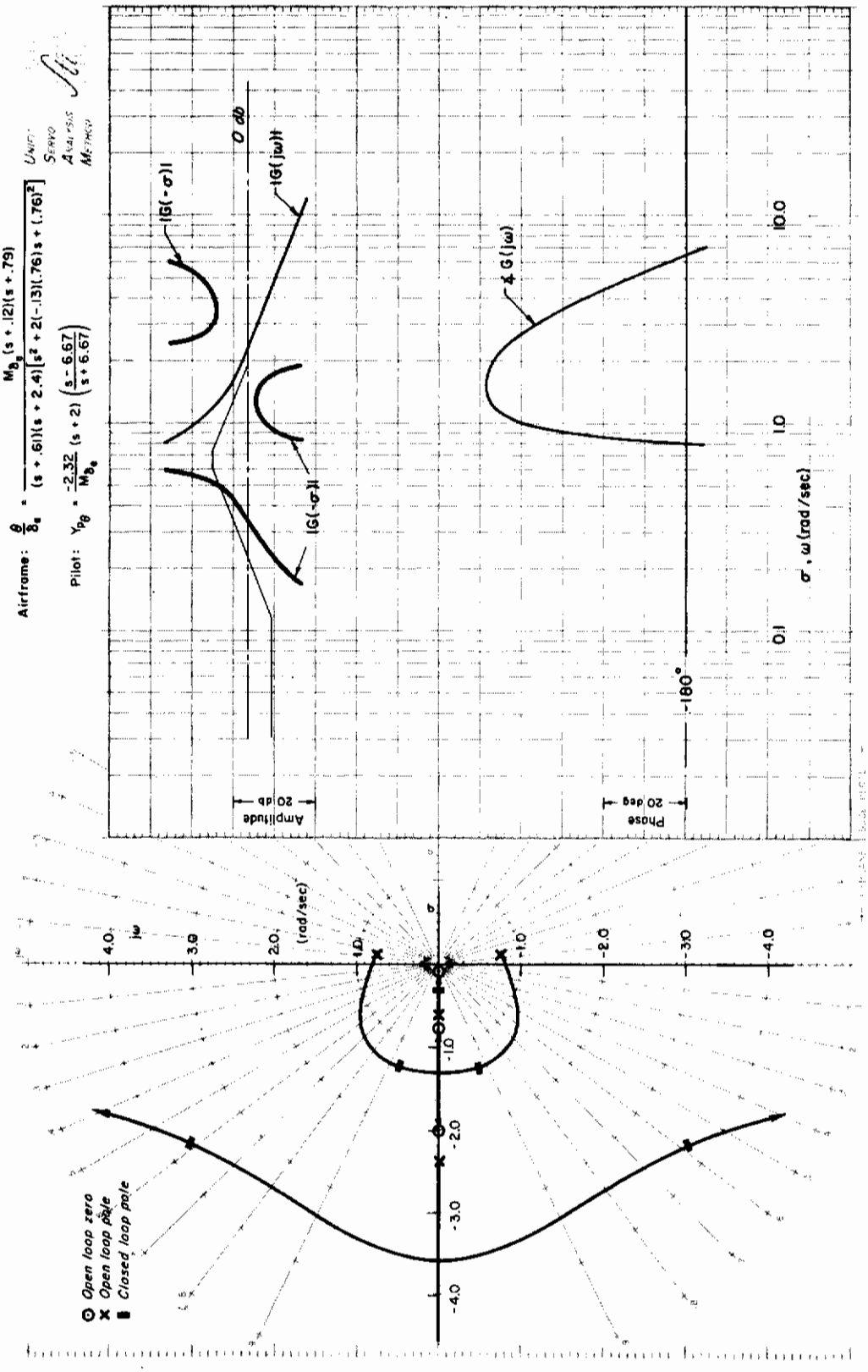

(a) V = 30 Kt, $\dot{V}$ = −0.3g

Figure 22. $\theta \rightarrow \delta_e$ Closure for Tilt Wing

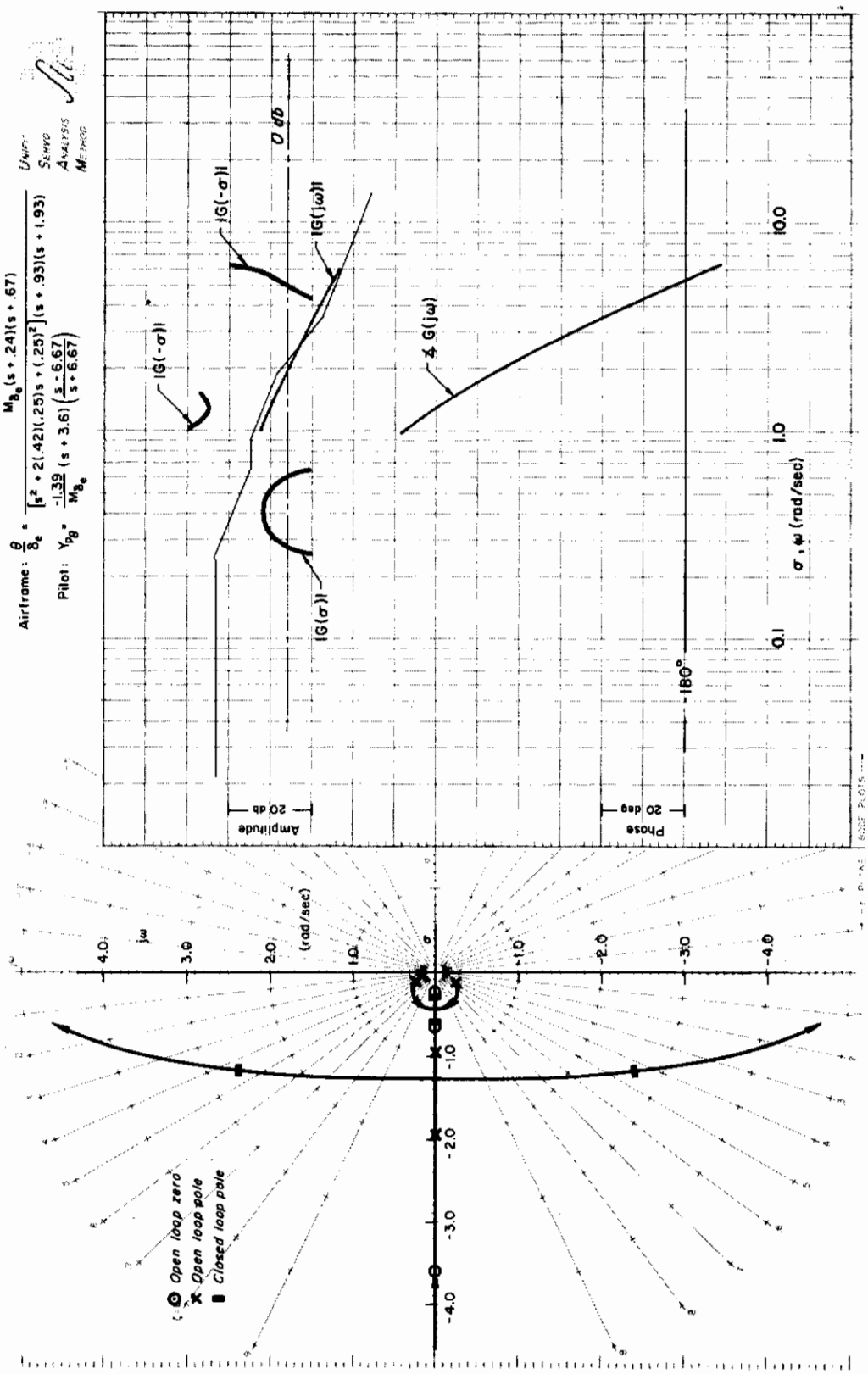

(b) V = 100 Kt, $\dot{V}$ = −0.1g

Figure 22 (Continued)

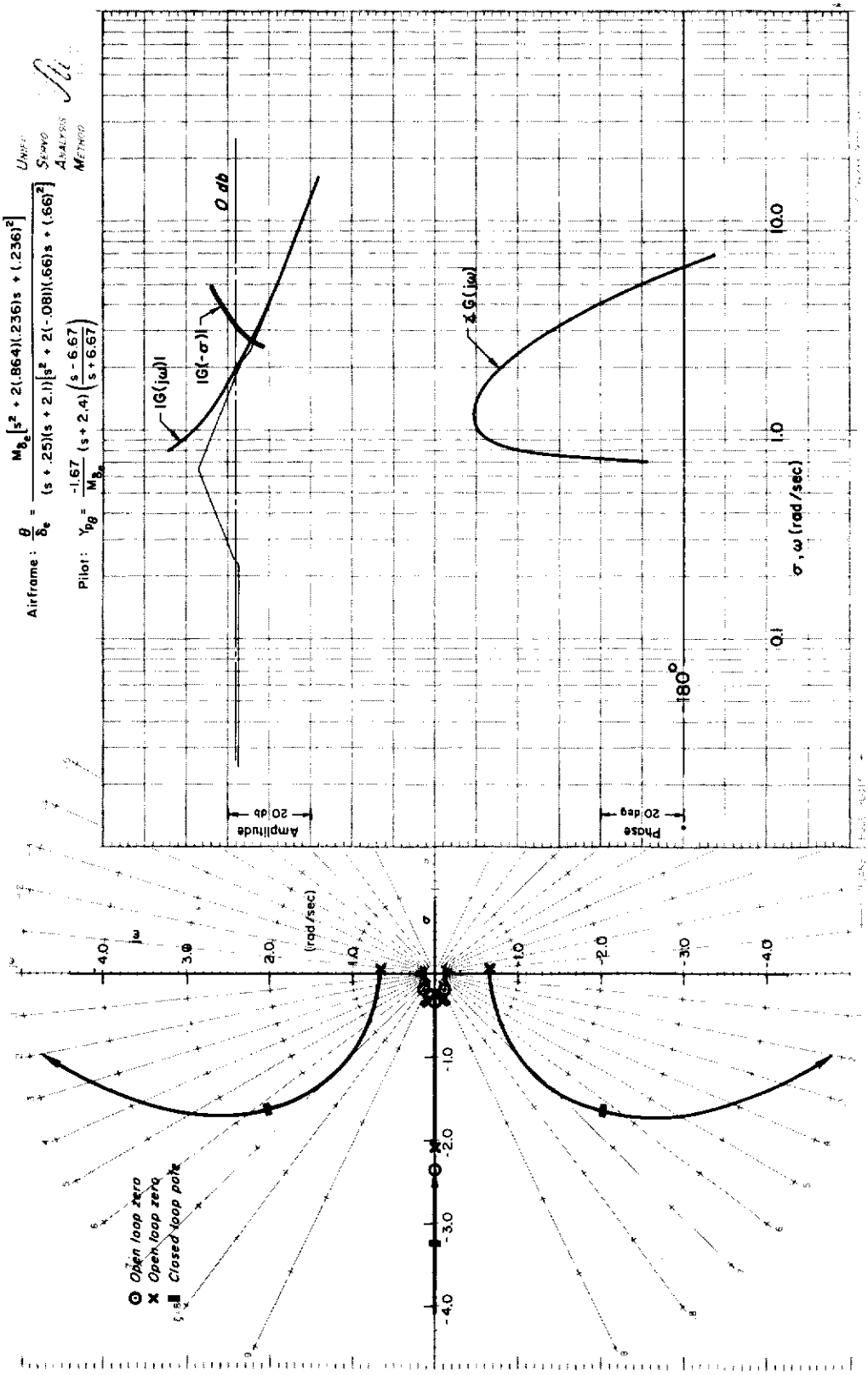

(c) V = 30 Kt, $\dot{V}$ = 0.07g

Figure 22 (Concluded)

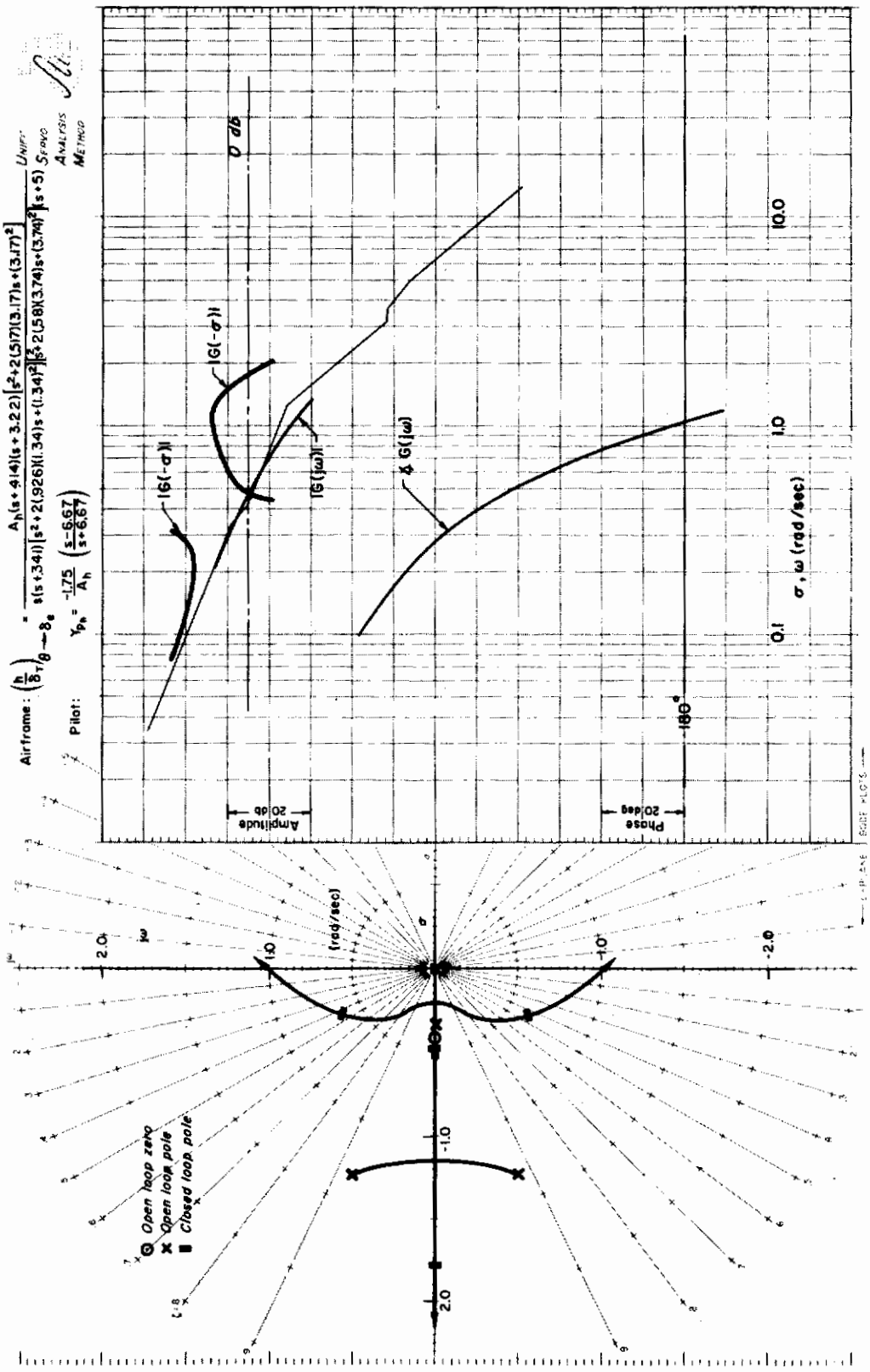

(a) V = 30 Kt, $\dot{V}$ = −0.3g

Figure 23. h ⟶ δ_T Closure for Tilt Wing

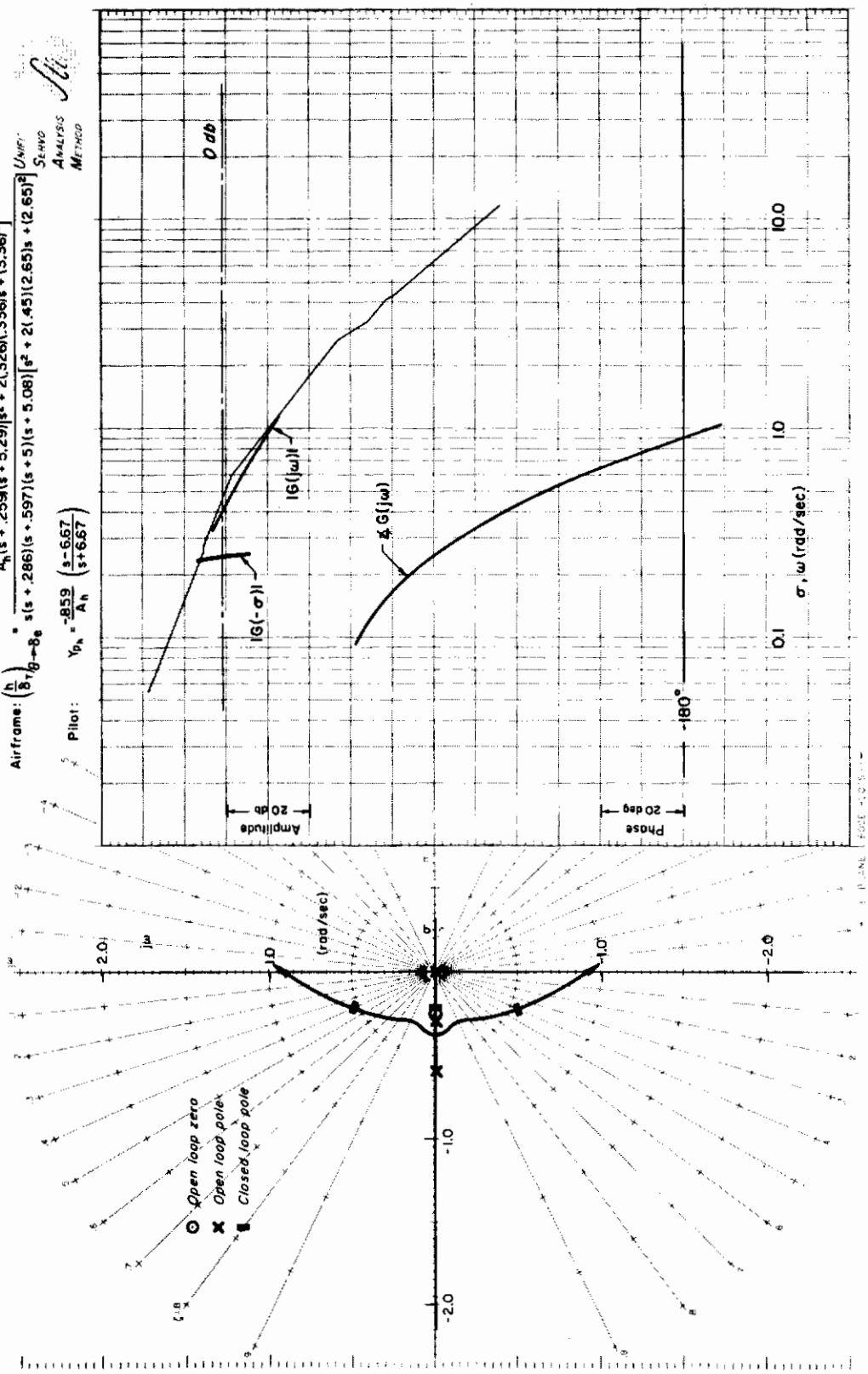

(b) V = 100 Kt, $\dot{V}$ = −0.1g

Figure 23 (Continued)

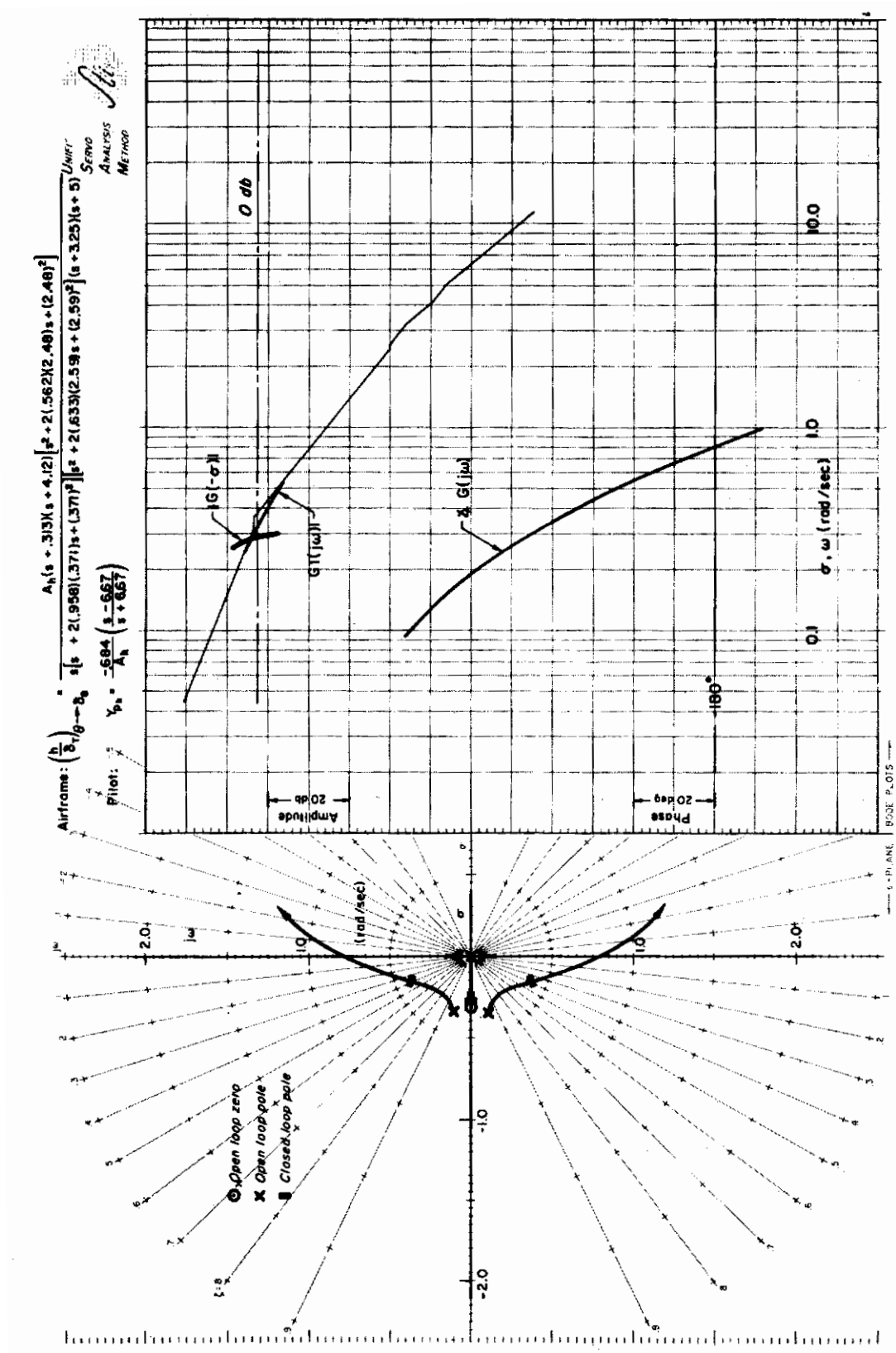

(c) V = 30 Kt, $\dot{V}$ = 0.07g

Figure 23 (Concluded)

Altitude control with throttle for the tilt wing is much easier than for the tilt duct; the primary cause appears to be the higher Z_w for the tilt wing. As with the ducted vehicle, altitude control is more difficult during takeoff than landing, but the difference is small. To obtain insight into why this is so, consider the metric ω_o, Eq 46, which is also valid for the tilt wing. For the tilt wing Z_w, $X_{\delta_T}/Z_{\delta_T}$, and Z_u are relatively constant for all nine flight conditions, as shown in Table XIII.

TABLE XIII

$h \rightarrow \delta_T$ METRIC FOR TILT WING

VELOCITY	ACCELERATION	$-Z_w$	$-\frac{X_{\delta_T}}{Z_{\delta_T}}$	$-Z_u$	PREDICTED ω_o	ACTUAL ω_o
knots		sec^{-1}		sec^{-1}	rad/sec	rad/sec
30	+	0.304	0.168	0.424	0.68	0.81
30	0	0.457	0.168	0.438	0.88	0.90
30	−	0.820	0.168	0.479	1.22	1.07
65	+	0.347	0.213	0.428	0.72	NA
65	0	0.475	0.213	0.475	0.86	0.85
65	−	0.570	0.213	0.520	0.96	0.90
100	+	0.573	0.178	0.360	1.01	NA
100	0	0.612	0.178	0.350	1.05	0.87
100	−	0.664	0.178	0.414	1.09	0.91

This is in direct contrast to a change in $X_{\delta_T}/Z_{\delta_T}$ by a factor of 10 and sizable changes in Z_w and Z_u for the tilt duct.

For the tilt wing in the speed range of 30 to 100 knots, speed has little effect on the altitude control primarily because $X_{\delta_T}/Z_{\delta_T}$ does not change significantly.

D. GENERAL COMMENTS

Before the study reported in this section was undertaken, it was felt that several handling qualities problems might arise during transitions which would not occur for constant velocity flight at any speed. The anticipated problems were due to

1. Trim control requirements
2. Time variations resulting from accelerating operating points
3. Changes in perturbation dynamics (transfer functions) about the operating points with acceleration

For the two cases which were analyzed the trim problem was the only one of the three that materialized. Time variations and the effects of acceleration on the operating points were not important. It would be presumptuous to conclude from the analysis of two vehicles that this result is valid for all V/STOL vehicles, but it is certainly reasonable to expect that it will be true in many cases.

A general remark on the interpretation of the effects of parameter variations on the transition maneuver seems pertinent here. In simulator experiments the aerodynamic characteristics of the vehicle may be altered to study the effects of changes in such parameters as M_α. Because the changes normally affect both the trim and perturbation control tasks,* it is difficult to determine which effect is the predominant influence on the pilot ratings. This problem in interpreting the results could be eased if constant velocity flight at several speeds, as well as complete transitions, were simulated.

*A notable exception is changing M_q, which does not affect the trim task.

SECTION V

SUMMARY

A. HOVER

The most significant effects of changes in individual stability derivatives on handling qualities in hover are:

1. Increasing M_u (making L'_v more negative):
   a. Greatly increases control deflections in gusty air, rms control deflections being roughly proportional to M_u $(-L'_v)$.
   b. Increases attitude response to gusts, with rms attitude deviations roughly proportional to the square root of M_u $(-L'_v)$.
   c. Destabilizes the open-loop second-order mode.
   d. Slightly improves position control and slightly degrades attitude control.
2. Making M_q (L'_p) more negative:
   a. Improves attitude control by reducing the required pilot lead; but at 2 sec^{-1} the required lead approaches zero and increasing the damping beyond this value will normally not give any further improvement.
   b. Increases the damping of the open-loop modes.
   c. Slightly reduces required control deflections and attitude responses in gusty air.
3. Within the normally encountered limits, making X_u $(+Y_v)$ more negative has small effects.
4. Within the normally encountered limits, making $X_{\delta_e}/M_{\delta_e}$ more negative $(Y_{\delta_a}/L'_{\delta_a}$ more positive) has negligible effects.

An important implication of the above is that the familiar experimental studies of control power versus damping must consider the effects of M_u $(-L'_v)$ and must include horizontal gust disturbances. This statement is clearly substantiated by the experimental results of Ref. 8. In those variable-stability helicopter tests, which included an artificial gust

disturbance, an increase in M_u from 0.0087 to 0.105 $(ft\text{-}sec)^{-1}$ with $M_q = -1.98\ sec^{-1}$ had the following effects:

1. The pilot ratings for hover were not changed when the gust magnitude was reduced so that the moment disturbance was constant.

2. Degraded the pilot ratings for hover from 3.2 to 6.6 on the Cooper scale when the gust magnitude was held constant.

B. SIZE AND GEOMETRY

The two most difficult control power requirements to evaluate are those relating to the control power needed to:

1. Maintain or quickly recover attitude in gusty air.

2. Perform required maneuvers consistent with the aircraft's effective utilization.

The first requirement is significantly affected by vehicle size because of variations in M_u (L_v'). For geometrically similar vehicles the variation in M_u (L_v') with size makes the necessary control angular acceleration vary roughly inversely with the square root of vehicle weight. The meager amount of available information indicates that the second requirement is a function of vehicle mission rather than size or geometry.

The most significant effect of size on hover is the variation in M_u (L_v'). For geometrically similar vehicles the variation of M_u (L_v') inversely with the square root of vehicle weight supports the lowering of required pitch (roll) damping, M_q (L_p'), with increasing size. This support comes from the fact that M_u and M_q have somewhat opposite overall effects (see Subsection A above). However, the extent to which the damping can be lowered because of increased vehicle size appears limited to values greater than about $0.8\ sec^{-1}$.

A new nondimensionalized set of hover equations of motion has been derived. These equations should be useful in understanding the effects of vehicle size and geometry.

C. TRANSITION

Although only two specific vehicles, a tilt duct and a tilt wing, were analyzed in detail, the following conclusions should be valid for most V/STOL vehicles:

1. The landing transition is more difficult than the takeoff transition because the trim control is more difficult and the position control requirements are more stringent.

2. The attitude stabilization task (control of attitude perturbations) is not significantly affected by either the time-varying operating point during transition or the differences between takeoff and landing transitions.

3. Altitude control with throttle is easier for landing transition than take-off transition, and easier at low speed than high speed (at high speed it may be necessary to switch to altitude control with elevator). The time-varying operating point is not a significant problem.

REFERENCES

1. Ashkenas, I. L., and D. T. McRuer, Approximate Airframe Transfer Functions and Application to Single Sensor Control Systems, WADC-TR-58-82, June 1958.

2. Wolkovitch, J., and R. P. Walton, VTOL and Helicopter Approximate Transfer Functions and Closed-Loop Handling Qualities, Systems Technology, Inc., Tech. Rept. 128-1, Sept. 1963.

3. Ashkenas, I. L., and D. T. McRuer, "A Theory of Handling Qualities Derived from Pilot-Vehicle System Considerations, Aerospace Eng., Vol. 21, No. 2, Feb. 1962, pp. 60, 61, 83-102.

4. Henderson, C., J. Kroll, and A. Hesby, Control Characteristics of V/STOL Aircraft in Transition, Bell Aerosystems Company Rept. 2023-917002, 1 July 1962.

5. Stapleford, R. L., D. E. Johnston, G. L. Teper, and D. H. Weir, Development of Satisfactory Lateral-Directional Handling Qualities in the Landing Approach, Systems Technology, Inc., Tech. Rept. 131-1, Dec. 1963.

6. Durand, T. S., and G. L. Teper, An Analysis of Terminal Flight Path Control in Carrier Landings, Systems Technology, Inc., Tech. Rept. 137-1, Aug. 1964.

7. Ashkenas, I. L., A Study of Roll Handling Qualities Requirements, AFFDL-TR-65-138, Pt. I, May 1965.

8. Seckel, E., J. J. Traybar, and G. E. Miller, Longitudinal Handling Qualities for Hovering, Princeton Univ., Dept. of Aeron. Eng., Rept. 594, Dec. 1961.

9. Etkin, B., Dynamics of Flight, John Wiley and Sons, Inc., New York, 1959.

10. Newton, G. C., Jr., L. A. Gould, and J. F. Kaiser, Analytical Design of Linear Feedback Controls, John Wiley and Sons, Inc., New York, 1957.

11. Klinar, W. J., and S. J. Craig, Study of VTOL Control Requirements During Hovering and Low-Speed Flight Under IFR Conditions, IAS Paper 61-60, Jan. 1961.

12. Klinar, W. J., and S. J. Craig, Jr., Gust Simulation as Applied to VTOL Control Problems, SAE Preprint 370C, 1961.

13. Ashkenas, I. L., and D. T. McRuer, The Determination of Lateral Handling Quality Requirements from Airframe/Human-Pilot System Studies, WADC-TR-59-135, June 1959.

14. Durand, T. S., and H. R. Jex, Handling Qualities in Single-Loop Roll Tracking Tasks: Theory and Simulator Experiments, ASD-TDR-62-507, Nov. 1962.

15. Walton, R. P., Transfer Function Description of XC-142 and X-22A VTOL Configurations in Transition Flight, Systems Technology, Inc., Tech. Memorandum 135-I-1, 20 Apr. 1964.

16. Michaels, J. L., and A. T. Hesby, Aerodynamic Stability and Control and Flying Qualities, X-22A, Bell Aerosystems Company Rept. 2127-917003, 28 Dec. 1962 (Rev. 1, Apr. 15, 1963).

17. McRuer, D., D. Graham, E. Krendel, and W. Reisener, Jr., Human Pilot Dynamics in Compensatory Systems — Theory, Models, and Experiments with Controlled Element and Forcing Function Variables, AFFDL-TR-65-15, Jan. 1965.

18. McKinney, M. L., "NACA Research on VTOL and STOL Aeroplanes, Sixth Annual Anglo-American Aeronautical Conference (Folkstone), Royal Aeronautical Society, 1959.

19. Kuhn, R. E., Semi-empirical Procedure for Estimating Lift and Drag Characteristics of Propeller-Wing-Flap Comfigurations for Vertical- and Short-Take-Off-and-Landing Airplanes, NASA Memo 1-16-59L, 1959.

20. Durand, W. F.,(ed), Aerodynamic Theory, Vol. V, Div. N, reprinted by Dover Pub., Inc., New York, 1962.

21. Bryant, L. W., and S. B. Gates, Nomenclature for Stability Coefficients, Aeronautical Research Council R and M 1801, 1937.

22. Duncan, W. J., Principles of the Control and Stability of Aircraft, Cambridge Univ. Press, New York, 1952.

23. Perkins, C. D., and R. E. Hage, Airplane Performance, Stability, and Control, John Wiley and Sons, Inc., New York, 1949.

24. Helicopter Flying and Ground Handling Qualities; General Requirements for, MIL-H-8501A, 7 Sept. 1961, Amend. 1, 3 Apr. 1962.

25. Halfman, R. L., Dynamics, Vol. I, Addison-Wesley Pub. Co., Inc., Reading, Mass., 1962.

26. Johnson, H. B., Estimation of Control Laws for Helicopter Autopilots, Royal Airc. Estab. Tech. Note I.A.P. 1107, June 1961.

27. Bramwell, A. R. S., Longitudinal Stability and Control of the Single-Rotor Helicopter, Aeronautical Research Council R and M 3104, Jan. 1957.

28. Dukes, T. A., J. M. Carballal, and P. M. Lion, Some Dynamic Aspects of Stability in Low-Speed Flying Machines, Princeton Univ. Rept. 640, Oct. 1963. (Also TRECOM-TR-63-56, Nov. 1963.)

29. Durand, W. F. (ed), Aerodynamic Theory, Vol. II, Div. E, Sec. 12, reprinted by Dover Pub., Inc., New York, 1963, p. 20.

30. Williams, J., "Some British Research on the Basic Aerodynamics of Powered Lift Systems," J. Royal Aeron. Society, Vol. 64, July 1960.

31. Davidson, I. M., "The Jet Flap," J. Royal Aeron. Society, Vol. 60, Jan. 1956.

32. Kuhn, R. E., Investigation of Effectiveness of a Wing Equipped with a 50-Percent-Chord Sliding Flap, a 30-Percent-Chord Slotted Flap, and a 30-Percent-Chord Slat in Deflecting Propeller Slipstreams Downward for Vertical Take-Off, NACA TN 3919, Jan. 1957.

33. Koenig, D. G., and J. A. Brady, A Large-Scale Wind-Tunnel Investigation of a Wingless Vertical Take-Off and Landing Aircraft, NASA TN D-1335, Feb. 1963.

34. Green, W., The Observer's Book of Aircraft, Warne and Co., London, 1964, p. 153.

35. Parlett, L. P., Aerodynamic Characteristics of a Small-Scale Shrouded Propeller at Angles of Attack from 0° to 90°, NACA TN 3547, Nov. 1955.

36. Reichert, J. B., and J. R. Ulyate, Final Report on Doak Model 16, Doak Aircraft Company Rept. DS-215, 15 Aug. 1960.

37. Kriebel, A. R., A. H. Sacks, and J. N. Nielsen, Theoretical Investigation of Dynamic Stability Derivatives of Ducted Propellers, Vidya Tech. Rept. 63-95, Jan. 9, 1963.

38. Grunwald, K. J., and K. W. Goodson, Division of Aerodynamic Loads on a Semispan Tilting-Ducted-Propeller Model in Hovering and Transition Flight, NASA TN D-1257, May 1962.

39. Parlett, L. P., Experimental Investigation of Some of the Parameters Related to the Stability and Control of Aerial Vehicles Supported by Ducted Fans, NASA TN D-616, Nov. 1960.

40. Wattson, R. K., Jr., and V. O. Hoehne, Wind Tunnel Tests of Shrouded Propellers and Their Application, IAS Paper 59-107, 1959.

41. Davenport, E. E., and K. P. Spreemann, Transition Characteristics of a VTOL Aircraft Powered by Four Ducted Tandem Propellers, NASA TN D-2254, Apr. 1964.

42. Tapscott, R. J., and H. L. Kelley, A Flight Study of the Conversion Maneuver of a Tilt-Duct VTOL Aircraft, NASA TN D-372, Nov. 1960.

43. McKinney, M. O., and W. A. Newsom, Experimental Research on 4-Duct Tandem VTOL Aircraft Configurations, paper presented at 18th Annual Forum of the American Helicopter Society, May 3-5, 1962.

44. Yaggy, P. F., and K. W. Goodson, Aerodynamics of a Tilting Ducted Fan Configuration, NASA TN D-785, Mar. 1961.

45. Newsom, W. A., Jr., Aerodynamic Characteristics of Four-Duct Tandem VTOL-Aircraft Configurations, NASA TN D-1481, Jan. 1963.

46. Goodson, K. W., and K. J. Grunwald, Aerodynamic Characteristics of a Powered Semispan Tilting-Shrouded-Propeller VTOL Model in Hovering and Transition Flight, NASA TN D-981, Jan. 1962.

47. Mort, K. W., and P. F. Yaggy, Aerodynamic Characteristics of a 4-Foot-Diameter Ducted Fan Mounted on the Tip of a Semispan Wing, NASA TN D-1301, Apr. 1962.

48. Ritter, A., and D. E. Ordway, "Some Results of Finite-Bladed Ducted-Propeller Theory for VTOL," Aerospace Engineering, Vol. 21, No. 7, July 1962, pp. 54–55.

49. Sacks, A. H., and J. A. Burnell, "Ducted Propellers — A Critical Review of the State of the Art," Progress in Aeronautical Sciences, Vol. 3, Pergamon Press, New York, 1962, pp. 85–135.

50. Maki, R. L., and D. H. Hickey, Aerodynamics of a Fin-in-Fuselage Model, NASA TN D-789, May 1961.

51. Goldsmith, R. H., and D. H. Hickey, Characteristics of Aircraft with Lifting-Fan Propulsion Systems for V/STOL, IAS Paper 63-27, Jan. 1963.

52. Seckel, E., Stability and Control of Airplanes and Helicopters, Academic Press, New York, 1964.

53. Fundamentals of Helicopter Stability and Control, Vertol, Division of Boeing, Rept. R-242, 1961.

54. Shapiro, J., Principles of Helicopter Engineering, McGraw-Hill, New York, 1952.

55. Heyson, H. H., Nomographic Solution of the Momentum Equation for VTOL-STOL Aircraft, NASA TN D-814, Apr. 1961.

56. Gessow, A., Review of Information on Induced Flow of a Lifting Rotor, NACA TN 3238, 1954.

57. Gessow, A., and G. C. Myers, Aerodynamics of the Helicopter, Macmillan, New York, 1952.

58. Durand, W. F. (ed), Aerodynamic Theory, Vol. IV, Division L, Section 12, first published by Julius Springer, Berlin, 1935, reprinted by Dover, New York, 1963.

59. von Mises, R., Theory of Flight, Dover, New York, 1959.

60. Küchemann, D., and J. Weber, Aerodynamics of Propulsion, McGraw-Hill, New York, 1951.

61. Meijer Drees, J., "A Theory of Airflow Through Rotors and Its Application to Some Helicopter Problems," J. Helicopter Assoc. of Great Britain, Vol. 3, No. 2, 1949, pp. 79–104.

62. Yaggy, P. F., and K. W. Mort, Wind-Tunnel Tests of Two VTOL Propellers in Descent, NASA TN D-1766, Mar. 1963.

63. Yaggy, P. F., and V. L. Rogallo, A Wind-Tunnel Investigation of Three Propellers Through an Angle-of-Attack Range from 0° to 85°, NASA TN D-318, May 1960.

64. Greenman, R. N., and M. G. Gaffney, Dynamic Stability Analysis of Ducted Fan Type Flying Platforms, Hiller Aircraft, Advanced Research Division, Rept. ARD-233, 29 May 1959. (ASTIA AD-218 994)

65. Vetter, H. C., "Effect of a Turbojet Engine on the Dynamic Stability of an Aircraft," J. Aeron. Sciences, Vol. 20, Nov. 1953, pp. 797–798.

66. Kriebel, A. R., "Theoretical Stability Derivatives for a Ducted Propeller," J. Aircraft, Vol. 1, No. 4, July–Aug. 1964.

67. Aeroelasticity in Stability and Control, WADC-TR-55-173, Mar. 1957.

68. McRuer, D. T., Unified Analysis of Linear Feedback Systems, ASD-TR-61-118, Mar. 1961.

APPENDIX A

APPROXIMATE FACTORS

The formulation of approximate factors for V/STOL vehicles is more complicated than for conventional aircraft. The extra complexity stems from the addition of low speed flight. In this flight regime certain important stability derivatives differ greatly from their values at conventional aircraft speeds and also differ substantially from one type of V/STOL to another. As a result it is necessary to use several sets of approximate factors to adequately cover the speed range and the types of vehicles.

This Appendix contains a summary of the best approximations currently known. Some of these represent original work done during this study, but most are taken from earlier reports and are repeated here for completeness. In several high speed cases the conventional airplane factors of Ref. 1 are used. Most of the factors unique to V/STOLs were taken from Ref. 2. About half of the denominator factors were derived in this study and are not documented elsewhere. The method of deriving these new factors is outlined below.

Briefly, the quartics were factored by finding the real roots, and then using these real roots to determine the remaining damping and frequency terms. The real roots were found by making an initial "guess," s_1, of a root location (via use of a Siggy sketch, Ref. 1, for example) and then assuming the exact root location to be at $s_1 + \epsilon$. By plugging $s_1 + \epsilon$ into the literal equation to be factored, a polynomial in ϵ was obtained. An approximate solution of this polynomial in ϵ then enabled a root location to be quite accurately expressed as a simple function of the stability derivatives. The approximate solution for ϵ was made possible by knowing the exact solution in advance. Thus, the significant terms in the equation were easily determined.

Table A-I lists the configurations and forward speeds which were used to check the validity of the approximate factors. In all cases the

approximate factors were within 5 percent of the exact values. The general forms of the transfer functions are given in Table A-II. Table A-III shows which approximate factors are available for each type of vehicle and gives the key for the "locations" of the factors, which are separately listed in Table A-IV. All the approximate factors are for straight and level flight and for stability axis derivatives. If the conditions of validity are met, the approximate factors should generally be accurate within ±10 percent of the magnitude of the root, i.e., for a second-order pair the errors in the real and imaginary parts of the roots should be less than 10 percent of the frequency.

TABLE A-I

CONDITIONS USED TO CHECK VALIDITY OF APPROXIMATE FACTORS

VEHICLE	U_o (ft/sec)	LONGITUDINAL	LATERAL
VZ-2 tilt-wing	0 25 45 60	Yes	No
XC-142 tilt-wing	1 35 60	Yes	No
AC-1 tilt-wing (Fig. 15)*	15 80 170	Yes	No
H-19 single-rotor helicopter	1 50 70 115	Yes	Yes
HUP-1 tandem-rotor helicopter	1 40 80 120	Yes	Yes
VZ-4 tilt-duct	0 60 75 125	Yes	Yes
X-22 tandem tilt-duct	1 35 70 100	Yes	Yes
Bell D-2064 tandem tilt-duct (Fig. 14)	15 135 270	Yes	No
Bell D-252 tilt-rotor	15 135 235	Yes	No

*Scaled-up version of Kaman K-16B as used in Ref. 4

TABLE A-II

TRANSFER FUNCTION FORMS

GENERAL:

$$\frac{\lambda(s)}{\delta(s)} = \frac{N_\lambda(s)}{\Delta(s)}$$

LONGITUDINAL:

$$\Delta(s) = \left(s^2 + 2\zeta_p\omega_p s + \omega_p^2\right)\underbrace{\left(s^2 + 2\zeta_{sp}\omega_{sp}s + \omega_{sp}^2\right)}_{\text{or}}$$

$$\left(s + \frac{1}{T_{sp_1}}\right)\left(s + \frac{1}{T_{sp_2}}\right)$$

$$N_\theta(s) = K_\theta\left(s + \frac{1}{T_{\theta_1}}\right)\left(s + \frac{1}{T_{\theta_2}}\right)$$

$$N_w(s) = K_w\left(s + \frac{1}{T_{w_1}}\right)\underbrace{\left(s + \frac{1}{T_{w_2}}\right)\left(s + \frac{1}{T_{w_3}}\right)}_{\text{or}}$$

$$\left(s^2 + 2\zeta_w\omega_w s + \omega_w^2\right)$$

$$N_u(s) = K_u\left(s + \frac{1}{T_{u_1}}\right)\underbrace{\left(s + \frac{1}{T_{u_2}}\right)\left(s + \frac{1}{T_{u_3}}\right)}_{\text{or}}$$

$$\left(s^2 + 2\zeta_u\omega_u s + \omega_u^2\right)$$

$$N_h(s) = K_h\left(s + \frac{1}{T_{h_1}}\right)\underbrace{\left(s + \frac{1}{T_{h_2}}\right)\left(s + \frac{1}{T_{h_3}}\right)}_{\text{or}}$$

$$\left(s^2 + 2\zeta_h\omega_h s + \omega_h^2\right)$$

Table A-II (Contd.)

LATERAL:

$$\Delta(s) = \left(s + \frac{1}{T_s}\right)\left(s + \frac{1}{T_R}\right)\left(s^2 + 2\zeta_d\omega_d s + \omega_d^2\right)$$

$$N_\varphi(s) = K_\varphi\underbrace{\left(s^2 + 2\zeta_\varphi\omega_\varphi s + \omega_\varphi^2\right)}_{\text{or}}$$

$$\left(s + \frac{1}{T_{\varphi_1}}\right)\left(s + \frac{1}{T_{\varphi_2}}\right)$$

$$N_r(s) = K_r\left(s + \frac{1}{T_r}\right)\left(s^2 + 2\zeta_r\omega_r s + \omega_r^2\right)$$

$$N_v(s) = K_v\left(s + \frac{1}{T_{v_1}}\right)\underbrace{\left(s + \frac{1}{T_{v_2}}\right)\left(s + \frac{1}{T_{v_3}}\right)}_{\text{or}}$$

$$\left(s^2 + 2\zeta_v\omega_v s + \omega_v^2\right)$$

TABLE A-III

AVAILABILITY AND KEY TO LOCATION OF APPROXIMATE FACTORS

				TILT-WING		HELICOPTER				TILT-DUCT		TILT-ROTOR
						SINGLE-ROTOR		TANDEM-ROTOR				
				LOW SPEED[1,3]	HIGH SPEED[2,3]	Hover ($U_o \doteq 0$)	High Speed ($U_o > 50$ fps)	Hover ($U_o \doteq 0$)	High Speed ($U_o > 40$ fps) ($U_o < 120$ fps)	Hover ($U_o \doteq 0$)	High Speed ($U_o > 100$ fps)	All Speeds
LONGITUDINAL	Denominator			AA	AB	AC	AB	AC	AD	AA	AB	AB
	NUMERATORS	Elevator (Pitching Moment Control)	θ	BB	BB	BC	BC	BC	BC	BB	BB	BC
			w	None	CC	Zero	CD	Zero	CD	None	CC	CD
			u	DD	DD	DE	DE	DE	DE	DD	DD	DE
			$\dot{h}$	None	None	Zero	EF	Zero	EF	None	EE	None
		Throttle (Thrust Control)	θ	BB	BB	Zero	FF	Zero	FG	Zero	BB	BB
			w	None*	None	None*	GG	None*	GG	None*	None	None
			u	None	None	Zero	HH	Zero	HI	Zero	None	None
			$\dot{h}$	None*	None	None*	None	None*	II	None*	None	None
LATERAL	Denominator			None	None	None	JK	JL	JL	JJ	None	None
	NUMERATORS	Aileron (Rolling Moment Control)	φ	NN	NN	KL	KL	KM	KM	KK	KK	NN
			r	None	None	LL	LL	LM	LM	None	None	None
			v	None	None	None	None	None	None	MM	MM	None
		Rudder (Yawing Moment Control)	φ	NN	NN	NP	NP	NN	NP	NN	NN	NN
			r	None	None	PP	PP	PP	PP	None*	None	None
			v	None	None	None	QR	QS	QS	None	QQ	None

Notes: [1]Including range of speed for which wing incidence is within 45 deg of wing incidence at hover.

[2]Wing incidence greater than 45 deg from incidence at hover.

[3]The separation of high and low speed factors by wing incidence is empirical.

*Although there is not an approximate factor available, the numerator factors will cancel with denominator factors to give a known transfer function.

"None" indicates approximate factors not available.

"Zero" indicates response is approximately zero.

Letters indicate appropriate approximate factor from Table A-IV.

TABLE A-IV

APPROXIMATE FACTORS REFERRED FROM TABLE A-III

	FIRST COEFF.	APPROXIMATE FACTORS	CONDITIONS OF VALIDITY
AA	1	$\frac{1}{T_{sp_1}} \doteq -Z_w$ $\frac{1}{T_{sp_2}} \doteq \sqrt[3]{gM_u} + \frac{-X_u - M_q}{3}$ $2\zeta_p\omega_p \doteq -\sqrt[3]{gM_u} + \frac{2}{3}(-X_u - M_q)$ $\omega_p^2 \doteq gM_uT_{sp_1}$	$\lvert U_oM_w\rvert \ll \lvert Z_wM_q\rvert$ $\lvert\frac{gM_u}{M_q^3}\rvert > 1$ $\lvert\frac{gM_u}{X_u^3}\rvert > 1$
AB	1	$\frac{1}{T_{sp_1}}\frac{1}{T_{sp_2}}$ or $\omega_{sp}^2 \doteq Z_wM_q - U_oM_w$ $\frac{1}{T_{sp_1}} + \frac{1}{T_{sp_2}}$ or $2\zeta_{sp}\omega_{sp} \doteq -Z_w - M_q - U_oM_w^{\cdot}$ $\frac{1}{T_{p_1}}\frac{1}{T_{p_2}}$ or $\omega_p^2 \doteq \frac{g(M_wZ_u - M_uZ_w)}{Z_wM_q - U_oM_w}$ $\frac{1}{T_{p_1}} + \frac{1}{T_{p_2}}$ or $2\zeta_p\omega_p \doteq -X_u - \frac{M_u(X_wU_o - g)}{Z_wM_q - U_oM_w}$	ω_{sp}^2 or $\lvert\frac{1}{T_{sp_1}}\frac{1}{T_{sp_2}}\rvert > 4\omega_p^2$ or $4\lvert\frac{1}{T_{p_1}}\cdot\frac{1}{T_{p_2}}\rvert$ $\lvert X_u\rvert \ll \lvert M_q + Z_w + U_oM_w^{\cdot}\rvert$ $\lvert X_u(M_q + Z_w + U_oM_w^{\cdot})\rvert \ll \lvert M_qZ_w - U_oM_w\rvert$ $\lvert Z_u(gM_w^{\cdot} + X_wM_q)\rvert \ll \lvert M_u(g - U_oX_w) - X_u(Z_wM_q - U_oM_w)\rvert$
AC	1	$\frac{1}{T_{sp_1}} \doteq -Z_w$ $\frac{1}{T_{sp_2}} \doteq \frac{-3M_q}{4} + \sqrt{\frac{M_q^2}{16} - \frac{gM_u}{2M_q}}$ $2\zeta_p\omega_p \doteq -X_u - \frac{M_q}{4} - \sqrt{\frac{M_q^2}{16} - \frac{gM_u}{2M_q}}$ $\omega_p^2 \doteq \frac{gM_u}{\frac{-3M_q}{4} + \sqrt{\frac{M_q^2}{16} - \frac{gM_u}{2M_q}}}$	$\lvert M_q\rvert \gg \lvert X_u\rvert$ $\lvert\frac{gM_u}{M_q^3}\rvert < 1$ If $\lvert X_u\rvert \gg \lvert M_q\rvert$ and $\lvert\frac{gM_u}{X_u^3}\rvert < 1$ interchange X_u and M_q in equations

TABLE A-IV (Contd.)

	FIRST COEFF.	APPROXIMATE FACTORS	CONDITIONS OF VALIDITY
AD	1	$\frac{1}{T_{sp_1}} \doteq -\left(\frac{M_q + Z_w + U_o M_{\dot{w}}}{2}\right) + \sqrt{\left(\frac{M_q + Z_w + U_o M_{\dot{w}}}{2}\right)^2 + U_o M_w - M_q Z_w}$ $\frac{-1}{T_{sp_2}} \doteq \omega_p \doteq -\left[g T_{sp_1}(M_w Z_w - M_u Z_w)\right]^{1/3}$ $2\zeta_p \omega_p \doteq -X_u - \frac{1}{T_{sp_2}}$	$\left\lvert\frac{1}{T_{sp_1}}\right\rvert > 5\left\lvert\frac{1}{T_{sp_2}}\right\rvert$ $\lvert g M_u \rvert \gg \lvert -X_u(M_q Z_w - U_o M_w) - M_u U_o X_w + M_q X_w Z_u + g Z_u M_{\dot{w}} \rvert$ If M_u is too small to satisfy this condition, use AB
BB	M_δ	$\frac{1}{T_{\theta_1}} + \frac{1}{T_{\theta_2}} \doteq \frac{X_\delta}{M_\delta}(Z_u M_{\dot{w}} + M_u) + \frac{Z_\delta}{M_\delta}(M_w - X_u M_{\dot{w}}) - (X_u + Z_w)$ $\frac{1}{T_{\theta_1}}\frac{1}{T_{\theta_2}} \doteq \frac{X_\delta}{M_\delta}(Z_u M_w - Z_w M_u) + \frac{Z_\delta}{M_\delta}(M_u X_w - M_w X_u) + (Z_w X_u - X_w Z_u)$	$\lvert Z_\delta M_{\dot{w}} \rvert \ll \lvert M_\delta \rvert$
BC	M_δ	$\frac{1}{T_{\theta_1}} \doteq \frac{X_\delta(M_u Z_w - Z_u M_w) + Z_\delta(X_u M_w - M_u X_w) + M_\delta(Z_u X_w - X_u Z_w)}{Z_w M_\delta}$ $\frac{1}{T_{\theta_2}} \doteq -Z_w$	$\left\lvert\frac{1}{T_{\theta_1}}\right\rvert \ll \left\lvert\frac{1}{T_{\theta_2}}\right\rvert$
CC	Z_δ	$\frac{1}{T_w} \doteq \frac{U_o M_\delta}{Z_\delta}$ $\omega_w^2 \doteq \frac{g}{U_o}\left(\frac{M_u Z_\delta}{M_\delta} - Z_u\right)$ $2\zeta_w \omega_w \doteq -X_u$	$\lvert Z_\delta(M_q + X_u) - X_\delta Z_u \rvert \ll \lvert U_o M_\delta \rvert$ $\lvert X_\delta(U_o M_u - Z_u M_q) \rvert \ll \lvert X_u(Z_\delta M_q - U_o M_\delta) \rvert$
CD	Z_δ	$\frac{1}{T_w} \doteq \frac{U_o M_\delta}{Z_\delta}$ $\omega_w^2 \doteq \frac{g}{U_o}\left(\frac{M_u Z_\delta}{M_\delta} - Z_u\right)$ $2\zeta_w \omega_w \doteq \frac{1}{U_o M_\delta}\left[U_o(X_\delta M_u - X_u M_\delta) + M_q(X_u Z_\delta - X_\delta Z_u) - Z_\delta \omega_w^2\right]$	$\left\lvert\frac{1}{T_w}\right\rvert \gg \lvert M_q \rvert$ $U_o \neq 0$ (at $U_o = 0$, $Z_\delta = 0$) $\left\lvert\frac{1}{T_w}\right\rvert \gg \omega_w$ $\lvert U_o M_\delta \rvert \gg \lvert X_u Z_\delta \rvert$

TABLE A-IV (Contd.)

	FIRST COEFF.	APPROXIMATE FACTORS	CONDITIONS OF VALIDITY
DD	$Z_\delta X_w$	$\frac{1}{T_{u_1}} \doteq \frac{M_\delta(U_o X_w - g)}{Z_\delta X_w}$ $\frac{1}{T_{u_2}} \doteq \frac{g\left(Z_w - \frac{Z_\delta}{M_\delta} M_w\right)}{(U_o X_w - g)}$	$\lvert Z_\delta(gM_{\dot{w}} + M_q X_w)\rvert \ll \lvert M_\delta(U_o X_w - g)\rvert$ $\left\lvert\frac{X_w Z_\delta}{X_\delta}\right\rvert \gg \left\lvert\frac{1}{T_{u_2}}\right\rvert \gg \left\lvert\frac{1}{T_{u_1}}\right\rvert$ For $U_o \doteq 0$, $\frac{1}{T_{u_2}} = -Z_w$, $\frac{1}{T_{u_1}} \to \infty$
DE	X_δ	$\frac{1}{T_u} \doteq -Z_w$ $\omega_u^2 \doteq \frac{-g}{X_\delta}\left(M_\delta - Z_\delta \frac{M_w}{Z_w}\right)$ $2\zeta_u\omega_u \doteq -M_q$	$\lvert X_\delta(M_q + Z_w)\rvert \gg \lvert U_o X_\delta M_{\dot{w}} - Z_\delta X_w)\rvert$ $\lvert X_\delta Z_w M_q - gM_\delta\rvert \gg \lvert U_o(X_w M_\delta - X_\delta M_w) - Z_\delta(gM_{\dot{w}} + X_w M_q)\rvert$
XE	$-Z_\delta$	$\frac{1}{T_{h_1}} \doteq -X_u + (U_o X_w - g)\frac{M_u - \frac{M_\delta}{Z_\delta} Z_u}{U_o\left(M_w - \frac{M_\delta}{Z_\delta} Z_w\right)}$ $-\frac{1}{T_{h_2}} \doteq \frac{1}{T_{h_3}} \doteq \sqrt{U_o\left(M_w - \frac{M_\delta}{Z_\delta} Z_w\right)}$	$\left(\frac{1}{T_{h_2}}\right)^2 \gg \left\lvert\left(X_u - \frac{X_\delta Z_u}{Z_\delta}\right)(M_q + U_o M_{\dot{w}})\right\rvert$ $\left\lvert\frac{1}{T_{h_1}}\frac{1}{T_{h_2}}\frac{1}{T_{h_3}}\right\rvert \gg \left\lvert\frac{X_\delta}{Z_\delta} U_o(Z_w M_u - Z_u M_w)\right\rvert$ For $U_o \doteq 0$, $h \doteq -w$
EF	$-Z_\delta$	$\frac{1}{T_h} \doteq -\frac{gZ_u}{U_o Z_w} + \frac{Z_\delta}{M_\delta}\frac{gM_u}{U_o Z_w} + \frac{X_\delta}{M_\delta}\left(M_u - \frac{M_w Z_u}{Z_w}\right)$ $\omega_h^2 \doteq \frac{M_\delta U_o Z_w}{Z_\delta}$ $2\zeta_h\omega_h \doteq -M_q - U_o M_{\dot{w}}$	$\left\lvert\frac{1}{T_h}\right\rvert \ll \omega_h$ $\lvert M_w Z_\delta\rvert \ll \lvert Z_w M_\delta\rvert$ $\left\lvert\frac{1}{T_h}\omega_h^2\right\rvert \gg U_o\left\lvert(M_u X_w - M_w X_u) + \frac{M_\delta}{Z_\delta}(X_u Z_w - X_w Z_u)\right\rvert$
FF	M_δ	$\frac{1}{T_{\theta_1}} \doteq -X_u - \frac{M_u(Z_w X_\delta - X_w Z_\delta)}{M_w Z_\delta - Z_w M_\delta}$ $\frac{1}{T_{\theta_2}} \doteq -Z_w + \frac{M_w Z_\delta + M_u X_\delta}{M_\delta} \doteq -Z_w + \frac{M_w}{M_\delta} Z_\delta$	$\left\lvert\frac{1}{T_{\theta_1}}\right\rvert \ll \lvert Z_w\rvert$ $\left\lvert\frac{1}{T_{\theta_1}}\right\rvert \ll \left\lvert\frac{1}{T_{\theta_2}}\right\rvert$ $M_\delta \neq 0$

TABLE A-IV (Contd.)

	FIRST COEFF.	APPROXIMATE FACTORS	CONDITIONS OF VALIDITY
FG	$Z_\delta M_{\dot{w}}$	$\frac{1}{T_{\theta_1}} \doteq \frac{M_w}{M_{\dot{w}}}$ $\frac{1}{T_{\theta_2}} \doteq -X_u + M_u \frac{X_w}{M_w}$	$M_{\dot{w}} \neq 0$ $\lvert M_\delta \rvert \ll \lvert Z_\delta M_{\dot{w}} \rvert$ $\lvert X_\delta \rvert \ll \lvert Z_\delta \rvert$ $U_o \neq 0$
GG	Z_δ	$\frac{1}{T_{w_1}} \doteq -M_q.$ $\frac{1}{T_{w_2}} \frac{1}{T_{w_3}}$ or $\omega_w^2 \doteq \frac{gM_u}{-M_q}$ $\frac{1}{T_{w_2}} + \frac{1}{T_{w_3}}$ or $2\zeta_w\omega_w \doteq -X_u - \frac{gM_u}{M_q^2}$	$U_o \neq 0$ $\left[\text{for } U_o = 0, \frac{w(s)}{\delta(s)} = \frac{Z_\delta}{s - Z_w}\right]$ $\lvert X_u \rvert \ll \lvert 1/T_w \rvert$ $\lvert X_u \rvert \ll \lvert \omega_w \rvert$ $\lvert X_\delta \rvert \ll \lvert Z_\delta \rvert$ $\lvert U_o M_\delta \rvert \ll \lvert Z_\delta M_q \rvert$
HH	X_δ	$\frac{1}{T_u} \doteq -Z_w + X_w \frac{Z_\delta}{X_\delta}$ $\omega_u^2 \doteq \frac{-gM_\delta}{X_\delta}$ $2\zeta_u\omega_u \doteq -M_q$	$X_\delta \neq 0$ (Note: $X_\delta = 0$ at $U_o = 0$) $\lvert X_w Z_\delta \rvert < \lvert Z_w X_\delta \rvert$
II	$Z_\delta X_w$	$\frac{1}{T_{u_1}} \frac{1}{T_{u_2}} \doteq \frac{-gM_w}{X_w}$ $\frac{1}{T_{u_1}} + \frac{1}{T_{u_2}} \doteq -M_q - \frac{gM_{\dot{w}}}{X_w}$	$X_\delta = M_\delta = 0$ $U_o \neq 0$
KK	$-Z_\delta$	$\frac{1}{T_{h_1}} \doteq X_u + (g - U_o X_w) \frac{M_u}{U_o M_w}$ $\frac{1}{T_{h_2}} + \frac{1}{T_{h_3}}$ or $2\zeta_h\omega_h \doteq -M_q$ $\frac{1}{T_{h_2}} \frac{1}{T_{h_3}}$ or $\omega_h^2 \doteq -U_o M_w$	$U_o \neq 0$ $\left[\text{for } U_o = 0, \frac{\dot{h}(s)}{\delta(s)} = \frac{-Z_\delta}{s - Z_w}\right]$ $\lvert Z_u \rvert \ll \lvert U_o Z_w \rvert$ $\lvert M_u \rvert \ll \lvert U_o M_w \rvert$ $X_\delta = M_\delta = 0$

TABLE A-IV (Contd.)

	FIRST COEFF.	APPROXIMATE FACTORS	CONDITIONS OF VALIDITY
JJ	1	$\frac{1}{T_s} \doteq -N_r'$ $\frac{1}{T_R} \doteq -\sqrt[3]{gL_v'} + \frac{-L_p' - Y_v}{3}$ $2\zeta_d\omega_d \doteq \sqrt[3]{gL_v'} + \frac{2}{3}(-L_p' - Y_v)$ $\omega_d^2 \doteq (gL_v')^{2/3}\left[1 + \frac{-L_p' - Y_v}{3\sqrt[3]{gL_v'}}\right]$	$\lvert U_o N_v' \rvert \ll \lvert N_r' L_p' \rvert$ $\lvert L_p' \rvert > \lvert Y_v \rvert$ $\left\lvert \frac{gL_v'}{L_p'^3} \right\rvert > 1$
JK	1	$\omega_d^2 \doteq U_o N_v'$ $2\zeta_d\omega_d \doteq -(Y_v + N_r') - \frac{L_v'}{N_v'}\left(N_p' - \frac{g}{U_o}\right)$ $\frac{1}{T_R} \doteq -L_p'$ $\frac{1}{T_s} \doteq -\frac{g}{U_o L_p'}\left(\frac{L_v'}{N_v'} N_r' - L_r'\right)$	$U_o \neq 0$ $N_v \neq 0$ $\left\lvert \frac{1}{T_s} \right\rvert \ll \left\lvert \frac{1}{T_R} \right\rvert$ $Y_r \doteq Y_p \doteq 0$ $\left\lvert \frac{L_r' g}{U_o} \right\rvert \ll L_p'^2$ $\lvert gL_v' \rvert \ll \lvert L_p'^3 \rvert$
JL	1	$\frac{1}{T_s} \doteq -N_r'\left[1 + \frac{U_o}{g}\left(N_p' - \frac{N_v' L_p'}{L_v'}\right) - \frac{L_r' N_v'}{N_r' L_v'}\right]$ $\frac{1}{T_R} \doteq -L_p' - \frac{gL_v'}{L_p'^2}$ $2\zeta_d\omega_d \doteq -Y_v + \frac{gL_v'}{L_p'^2}$ In hover, a better approximation is: $2\zeta_d\omega_d \doteq -Y_v - \frac{L_p'}{4} - \sqrt{\frac{L_p'^2}{16} + \frac{gL_v'}{2L_p'}}$ $\omega_d^2 \doteq \frac{-gL_v' + U_o(L_v' N_p' - N_v' L_p')}{-L_p' - \frac{gL_v'}{L_p'^2}}$	

TABLE A-IV (Contd.)

	FIRST COEFF.	APPROXIMATE FACTORS	CONDITIONS OF VALIDITY
KK	L'_{δ_a}	$2\zeta_\phi\omega_\phi \doteq -N'_r - Y_v$ $\omega_\phi^2 \doteq U_o N'_v + Y_v N'_r - \frac{N'_{\delta_a}}{L'_{\delta_a}}(L'_v U_o)$	$Y_{\delta_a} = 0$
KL	L'_{δ_a}	$2\zeta_\phi\omega_\phi \doteq -N'_r - Y_v$ $\omega_\phi^2 \doteq U_o N'_v$	$\lvert Y_{\delta_a} L'_r\rvert \ll \lvert U_o L'_{\delta_a}\rvert$ $(-Y_v - N'_r)^2 < \lvert 4U_o N'_v\rvert$ For $U_o \doteq 0$, use exact expression NN
KM	L_{δ_a}	$\frac{1}{T_{\phi_1}T_{\phi_2}}$ or $\omega_\phi^2 \doteq U_o N_v + Y_v N_r$ $\frac{1}{T_{\phi_1}} + \frac{1}{T_{\phi_2}}$ or $2\zeta_\phi\omega_\phi \doteq -Y_v - N_r$	$\lvert N_{\delta_a} I_{xz}\rvert \ll \lvert L_{\delta_a} I_x\rvert$ $\left\lvert \frac{Y_{\delta_a}}{L_{\delta_a}}\left(L_v + \frac{I_{xz}}{I_x}N_v\right) + \frac{N_{\delta_a}}{L_{\delta_a}}\left(L_r - \frac{I_{xz}}{I_x}Y_v\right)\right\rvert \ll \lvert N_r + Y_v\rvert$ $\lvert Y_{\delta_a}(L_r N_v + L_v N_r) - N_{\delta_a}(U_o L_v + Y_v L_r)\rvert \ll \lvert L_{\delta_a}(U_o N_v + Y_v N_r)\rvert$ For $U_o \doteq 0$, use $\frac{1}{T_{\phi_1}} \doteq -N_r$, $\frac{1}{T_{\phi_2}} \doteq -Y_v + \left(\frac{Y_{\delta_a}}{L_{\delta_a}}\right) L_v$
LL	$Y_{\delta_a}N'_v + L'_{\delta_a}N'_p$	$2\zeta_r\omega_r \doteq \frac{Y_{\delta_a}(L'_v N'_p - N'_v L'_p) - L'_{\delta_a} Y_v N'_p}{L'_{\delta_a}N'_p + Y_{\delta_a}N'_v}$ $\omega_r^2 \doteq g\frac{L'_{\delta_a}N'_v}{L'_{\delta_a}N'_p + Y_{\delta_a}N'_v}$	Expressions are exact for $N_{\delta_a} = 0$ $N_{\delta_a} \neq 0$ introduces third root and changes first coefficient to N_{δ_a}
LM	N'_{δ_a}	$\frac{1}{T_r} \doteq \left[g\left(-L'_v + N'_v\frac{L'_{\delta_a}}{N'_{\delta_a}}\right)\right]^{1/3}$ $\omega_r \doteq \lvert 1/T_r\rvert$ $\zeta_r \doteq 0.5$ for $1/T_r < 0$ $\zeta_r \doteq -0.5$ for $1/T_r > 0$	$\frac{L_p}{N_p} \doteq \frac{L_{\delta_a}}{N_{\delta_a}}$

TABLE A-IV (Contd.)

	FIRST COEFF.	APPROXIMATE FACTORS	CONDITIONS OF VALIDITY
MM	$-U_o N'_{\delta_a}$	$2\zeta_v\omega_v \doteq \frac{L'_{\delta_a}}{N'_{\delta_a}}\left(N'_p - \frac{g}{U_o}\right) = \frac{1}{T_{v_1}} + \frac{1}{T_{v_2}}$ $\omega_v^2 \doteq \frac{g}{U_o}\left(\frac{L'_{\delta_a}}{N'_{\delta_a}} N'_r - L'_r\right) = \frac{1}{T_{v_1}}\frac{1}{T_{v_2}}$	$Y_{\delta_a} = 0$, $N'_{\delta_a} \neq 0$ For hover, if $N'_{\delta_a} = 0$, first coefficient $= gL'_{\delta_a}$, $\frac{1}{T_v} = -N'_r$
MM	L'_{δ_r}	$\frac{1}{T_{\varphi_1}} + \frac{1}{T_{\varphi_2}}$ or $2\zeta_\varphi\omega_\varphi \doteq -(N'_r + Y_v) + \frac{N'_{\delta_r}}{L'_{\delta_r}} L'_r + \frac{Y_{\delta_r}}{L'_{\delta_r}} L'_v$ $\frac{1}{T_{\varphi_1}}\frac{1}{T_{\varphi_2}}$ or $\omega_\varphi^2 \doteq -\frac{N'_{\delta_r}}{L'_{\delta_r}}(L'_v U_o + Y_v L'_r) + (Y_v N'_r + U_o N'_v) + \frac{Y_{\delta_r}}{L'_{\delta_r}}(L'_r N'_v - L'_v N'_r)$	None; this is exact expression
MP	L'_{δ_r}	$2\zeta_\varphi\omega_\varphi \doteq -Y_v - N'_r + \frac{N'_{\delta_r}}{L'_{\delta_r}} L'_r$ $\omega_\varphi^2 \doteq U_o N'_v + \frac{Y_{\delta_r}}{L'_{\delta_r}} L'_v N'_r - \frac{N'_{\delta_r}}{L'_{\delta_r}} U_o L'_v$	$\lvert Y_{\delta_r} L'_v \rvert \ll \lvert N'_{\delta_r} L'_r + L'_{\delta_r}(Y_v + N'_r) \rvert$ $2\zeta_\varphi\omega_\varphi$ is given by small difference between $-Y_v - N'_r$ and $\frac{N_{\delta_r}}{L_{\delta_r}} L'_r$; hence, accuracy is low for small ζ
PP	N'_{δ_r}	$\frac{1}{T_r} \doteq -L'_p$ $\omega_r^2 \doteq -\frac{g}{L'_p}\left(-L'_v + \frac{L'_{\delta_r}}{N'_{\delta_r}} N'_v\right)$ For single rotor, $2\zeta_r\omega_r \doteq 0$ For tandem rotor, $\doteq -Y_v + \frac{\omega_r^2}{L'_p}$	$\lvert L'_p \rvert \gg \left\lvert \frac{L'_{\delta_r}}{N'_{\delta_r}} N'_p + \frac{Y_{\delta_r}}{N'_{\delta_r}} N'_v \right\rvert$ $Y_{\delta_r} \doteq 0$ $\left\lvert \frac{1}{T_r} \right\rvert \gg \omega_r$ $\left\lvert \frac{1}{T_r} \right\rvert \gg \lvert 2\zeta_r\omega_r \rvert$
QQ	Y_{δ_r}	$\frac{1}{T_{v_3}} \doteq -L'_p - N'_r - \frac{U_o N'_{\delta_r}}{Y_{\delta_r}}$ $\frac{1}{T_{v_1}}\frac{1}{T_{v_2}}$ or $\omega_v^2 \doteq \frac{gT_{v_3}}{Y_{\delta_r}}(-L'_{\delta_r} N'_r + L'_r N'_{\delta_r})$ $\frac{1}{T_{v_1}} + \frac{1}{T_{v_2}}$ or $2\zeta_v\omega_v \doteq T_{v_3}\left[(L'_p N'_r - L'_r N'_p) + \frac{U_o}{Y_{\delta_r}}(L'_p N'_{\delta_r} - L'_{\delta_r} N'_p) - \omega_v^2\right]$	$\left\lvert \frac{1}{T_{v_3}} \right\rvert \gg \left\lvert \frac{1}{T_{v_1}} \right\rvert$ $\left\lvert \frac{1}{T_{v_3}} \right\rvert \gg \left\lvert \frac{1}{T_{v_2}} \right\rvert$

TABLE A-IV (Contd.)

	FIRST COEFF.	APPROXIMATE FACTORS	CONDITIONS OF VALIDITY
QR	Y_{δ_r}	$\frac{1}{T_{v_1}} \doteq 0$ $\frac{1}{T_{v_2}} + \frac{1}{T_{v_3}} \doteq -L'_p - \frac{U_o N'_{\delta_r}}{Y_{\delta_r}}$ $\frac{1}{T_{v_2}} \frac{1}{T_{v_3}} \doteq \left[L'_p N'_r - L'_r N'_p - \frac{L'_{\delta_r}}{Y_{\delta_r}} (U_o N'_p - g) + \frac{N'_{\delta_r}}{Y_{\delta_r}} U_o L'_p \right]$	$U_o \neq 0$ $\left\lvert \frac{1}{T_{v_1}} \right\rvert \ll \frac{1}{T_{v_2}}$ $\left\lvert \frac{1}{T_{v_1}} \right\rvert \ll \frac{1}{T_{v_3}}$
QS	$-U_o N'_{\delta_r}$	$\frac{1}{T_{v_1}} + \frac{1}{T_{v_2}} \doteq -\left[L'_p + \frac{L'_{\delta_r}}{N'_{\delta_r}} \left(\frac{g}{U_o} - N'_p \right) \right]$ $\frac{1}{T_{v_1}} \frac{1}{T_{v_2}} \doteq -\left[\frac{g}{U_o} \left(L'_r - \frac{L'_{\delta_r}}{N'_{\delta_r}} N'_r \right) \right]$	$Y_{\delta_r} = 0$, $U_o \neq 0$ (but valid for $U_o \doteq 0$) At $U_o = 0$, numerator becomes first-order: $g\left[L'_{\delta_r} (s - N_r) + L'_r N'_{\delta_r} \right]$

APPENDIX B

ESTIMATION OF HOVER DERIVATIVES BY MOMENTUM THEORY

"Momentum theory" is the name given to that theory which predicts aerodynamic forces by considering the behavior of certain stream tubes of finite cross section. The most familiar application of momentum theory is the actuator disk theory of propeller performance. In this application it gives surprisingly accurate results, because the stream tube hypothesis corresponds closely to the physical slipstream. Momentum theory has also been used to calculate the forces on fixed wings, helicopter and autogiro rotors, ducts, ducted fans, and wing-propeller combinations. In these applications the stream tube does not correspond so obviously to the physical flow, but good results have been obtained when a satisfactory choice was made for the cross-sectional area of the hypothetical stream tube.

In this appendix we explore the application of momentum theory to the calculation of stability derivatives for hovering vehicles. It is found that most hover derivatives can be derived with sufficient accuracy for stability calculations. Momentum theory usually fails when large separated flows are present, or when structural flexibility due to hinged rotors is important, though even for hinged rotors momentum theory gives certain derivatives quite accurately.

This appendix is divided into the following parts:

1. u-Derivatives for a Ducted Fan
2. u-Derivatives for an Unshrouded Propeller
3. w-Derivatives for an Unshrouded Propeller
4. w-Derivatives for a Ducted Fan
5. q-Derivatives for Ducted and Unshrouded Propellers

Whenever possible, comparisons of the theoretical results are made with experimental data.

1. u-Derivatives for a Ducted Fan

Consider a ducted-fan vehicle moving very slowly forward with the ducts vertical, Sketch 1:

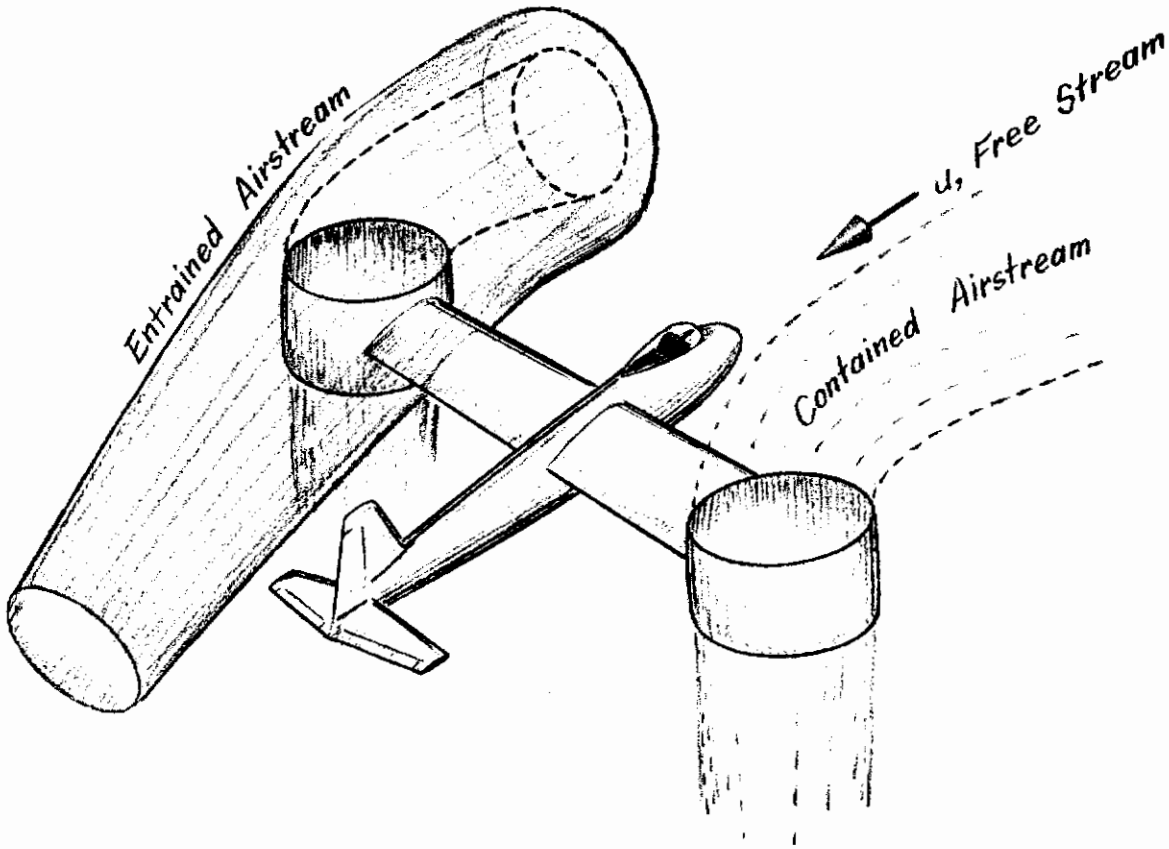

Sketch 1. Stream Tube Concept for a Ducted-Fan Vehicle Near Hover

The wings, fuselage, and tail are assumed to be nonlifting to simplify the analysis. Let us split the airflow into three parts — (a) that part which goes through the ducts (contained airstream), (b) an assumed stream tube which is deflected downward by an entrainment process (entrained airstream), and (c) a part which is unaffected by the ducts (free stream). Note that the contained airstream exists physically; the entrained stream tube is a hypothesis of momentum theory, since, actually, the region of entrainment is infinite.

The change per second in vertical momentum of the contained stream tube is

$$\underbrace{\underbrace{(\rho A_e V_e)V_e}}_{\text{contained mass flow}}$$

where A_e = the total duct exit area

V_e = the through-flow velocity at A_e

Making the reasonable assumption that the jet is at atmospheric pressure, this change in vertical momentum per second is equal to the total lift exerted on the propeller, stator blades, and ducts:

$$L = (\rho A_e V_e)V_e \tag{B-1}$$

The change in horizontal momentum per second equals the drag:

$$D = (\rho A_e V_e)u \tag{B-2}$$

We can differentiate these expressions with respect to u to obtain the contribution of the contained airstream to X_u and Z_u:

$$mZ_u = -2\rho A_e V_e \frac{\partial V_e}{\partial u} \tag{B-3}$$

$$mX_u = -\rho A_e \left(V_e + u \frac{\partial V_e}{\partial u}\right) \tag{B-4}$$

To determine the value to be assigned to $\partial V_e/\partial u$, let us first consider the case of constant power, although later we shall have to consider constant rpm. Constant power is the simplest case to handle analytically since it is tractable by momentum theory. The energy contained in the mass of air that flows into the duct in unit time is

$$E_1 = \frac{1}{2}(\rho A_e V_e)u^2 \tag{B-5}$$

and the outflow energy is

$$E_2 = \frac{1}{2}(\rho A_e V_e)V_e^2 \qquad \text{(B-6)}$$

Hence, the power is given by

$$P = \frac{1}{2}\rho A_e V_e(V_e^2 - u^2) \qquad \text{(B-7)}$$

The shaft power will exceed this by a factor determined by the fan efficiency, which we shall assume is unchanged by the u-perturbation. For constant power $\partial P/\partial u = 0$, hence

$$\frac{\partial P}{\partial u} = \frac{1}{2}\rho A_e \frac{\partial}{\partial u}(V_e^3 - V_e u^2)$$

$$= \frac{1}{2}\rho A_e \left[\frac{\partial V_e}{\partial u}(3V_e^2 - u^2) - 2V_e u\right] = 0 \qquad \text{(B-8)}$$

$$\frac{\partial V_e}{\partial u} = \frac{2V_e u}{3V_e^2 - u^2} \doteq \frac{2}{3}\frac{u}{V_e} \qquad \text{(B-9)}$$

Substituting from Eq B-9 in Eqs B-3 and B-4,

$$mZ_u = -\frac{4}{3}\rho A_e u \qquad \text{(B-10)}$$

Thus, in the equations of motion $Z_u u$ is second-order; hence, Z_u can be neglected.

$$mX_u = -\rho A_e\left(V_e + u\frac{2}{3}\frac{u}{V_e}\right) \qquad \text{(B-11)}$$
$$= -\rho A_e V_e, \text{ neglecting second-order terms}$$
$$= -\text{mass flow}$$

Thus, considering the contained mass flow alone has led us to the conclusions

$$Z_u = 0 \qquad \text{(B-12)}$$

$$X_u = \frac{-\text{ mass flow}}{\text{airplane mass}} = \frac{-\rho A_e V_e}{m} \qquad \text{(B-13)}$$

Since the drag results from the turning of the flow into the ducts, it should be felt as a pressure around the duct lip. Thus, M_u is determined by X_u and the height of the duct lip above the c.g.

$$M_u = -\frac{m}{I_y} X_u h_D$$

How does the entrained mass flow affect these values? The answer to this question cannot be found by momentum theory. Indeed, as far as the writer is aware, no theoretical solution has been published. However, considerable experimental evidence exists to indicate that the forces due to entrained air (i.e., airflow that does not pass through the actuator disk) are negligible in hover for most configurations. In support of this assertion we quote the following experimental data:

a. For the Bell X-22 quad-tilt-duct configuration in hover, Fig. 84 of Ref. 16 compares the total lift on the configuration including stub wings with the total thrust on the ducts and propellers. The difference is negligible.

b. For jet flap configurations at very high C_L, the resultant force approaches the jet momentum per second, indicating that the entrainment lift is very small (Refs. 30 and 31).

c. The numerous NASA tests on tilt-wing and deflected-slipstream vehicles show that in hover the total aerodynamic force approaches the propeller thrust. Usually the resultant force is less than the propeller thrust, due mainly to wing skin friction losses; in one or two instances the resultant aerodynamic force was a few percent in excess of the propeller thrust in the absence of the wing (see, for example, Ref. 32), but this was due to the wing removing swirl from the propeller slipstream, and would not have occurred with a more efficient propeller.

In addition to the above experimental data, two theoretical methods of calculating the lift and drag of wing-plus-propeller or ducted-fan configurations have been published. Kuhn in Ref. 19 uses momentum theory to calculate the aerodynamic forces on a slipstreamed wing, and the Lippisch method (see the Appendix of Ref. 33) is used to calculate the lift and drag of a ducted-fan ("aerodyne") configuration. The Kuhn and Lippisch methods both predict zero force due to entrained flow at hover.

It is only fair to mention a counterexample to these, i.e., the Lockheed "Hummingbird" configuration (Ref. 34). This configuration uses a unique "ejector" system to entrain air past the efflux of the jet engines. However, this is rather a special configuration and one would not attempt to apply inviscid flow theory to a configuration which depends so fundamentally on viscous effects.

On this basis we can calculate the derivatives of a configuration such as the Doak VZ-4, assuming that the forces and moments are due to effects of the appropriate perturbation on the contained airflow, plus the separate effects of the perturbation on the unpowered airframe. As we shall see in the next section, this assumption gives good agreement with experimental results except where separation effects are significant.

As one final modification to the X_u and M_u expressions, we note that for a hovering vehicle

$$L = mg = \rho A_e V_e^2$$

or

$$V_e = \sqrt{\frac{mg}{\rho A_e}}$$

Consequently,

$$X_u = -\sqrt{\frac{\rho g A_e}{m}}$$

$$M_u = \frac{m h_D}{I_y}\sqrt{\frac{\rho g A_e}{m}} = \frac{h_D}{k_y^2}\sqrt{\frac{\rho g A_e}{m}}$$

where k_y = pitch radius of gyration

Let us now compare the theory and experimental data. Table B-I summarizes the experimental data reviewed. Most of the data were not useful because they did not apply to hover conditions. References 37 and 49 contain summaries of other reports not listed in Table B-I. The configurations tested were either isolated ducted fans or configurations of the Doak or Bell X-22 types. A few other references exist on fan-in-fuselage or fan-in-wing configurations, but these were not included as it was felt that the effects of entrained flow would probably be important for such configurations and the applicability of momentum theory correspondingly smaller.

TABLE B-I

REFERENCES EXAMINED FOR DATA ON DUCTED FAN DERIVATIVES AT HOVER

REF. NO.	REPORT	COMMENTS
16	Bell Aerosystems Rept. 2127-917003 by Michaels and Hesby	Stability and control estimates and test data on several versions of the X-22. On p. 107, "L_u" and "D_u" quoted are not true partial derivatives. On pp. 149 and 151, summarized hover derivatives are inconsistent, e.g., $I_y M_u \neq -I_x L_v$. Not clear whether hover data are experimental or theoretical. Not used.
35	NASA TN 3547 by Parlett	Forces and moments on crude 18" diameter ducted propeller with various lip radii. Derivatives can be found for 0 to 90° duct angles at $0 < U_o < 60$ ft/sec. Used.
36	Doak Aircraft Company Rept. DS-215 by Reichert and Ulyate	Time histories of hover oscillations. No hover derivatives. Not used.
37	Vidya Tech. Rept. 63-95 by Kriebel, Sacks, and Nielsen. Also reported in Ref. 66, J. Aircraft, July-Aug. 1964, by Kriebel.	Sophisticated theoretical method for calculating loads and derivatives on ducted fans of short chord/diameter ratio (< 0.4). This ratio is shorter than most tested ducts and perhaps because of this agreement of theory with test results on division of thrust T_{prop}/T_{duct} is only fair. No useful experimental data on hover derivatives. Theory has more potential than momentum theory, but is much more complicated.
38	NASA TN D-1257 by Grunwald and Goodson	Tests on Doak wing + fan. Shows that T_{prop}/T_{duct} is unaffected by u-perturbations in hover. Not useful for derivatives because of simultaneous variation of duct angle and wing angle of attack with V.
39	NASA TN D-616 by Parlett	Tests on ducts of 28" diameter, 9" and 12" chord. Propeller located at exist. Useful data on u-derivatives analyzed here. Separation effects were important, probably due to crude duct lip shape. Used.
40	IAS Paper 59-107 by Wattson and Hoehne	Extensive tests on ducted fans at forward speed. No data useful for hover derivatives. Not used.

Table B-I (Contd.)

REF. NO.	REPORT	COMMENTS
41	NASA TN D-2254 by Davenport and Spreemann	Tests on X-22 model. No hover data. Not used.
42	NASA TN D-372 by Tapscott and Kelley	Doak VZ-4 transition time histories. Data insufficiently complete for extraction of hover derivatives. Not used.
43	18th Annual AHS Forum paper by McKinney and Newsom	Summary of NASA wind tunnel tests on X-22. No hover data. Not used.
44	NASA TN D-785 by Yaggy and Goodson	Wind tunnel tests on Doak-type model. Shows effect of pitch trim flaps on trim. Trim data only. Derivatives cannot be extracted because no data on effect of perturbations one at a time. Not used.
45	NASA TN D-1481 by Newsom	Wind tunnel tests on X-22. No hover data. Not used.
46	NASA TN D-981 by Goodson and Grunwald	Wind tunnel tests on Doak VZ-4. No hover data. Not used.
47	NASA TN D-1301 by Mort and Yaggy	Wind tunnel tests on Doak. Data on fan performance in axial flow $0 < J < 0.6$. Used here to get Z_w. (Other data used extensively in Ref. 2 to get derivatives in speed range 60 – 120 ft/sec.)
2	STI TR-128-1 by Wolkovitch and Walton	Appendix A presents Doak derivatives for 60 – 120 ft/sec calculated from test data and hover derivatives calculated by momentum theory without detailed justification. Doak periods and dampings predicted.
48	Aerospace Engineering, July 1962, article by Ritter and Ordway	Very sophisticated theory allows for finite number of blades. Assumes axial flow, zero duct thickness. Not clear whether theory remains applicable in hover. Much more complicated than momentum theory.
49	Progress in Aeronautical Sciences, Vol. 3, by Sacks and Burnell	Extremely complete. Review of ducted fan theory and experiments up to 1962.

The only data of real use for our present purpose were Refs. 35, 39, and 47. The configurations tested in Refs. 35 and 39 are illustrated in Fig. B-1. The configuration of Ref. 47 is of the Doak type; the test data permitted only the extraction of w-derivatives. The isolated ducted fan of Ref. 39 is rather unusual in that the fan is located at the exit of the duct. The effect of this on the static thrust efficiency may be adverse, because according to simple momentum theory the increased static thrust/power of a ducted fan compared to an unducted fan is due to the duct suppressing the contraction of the slipstream (see Ref. 49).

The isolated ducted fan of Ref. 35 is of a more orthodox configuration, with a chord/diameter of 0.67. However, the duct is rather crude compared with full-scale practice, being a straight, untapered tube and having a very "unstreamlined" nacelle. In addition, the lip radius employed in the tests useful for our present purposes was quite small, and separations were undoubtedly present.

Although none of the individual configurations of Refs. 35, 39, and 47 were completely suitable for purposes of correlating experimental with theoretical derivative data, by assembling pieces of information from each one can reach conclusions regarding the validity of momentum theory for calculating derivatives.

Let us commence by checking on the expression for X_u (Eq B-13). This has been derived assuming constant power. The relation between power and rpm for a vertical ducted-fan in a uniform flow of 2.1 and 6.1 knots has been studied in Ref. 39. The results are replotted in Fig. B-2. We see that for the forward speeds tested, power was proportional to $(\text{rpm})^3$ and essentially independent of forward speed.

It seems reasonable to extrapolate this result down to zero forward speed, since at hover it can be shown by dimensional analysis that power varies as $(\text{rpm})^3$ if Reynolds number and Mach number effects are unimportant. We can form an estimate of the range of validity of this relation by scaling the model tests of Ref. 39 as follows:

Typical lift value at 6.1 knots and 900 rpm = 6.0 lb

From momentum theory, hover lift = $\rho A_e V_e^2$

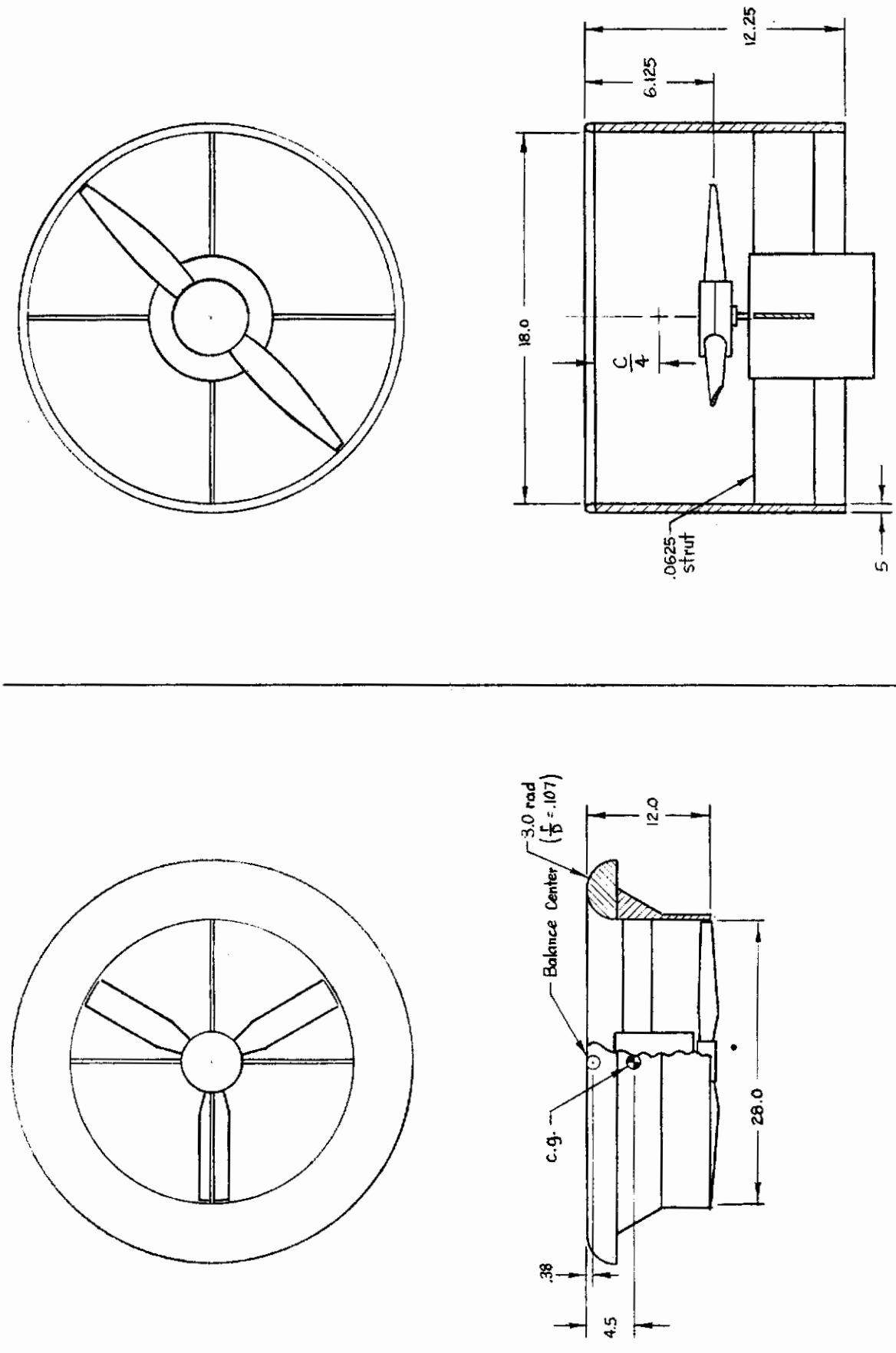

Figure B-1. Configuration of Ref. 39 and Configuration of Ref. 35

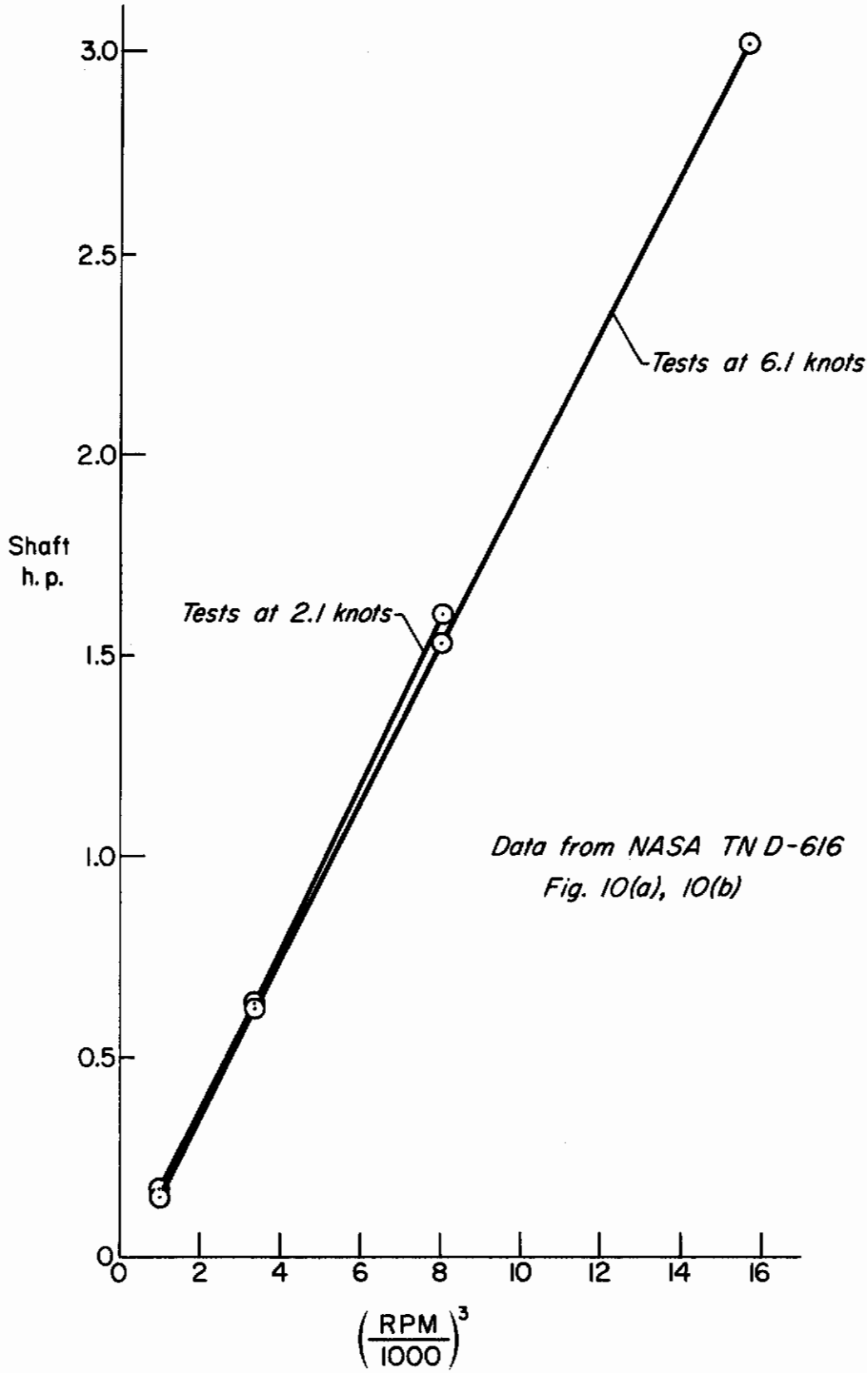

Figure B-2. Power Versus $(rpm)^3$ at Two Forward Speeds for Ducted Fan of Ref. 35

Therefore, $V_e = 24.5$ ft/sec

$$\frac{U_o}{V_e} = \frac{10.3}{24.5} = 0.42$$

This suggests that, for an isolated vertical ducted fan, power varies as rpm^3 for speeds far exceeding those associated with small perturbations in u. Hence, we conclude that the power–rpm relationship is essentially unaffected by u-perturbations; thus Eq B-13, which has been derived for constant power, applies equally to constant rpm. With this conclusion we may now check the X_u and Z_u predicted by momentum theory against experimental results obtained at constant rpm.

Figure B-3 summarizes the forward speed test data on a vertical duct given in Ref. 35. The slope of the drag-velocity graph, according to momentum theory, should be $D_u = \rho A_e V_e$. Assuming a constant lift of 6.1 lb ($= \rho A_e V_e^2$) gives $V_e = 38.1$ ft/sec. With this V_e, $D_u = 0.16$ lb sec/ft. The measured value is 0.20 lb sec/ft. In view of the crude nature of the duct and the existence of considerable separation around the duct lip (noted in Ref. 35) this agreement is about as good as one can expect.

So much for drag. The pitching moment displays a nonlinear trend with forward speed, peaking at 20 ft/sec. This is believed to be due to separation effects and, in any case, is outside the range of u/V_e appropriate to small perturbations from hover. Therefore we shall consider only the lower speed values, for which pitching moment in pound feet is 0.175 times measured drag in pounds, or 0.219 times predicted drag. Now according to momentum theory, the drag results from the turning of the airflow into the duct. This drag should therefore act close to the lip of the duct. Its moment arm should therefore be slightly less than the distance from the moment center to the top of the duct lip. This distance was 0.255 ft in the tests of Ref. 35. Subtracting the lip radius of 0.5 in. gives a suggested moment arm of 0.213 ft. This is in close agreement with the ratio

Measured pitching moment/theoretical drag = 0.219 ft

and again in fair agreement with

Measured pitching moment/measured drag = 0.175 ft

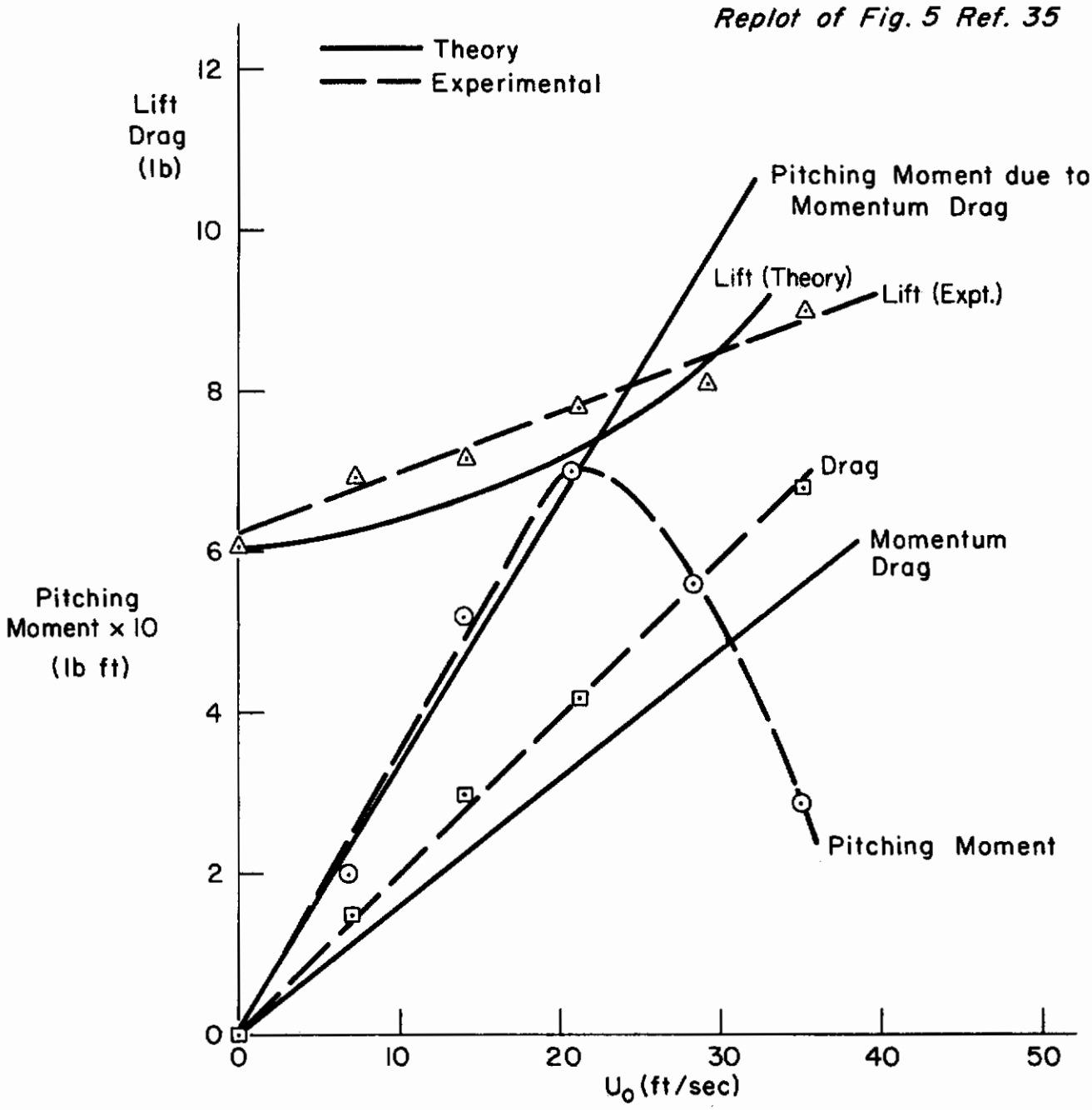

Figure B-3. Comparison of Experimental and Theoretical Lift, Drag, and Pitching Moment on Isolated Vertical Ducted Fan

On the basis of these results it appears that momentum theory can predict hovering X_u and M_u with fair accuracy.

However, we note that the measured Z_u is nonzero, whereas as predicted by momentum theory (Eq B-10) it should be second-order for small perturbations. How far is the discrepancy due to violation of the small perturbation restriction? To answer this, let us calculate $\Delta L = \int_o^u \frac{\partial L}{\partial u}\, du = -m\int_o^u Z_u\, du$ at several forward speeds. Here,

$$-mZ_u = \frac{4}{3}\rho A_e u = 0.0055u$$

Integrating, the perturbations in lift are given by $\Delta L = 0.00275u^2$. This is graphed in Fig. B-3. It is seen that most of the experimental data points lie outside the small perturbation region of u, and allowing for this the agreement between actual and predicted lift is fair.*

It is concluded that momentum theory predicts the effects of u-perturbations on the ducted-fan configuration of Ref. 35 with accuracy sufficient for most stability and control calculations.

Turning now to the data of Ref. 39, it must be first pointed out that the configuration is very unusual in that the propeller is located right at the exit, i.e., the flow downstream of the propeller is not shrouded (see Fig. B-1). Since the increased thrust/power of a ducted-fan over an unshrouded propeller is due to the fact that the slipstream contraction is suppressed one would suspect that the configuration of Ref. 39 is relatively inefficient. From our viewpoint the data of Ref. 39 are less useful than those of Ref. 35 because

a. The unusual and possibly inefficient configuration does not correspond to current practice in duct design as exemplified by the Doak VZ-4 and Bell X-22.

b. The short chord/diameter ratio will tend to encourage nonuniform flow conditions across the actuator disk, thus invalidating the tacit assumption of momentum theory that the fan is uniformly loaded.

---

*Allowing for large perturbation (u^2), drag effects might also improve the fit of the drag data. However we are primarily interested in examining the accuracy of momentum theory at small perturbations rather than reconstructing all the results of Ref. 35.

c. It is uncertain how far the standard ducted-fan momentum theory applies to a configuration with the fan at the exit.

Despite these drawbacks, the tests of Ref.39 do reveal some interesting points when analyzed with a view to checking momentum theory estimates of derivatives.

Tests were conducted at two forward speeds, 2.1 knots and 6.1 knots, and a range of rpm. Now, the dimensionless parameters C_L, C_D, and C_M should be dependent only on Reynolds number, tip Mach number, and a tip-speed/forward-speed parameter $J_\Omega = U_o/\Omega D$. Thus, with data available at two speeds and several rpm we might be able to check for scale effects by graphing C_L versus J_Ω from data obtained at 2.1 knots and 6.1 knots, and seeing whether or not the graphs coincide. In fact, the overlap between the 2.1 knot and 6.1 knot data was not quite sufficient to allow this; nevertheless the results are suggestive. Figure B-4 illustrates the variation of C_L with J_Ω. The 2.1 knot results fair quite smoothly into the 6.1 knot results. By contrast, the drag and pitching moment curves (Fig. B-5) do not fair into each other smoothly Curiously enough the jump in drag appears to occur as Reynolds number increases. This is true whether one takes Reynolds number as being proportional to forward speed, U_o, or exit-flow speed, V_e (calculated by momentum theory).

Another striking feature of Fig. B-5 is the similarity of the drag and pitching moment curves, suggesting that the pitching moment arises through the mechanism of the drag acting at some point away from the moment center. Let us now investigate how well the predictions of momentum theory tally with these results.

Measured lift, drag, and pitching moment at 2000 rpm and 2.1 and 6.1 knots are graphed in Fig. B-6. As predicted by momentum theory, the change in lift is given by

$$\Delta L = \frac{2}{3}\rho A_e u^2 = 0.00675u^2$$

Thus, over a speed range of 10 ft/sec the lift change is only 0.675 lb. This is in agreement with the almost constant measured values graphed in Fig. B-6.

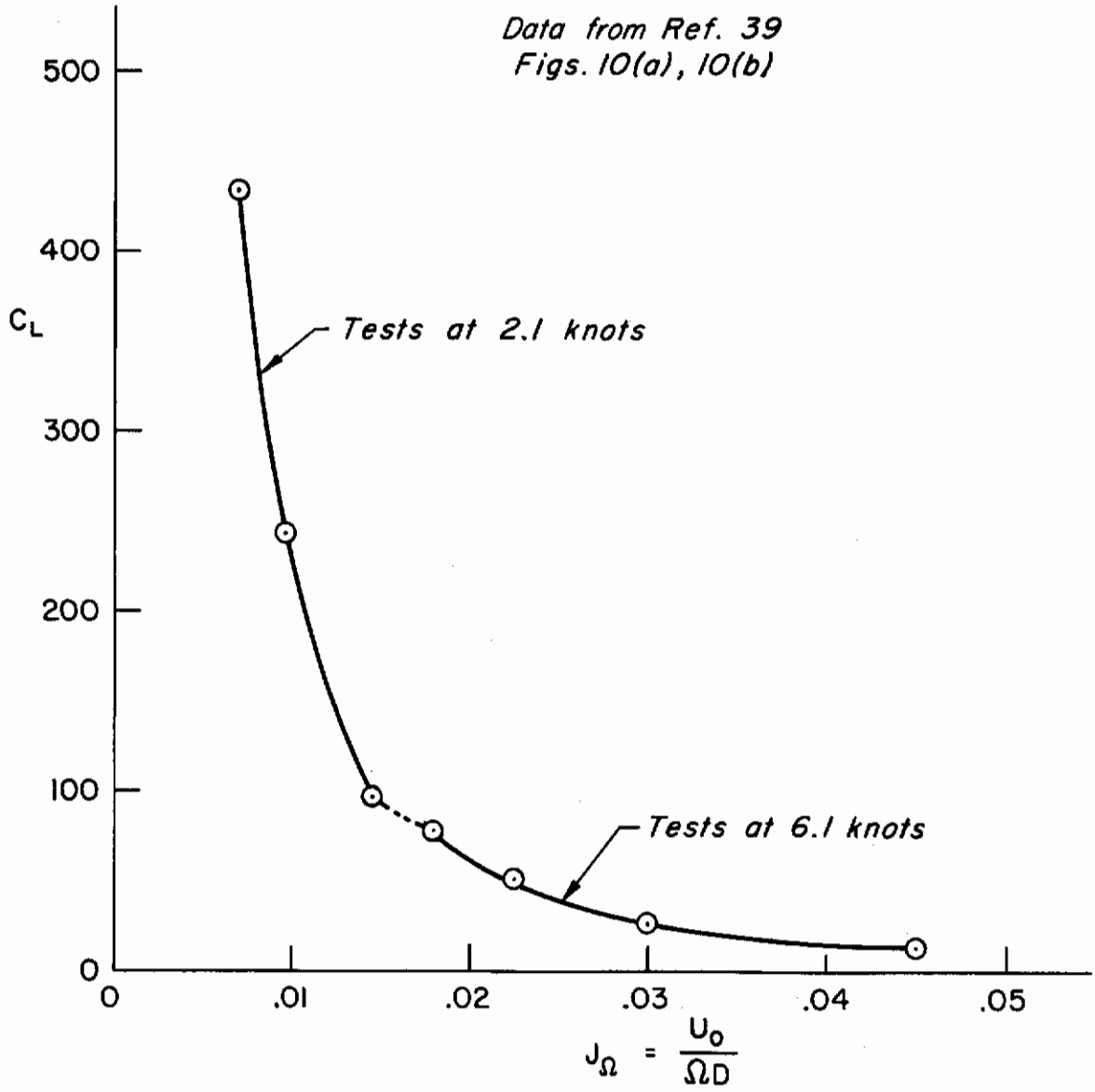

Figure B-4. Scale Effect on Lift Coefficient

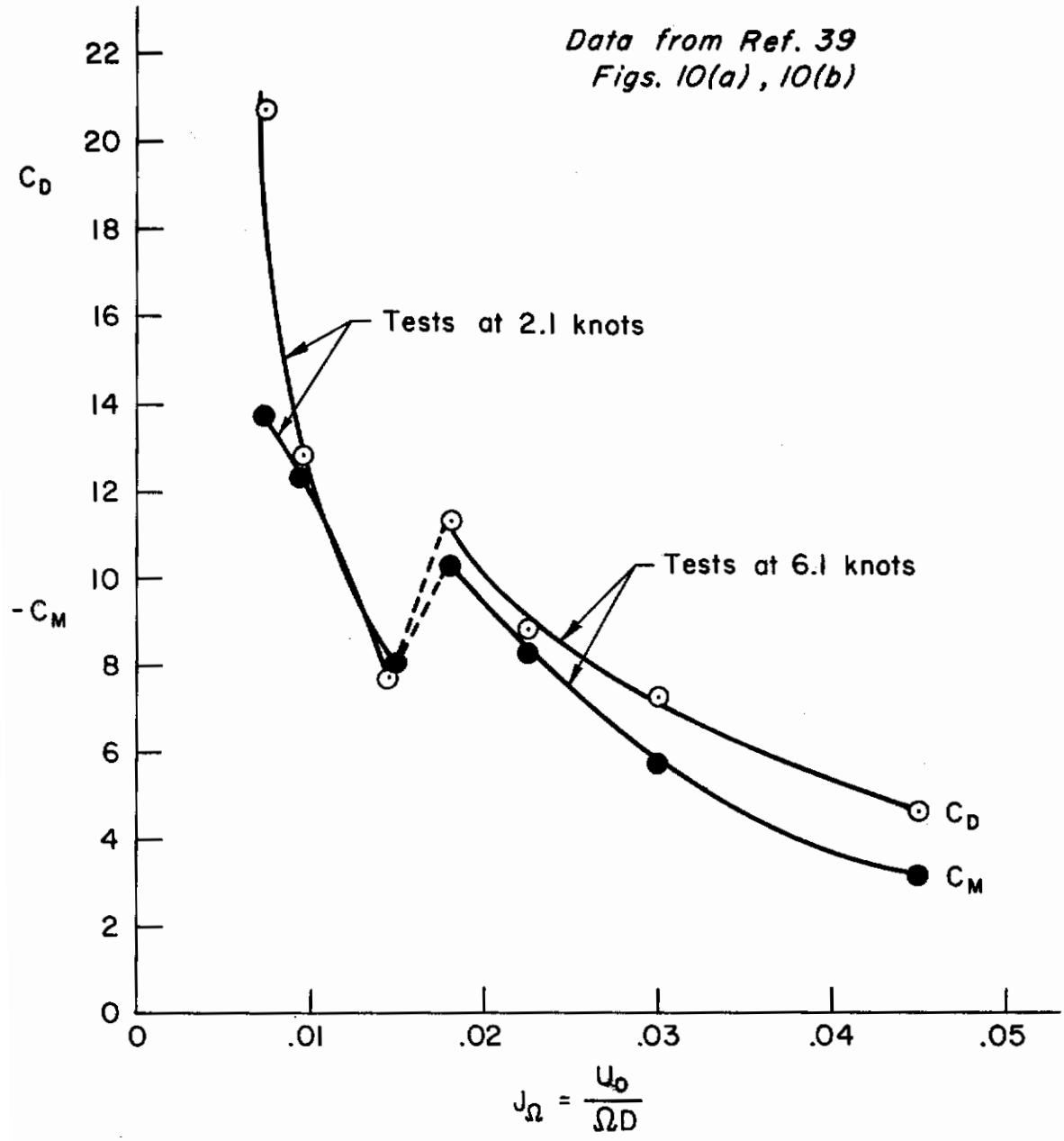

Figure B-5. Scale Effect on Duct Drag Coefficient and Pitching Moment

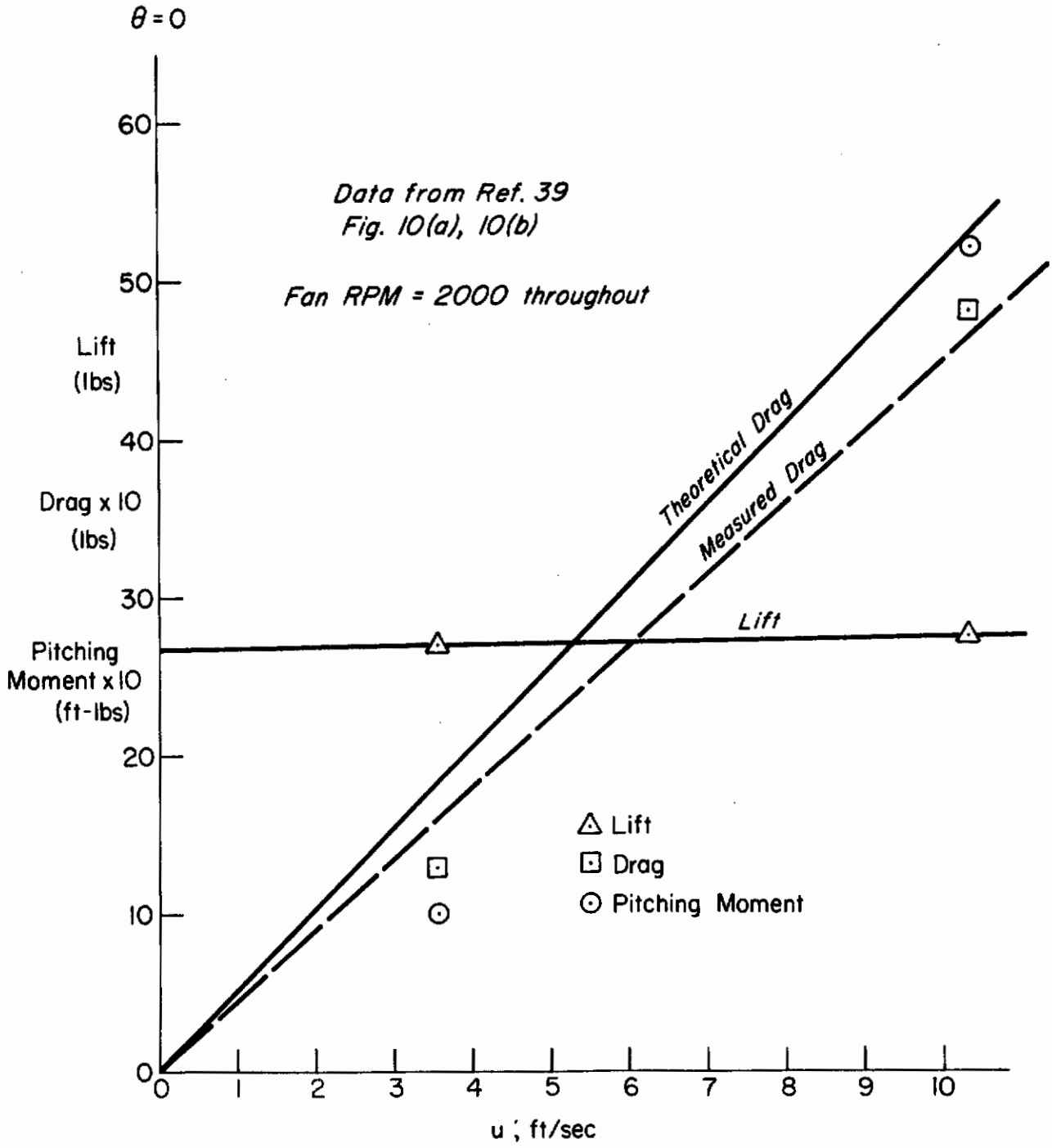

Figure B-6. Lift, Drag, and Pitching Moment on Ducted Fan of Ref. 39 for Small u-Perturbations from Hover

The drag has been calculated as before, assuming that there is no contraction of the slipstream. Thus, $V_e = (\text{lift}/\rho A_e)^{1/2}$. The momentum theory formula Drag = $\rho A_e V_e u$ gives quite good agreement with the measured values.

Assuming as before that the drag is centered one lip radius below the upper tip of the duct gives a moment arm of (3.00 - 0.38) = 2.62 in. = 0.218 ft below the balance center. Thus the pitching moment in pound feet should be -0.218 times the drag in pounds. In fact, the pitching moment is about equal to the drag in pounds. Thus, here, momentum theory fails to indicate the correct magnitude of the pitching moment and actually gives the wrong sign. This is very surprising, particularly in view of the successful prediction of drag and lift. Still more curious is the fact that the measured moment is nose-up; this would correspond to a drag force acting about the 1.0 ft above the top of the duct lip!

The explanation of this anomalous result appears to lie in the shape of the undersurface of the duct lip. It is believed that a large separated area existed in the downstream side, as sketched below. Similar pitch-up tendencies have been observed in many vehicles of the fan-in-wing and fan-in-fuselage type (see Refs. 50 and 51 for examples). Here, then, is an example of a case

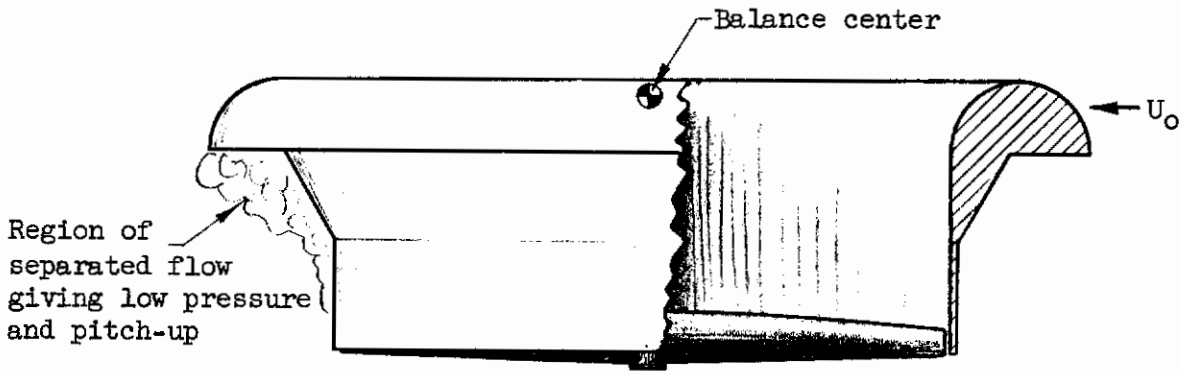

Sketch 2. Separated Region Beneath Aft Lip of Duct of Ref. 39

where entrained flow is important and momentum theory alone is inadequate (at least for pitching moment). This view is supported by other tests reported in Ref. 39, where the lip radius was decreased to 0.5 in., giving a duct shape as sketched below:

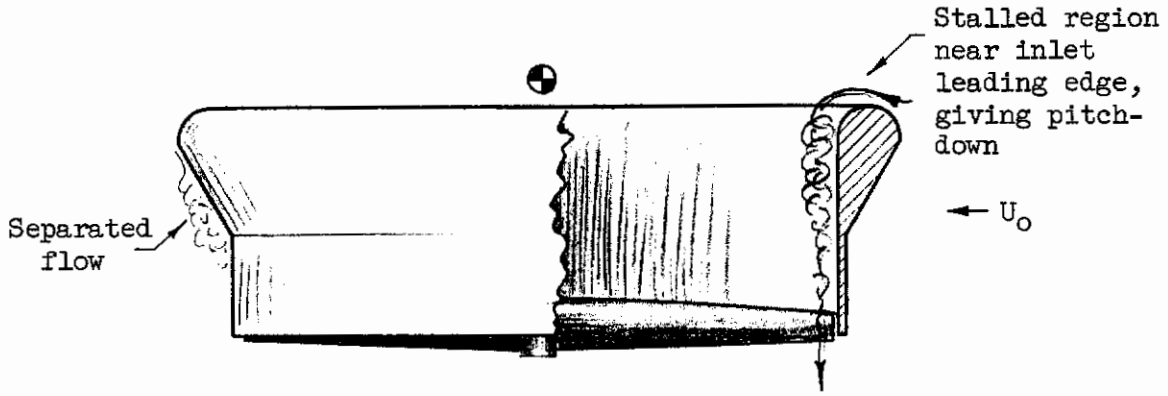

Sketch 3. Separated Region Inside Forward Lip of Duct of Ref. 39

Here, the measured ratio of pitching moment to drag was −0.025 ft, which is closer to the estimated value of −0.218 ft.* However, this pitching moment is still more nose-up than momentum theory predicts. As before, this discrepancy is ascribed to lee-side separations, but the discrepancy is smaller than previously because of the improved lip shape. This reduces flow separation and provides a smaller projected horizontal area for the low pressure to act on.

In Ref. 39 it is suggested that the discrepancy may be due to a region of stall near the leading edge. This may be a contributing factor, but it cannot be the sole reason because the loss of lift on the upwind side of the duct would cause the pitching moment to be more nose-down than the theory predicts. Similar lip-stalling appears to have occurred in the tests of Ref. 35, and Fig. B-5 suggests that the pitching moment was more nose-down when separation occurred. Separated flows around the duct lip are unlikely in full-scale vehicles because they induce undesirable lift losses, and therefore separations will be minimized by inlet slots, etc. It is less easy to obviate lee-side separations; these should be anticipated when applying momentum theory to full-scale configurations. Unfortunately, the currently available full-scale test data are insufficient to suggest any empirical correction factors to be applied to the theory.

*The change in lip radius did not affect this moment arm.

2. u-Derivatives for an Unshrouded Propeller

Momentum theory can be used to predict u-derivatives for unshrouded propellers, but it cannot account for flexibility and/or blade flapping effects which for most VTOLs and helicopters give the major contributions to X_u and M_u. Formulas for u-derivatives in terms of blade parameters are given in Refs. 52 and 53. The use of momentum theory to calculate drag on idealized helicopters is however described very clearly in Ref. 54, p. 17. References 55 and 56 are also of interest in this connection.

3. w-Derivatives for an Unshrouded Propeller

The calculation of the ideal thrust characteristics of propellers in axial flow is the most familiar application of momentum theory, and indeed the purpose for which momentum theory was originally developed by Rankine and Froude. Accounts of the use of momentum theory for this purpose are given in many standard texts (e.g., Refs. 57 and 58). However, the only rigorous account of which the writer is aware will be found in Ref. 59.

At or near hover special problems arise in the application of momentum theory. These problems consist of defining the stream tube area and ascertaining whether a slipstream exits at all. To apply momentum theory for typical VTOL flight conditions, it is necessary to have a good understanding of these points. Basic explanations will be found in Refs. 57, 58, and 60, but the clearest presentation is given in the rather inaccessible Ref. 61, so we feel that it is worthwhile repeating here in outline.

Figure B-7 illustrates the possible axial flows through an unshrouded rotor. Note that the ratio of climb velocity to through-flow velocity does not necessarily define the working state, because in some instances alternative working states are possible, depending on the torque on the propeller and its disk loading. From our viewpoint the particular interest centers on conditions close to hover. As indicated by Fig. B-7, for downward perturbation ($w > 0$) the rotor may enter the powered descent or vortex-ring region, whereas for upward velocity perturbations ($w < 0$) the rotor tends toward the normal "propeller" working state and a clearly defined slipstream exists, thus permitting the application of momentum theory.

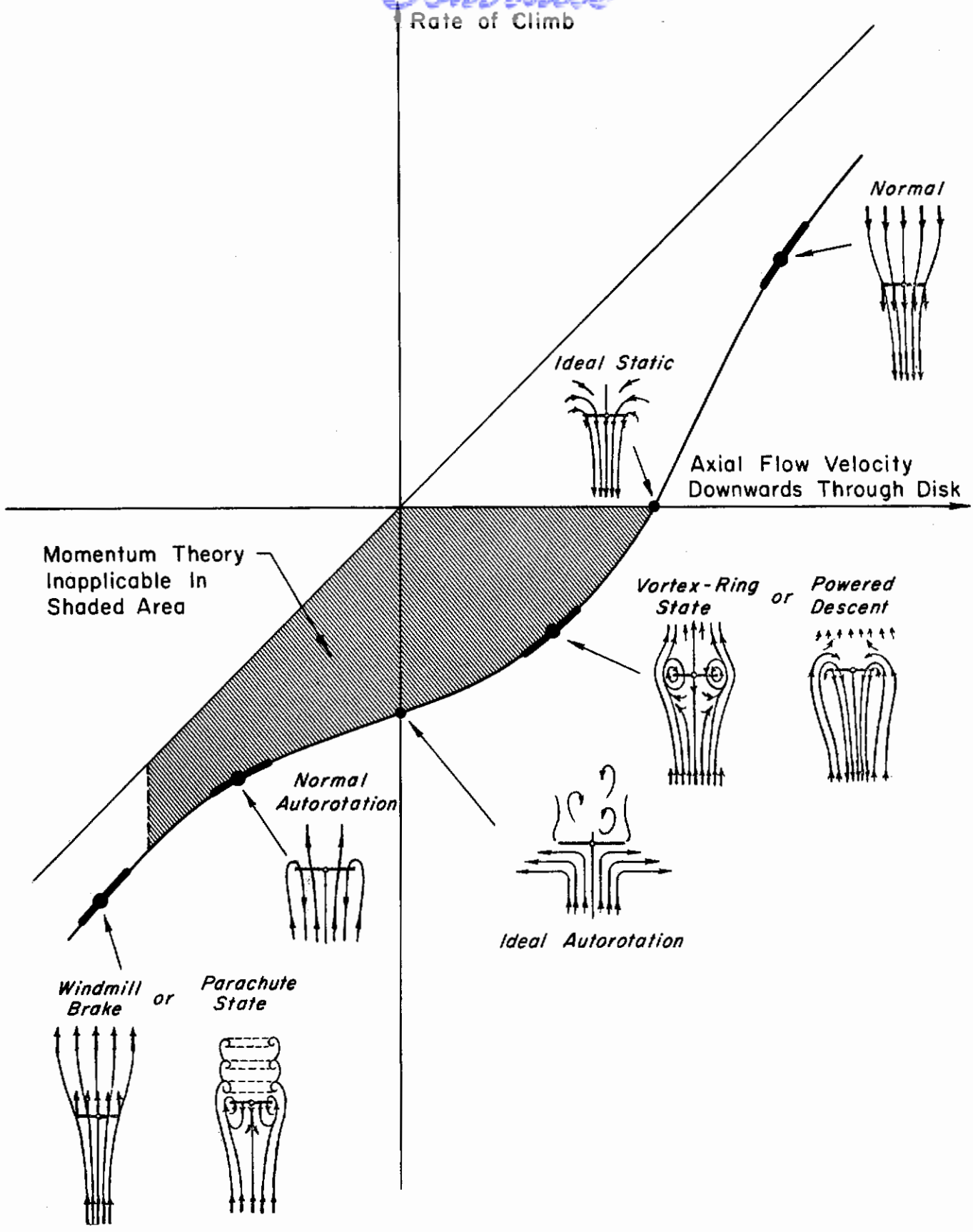

Figure B-7. Rotor Working States in Axial Flow

Actually the situation is not quite so simple. Understanding the transition from the climbing to the descending case demands more detailed consideration of the hovering situation. Although a definite slipstream exists in hover, the maximum area of the stream tube is less than the actuator disk area, due to a vortex ring formed at the tips of the propeller. The mechanism by which this arises is sketched below.

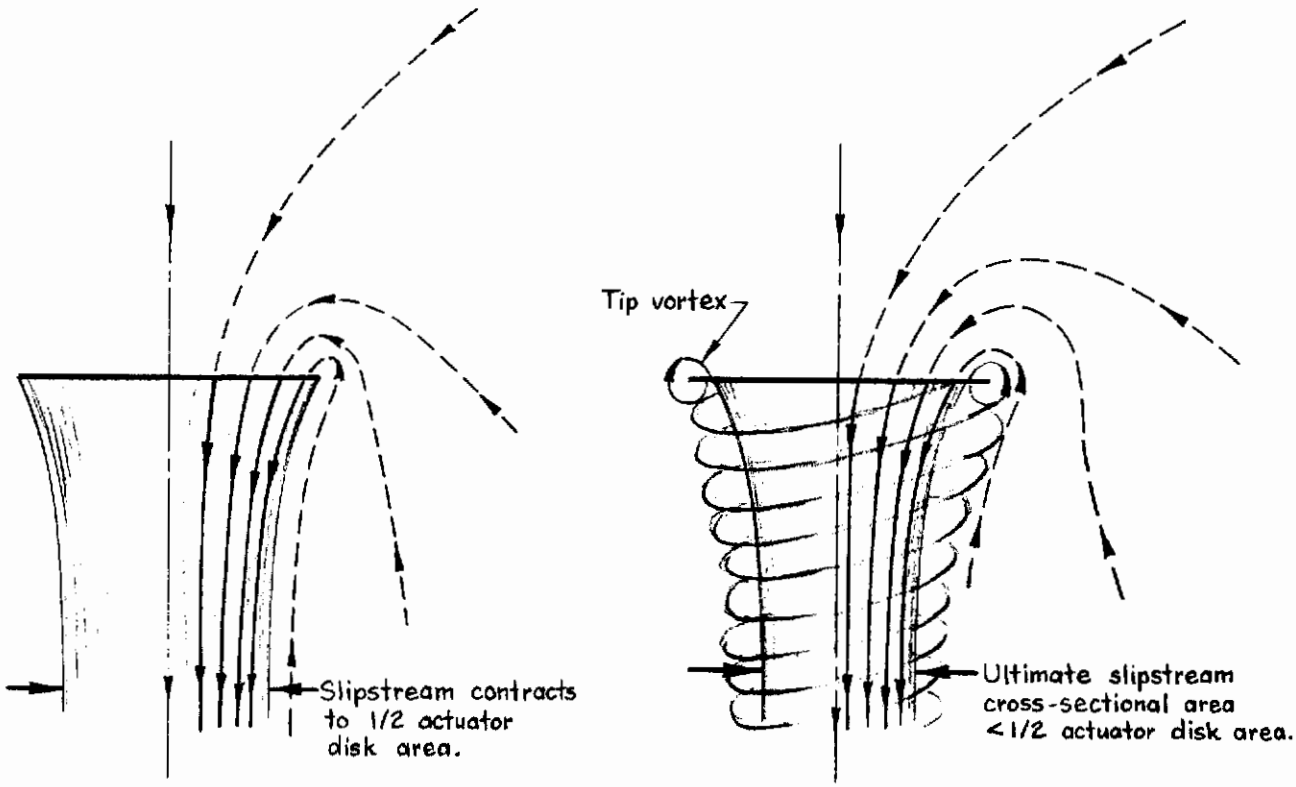

Ideal static streamlines Actual static streamlines

Sketch 4. Ideal and Actual Flow Through a Static Propeller

Due to viscosity the fluid cannot turn the sharp corner required to cross the tip of the actuator disk, and as a result vortices form on each blade tip. The vortex is continually shed and thus creates a tube of vorticity separating the high velocity slipstream from the almost static air just outside the slipstream. Air flows around the tip vortex in much the same way as it flows around the lip of a ducted-fan. The net result is that the effective

actuator disk area is decreased and the power required to produce a given static thrust increases. Typically this increase in power is of the order of 3 percent for a helicopter rotor (see p. 50 and p. 72 of Ref. 57). This corresponds to quite a small vortex and is well within the accuracy required for stability calculations. However, it should be noted that at high disk loadings the tip loss region increases. Ref. 57, p. 23, quotes an approximate formula for this effect:

$$B = 1 - \frac{\sqrt{2C_{T_\Omega}}}{b}$$

where B = a tip loss factor; blade elements outboard of radius BR are assumed to have profile drag but no lift

C_{T_Ω} = thrust coefficient = $T/\pi R^2 \rho(\Omega R)^2$

T = thrust
R = radius of rotor
Ω = rotor speed, rad/sec

b = number of blades

This gives $B \doteq 97$ percent for the Sikorsky H-19 single-rotor helicopter, and for the Curtiss X-19A VTOL, $B \doteq 90$ percent.

For purpose of calculating hover derivatives, we may therefore assume that a large tip vortex exists both at positive and at negative w perturbation velocities. At zero w it effectively changes the actuator disk area, as indicated by the above formula, but the size of the tip-loss region decreases for negative w, so it is not a simple matter to calculate its effect on Z_w.

Note that the vortex-ring flow regime is associated with large unsteady flows and oscillating loading with possibly positive average Z_w, which causes well-known difficulties in controlling helicopters at rates of descent exceeding about 400 ft/min. The rigidity of the rotor plays an important part in determining when the transition from "powered descent" to "vortex-ring" flow occurs. For disk loadings appropriate to VTOL it seems that the vortex-ring regime is not likely to be entered in small perturbations from hover. Figure B-8, based on data from Ref. 62, indicates that at small positive w

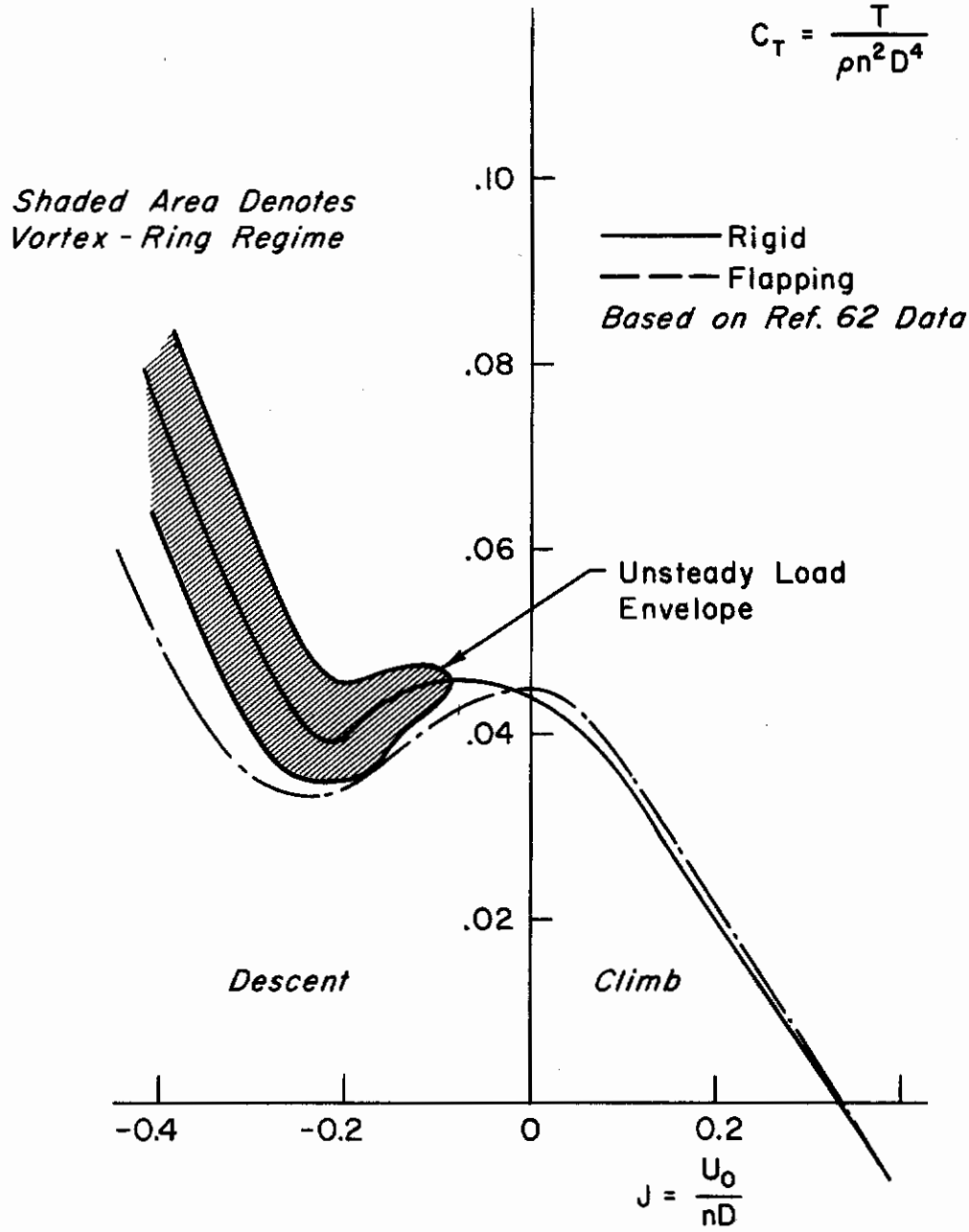

Figure B-8. Typical Variation of C_T Versus J for Rigid and Flapping Propellers (Illustrative only; not to scale)

(descending flight) the rotor remains in the "actual static-powered descent" condition. For larger positive w (rapid descent) the vortex-ring condition is approached, for corresponding climb velocities the tip-loss region becomes much smaller, and (as will be explained later) it is possible to calculate Z_w from momentum theory without allowing for the tip vortices.

Unlike u-perturbations, w-perturbations have roughly the same effect on a rotor Z-force irrespective of whether or not flapping and/or drag hinges are employed, provided the vortex-ring region is not approached. In the derivation of hovering Z_w for an unshrouded rotor that now follows, we use a combination of momentum theory and blade-element theory. The derivation is fairly lengthy, but the final formulas are quite simple. The treatment is essentially an extension of that given in Appendix C, Ref. 2, with the empirical constants of that reference replaced by logically based expressions. A comparison with experimental data is also presented.

Following standard practice (e.g., Ref. 54), the induced velocity through the disk, V_i', is assumed to be constant across the disk and the fully developed slipstream velocity, V_∞', is likewise constant across the slipstream. Initially, the effective reduction in actuator disk area due to tip losses will not be considered. All velocities are measured with respect to the earth and are positive in the directions shown. When w is zero (the equilibrium state) and conditions are steady, the appropriate V_i' and V_∞' will be denoted simply as V_i and V_∞.

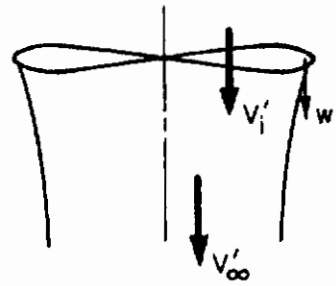

From Refs. 57 and 58 (for example) it is known that V_i' is the mean of the velocity of climb, $-w$, and the fully developed slipstream velocity, V_∞', i.e.,

$$V_i' = \frac{1}{2}(V_\infty' - w) \qquad \text{(B-14)}$$

The thrust T', measured positive upward, is given by momentum theory as

$$T' = \rho\pi R^2 V_i'(V_\infty' + w) = \frac{1}{2}\rho\pi R^2(V_\infty'^2 - w^2) \qquad \text{(B-15)}$$

where R = propeller radius

For greater accuracy R should be replaced by the effective radius allowing for the tip vortices. For simplicity we shall neglect this effect in the derivation. The effect of this simplification is discussed later. An alternative expression for T' can be obtained from blade-element theory

(e.g., Ref. 48), which gives, for an untwisted blade,*

$$T' = a_1 \pi\sigma \frac{1}{2} \rho\Omega^2 R^4 \left(\frac{\theta_o}{3} - \frac{V_i'}{2\Omega R}\right) \tag{B-16}$$

where a_1 = blade section lift-curve slope

σ = solidity = (number of blades x average chord)/πR

Ω = blade rotational speed in rad/sec

θ_o = angle between blade no-lift chord line and plane of rotation

Equations B-14, B-15, and B-16 provide the basis for determining Z_w for an unshrouded propeller operating at constant rpm. The assumption of constant rpm should be valid for frequencies of the order important in helicopter-plus-pilot system dynamics because rpm governors are widely used, and, to be effective, their time constants must be much less than the time constants important in helicopter rigid-body dynamics. Similar arguments apply to VTOLs.

Differentiating Eq B-14 with respect to w, and rearranging the result, gives

$$\frac{\partial V_i'}{\partial w} = -\frac{1}{2}\left(1 - \frac{\partial V_\infty'}{\partial w}\right) \tag{B-17}$$

$|\partial V_\infty'/\partial w|$ is usually $\ll 1$. Recourse has to be made to blade-element theory to show this (see below), but the remainder of the derivation of Z_w is quite simple and can be accomplished by momentum theory alone. Differentiating Eq B-15 with respect to w,

$$\frac{\partial T'}{\partial w} = \rho\pi R^2 \left(V_\infty' \frac{\partial V_\infty'}{\partial w} - w\right) \tag{B-18}$$

*As noted in Ref. 52, p. 304, if taper or twist are not excessive it should be satisfactory to apply the following results to twisted or tapered blades, basing σ and θ_o on conditions at 3/4 radius.

From Eq B-16 the corresponding expression in blade-element terms is

$$\frac{\partial T'}{\partial w} = -\frac{a_1 \pi \sigma \frac{1}{2} \rho \Omega^2 R^4}{2\Omega R} \frac{\partial V_i'}{\partial w} = -\frac{1}{4} a_1 \pi \sigma \rho \Omega R^3 \frac{\partial V_i'}{\partial w} \tag{B-19}$$

Since we are only interested here in evaluating Z_w at hover conditions ($T \equiv T'$, $V_\infty \equiv V_\infty'$, $w = 0$), Eq B-18 can be simplified to

$$\frac{\partial T}{\partial w} = \rho \pi R^2 \left(V_\infty \frac{\partial V_\infty}{\partial w} \right) \tag{B-20}$$

Equating the right sides of Eqs B-19 and B-20,

$$-\frac{1}{4} a_1 \pi \sigma \rho \Omega R^3 \frac{\partial V_i}{\partial w} = \rho \pi R^2 V_\infty \frac{\partial V_\infty}{\partial w} \tag{B-21}$$

Therefore,

$$\frac{\partial V_\infty}{\partial w} = -\frac{a_1 \sigma \Omega R}{4 V_\infty} \frac{\partial V_i}{\partial w} \tag{B-22}$$

and, from Eq B-14,

$$\frac{\partial V_\infty}{\partial w} = -\frac{a_1 \sigma \Omega R}{8 V_i} \frac{\partial V_i}{\partial w} \tag{B-23}$$

But substituting from Eq B-17 into Eq B-23,

$$\frac{\partial V_\infty}{\partial w} = -\frac{a_1 \sigma \Omega R}{8 V_i} \left(-\frac{1}{2} + \frac{1}{2} \frac{\partial V_\infty}{\partial w} \right) \tag{B-24}$$

and, combining terms,

$$\frac{\partial V_\infty}{\partial w} = \frac{\frac{a_1 \sigma \Omega R}{8 V_i}}{2 + \frac{a_1 \sigma \Omega R}{8 V_i}} \tag{B-25}$$

Using this result, and $V_i = (1/2) V_\infty$, in Eq B-20 yields

$$\frac{\partial T}{\partial w} = \rho\pi R^2 V_i \frac{\frac{a_1 \sigma \Omega R}{4V_i}}{2 + \frac{a_1 \sigma \Omega R}{8V_i}} \tag{B-26}$$

In helicopter work $V_i/\Omega R$ is usually called λ, the inflow factor; with this notation,

$$\frac{\partial T}{\partial w} = \rho\pi R^2 V_i \left(\frac{\frac{a_1 \sigma}{4\lambda}}{2 + \frac{a_1 \sigma}{8\lambda}} \right) \tag{B-27}$$

Expressing this in terms of $Z_w = -\frac{1}{m}\frac{\partial T}{\partial w} N$, where N = number of rotors, we note from Eq B-15 that

$$\frac{mg}{N} = T = 2\rho\pi R^2 V_i^2 \tag{B-28}$$

This yields

$$V_i = \left(\frac{\text{Disk loading}}{2\rho} \right)^{1/2} \tag{B-29}$$

whence

$$Z_w = -\frac{g}{2}\left(\frac{2\rho}{\text{Disk loading}} \right)^{1/2} \left(\frac{\frac{a_1 \sigma}{4\lambda}}{2 + \frac{a_1 \sigma}{8\lambda}} \right) \tag{B-30}$$

for the total configuration with any number of unshrouded rotors, provided that each is equally loaded

The terms a_1 and σ depend only on the geometry of the rotor, so for a rigid-rotor* configuration Z_w is inversely proportional to the square root of disk loading.

Comparison of theoretical with experimental Z_w — In Ref. 63 tests are reported on three full-size VTOL-type propellers. These propellers were of

*The effects of flapping hinges and blade flexibility on vertical response in hover have been examined in Ref. 67 (p. 394), where it is demonstrated that these effects are negligible at the frequencies of interest in handling qualities studies. Equation B-30 may therefore be applied to hinged as well as rigid rotors.

relatively high solidity and were designed for the Curtiss X-19 (Propellers 1 and 2) and the Vertol VZ-2 (Propeller 3). Figure B-9 illustrates the effect of axial velocity on thrust. In terms of our notation, the data have been nomdimensionalized as follows:

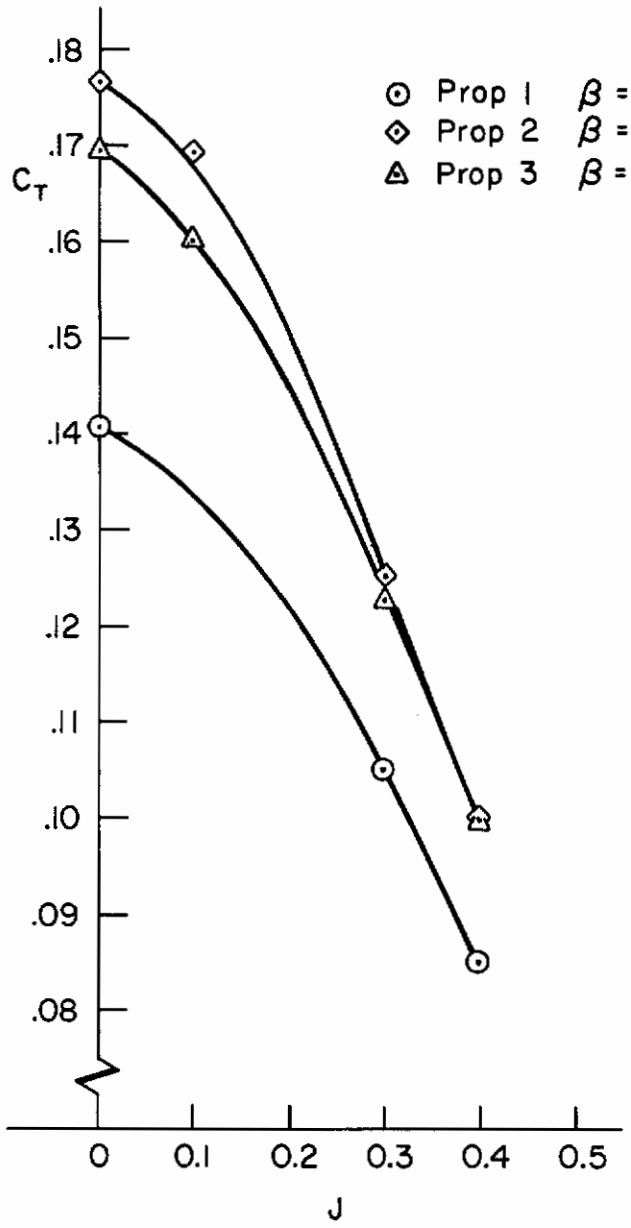

Figure B-9. C_T Versus J for Three VTOL Propellers (Data from Ref. 63)

$$C_T = \frac{\text{Thrust}}{\rho n^2 D^4}$$

$$J = \frac{-w}{nD}$$

where

n = rev/sec

D = diameter

$-w$ = perturbation upward velocity

The particular blade settings used for the data graphed in Fig. B-9 were those for the peak static thrust figure of merit, $C_T^{3/2}/C_p$ (see Fig. 15, Ref. 63). Reference 63 indicates that $\partial C_T/\partial J$ at a given J hardly varies with pitch setting, so these experimental data should be representative of a wide range of possible pitch settings. To facilitate the comparison of theory with experimental data (which are usually expressed in terms of C_T and J), we nondimensionalize the formula for Z_w, expressing it in terms of $\partial C_T/\partial J$ as follows.

Starting from Eq B-27,

$$\frac{\partial T}{\partial w} = \rho\pi R^2 v_i \left(\frac{\frac{a_1 \sigma}{4\lambda}}{2 + \frac{a_1 \sigma}{8\lambda}} \right)$$

Substituting $T = C_T \rho n^2 D^4$, $w = -JnD$, and assuming n constant gives

$$\frac{\partial C_T}{\partial J} = -\frac{\pi^2}{4} \lambda \left(\frac{2}{1 + \frac{16\lambda}{a_1 \sigma}} \right) \qquad \text{(B-31)}$$

To express λ in terms of C_T, we use Eqs B-14 and B-15, specialized for hover,

$$T = 2\pi\rho R^2 v_i^2$$

$$C_T = \frac{2\pi\rho R^2 v_i^2}{\rho n^2 D^4} = \frac{2\pi\rho R^2 v_i^2}{\rho \left(\frac{\Omega}{2\pi}\right)^2 (2R)^4} = \frac{\pi^3}{2} \lambda^2 \qquad \text{(B-32)}$$

$$\lambda = \left(\frac{2C_T}{\pi^3} \right)^{1/2} \qquad \text{(B-33)}$$

Substituting for λ in Eq B-31),

$$\frac{\partial C_T}{\partial J} = -\left(\frac{\pi C_T}{2} \right)^{1/2} \frac{1}{1 + \frac{16}{a_1 \sigma} \left(\frac{2C_T}{\pi^3} \right)^{1/2}} \qquad \text{(B-34)}$$

The characteristics of each propeller are tabulated in the following table. This table shows good agreement is obtained between theory and experiment if we measure $\partial C_T / \partial J$ at the straight part of the C_T versus J graph (Fig. B-9). This is because our theory has neglected tip losses, which are significant at hover but become progressively less important as J is increased. In other words, the theory gives good results outside the range of J for which

the tip vortex effects are important. For ducted fans, static tip losses are small and in Fig. B-10 it will be shown that for a ducted-fan-measured C_T gives a straight line graph when plotted against J for all J from zero to about 0.6.

Comparison of Theoretical and Measured $\partial C_T/\partial J$ (tests of Ref. 63)

	Propeller 1	Propeller 2	Propeller 3
Diameter, ft	12.0	10.0	9.75
Pitch setting, deg	12	12	18
Solidity, σ	0.15	0.222	0.173
a_1 (assumed)	5.73	5.73	5.73
$C_{T_{J=0}}$	0.141	0.169	0.177
$\partial C_T/\partial J$ (theoretical)	−0.168	−0.22	−0.191
$\partial C_T/\partial J$ (measured at J = 0)	−0.09	−0.07	−0.085
$\partial C_T/\partial J$ (measured at $0.2 < J < 0.4$)	−0.20	−0.25	−0.21

While this explains the discrepancy between calculated and measured $\partial C_T/\partial J$, it does not give us a simple method of calculating $\partial C_T/\partial J$ at J = 0. There are two effects we have not taken into account:

a. The reduction in effective rotor diameter at w = J = 0

b. The decrease in the size of the tip vortex with increasing negative w or positive J

Both effects are additive — the first decreases $|Z_w|$ through the increase of effective disk loading, and the second decreases $|Z_w|$ because of the loss in actuator disk area with increasing w, resulting in a smaller upward thrust. The first effect can be analyzed fairly simply, but the major part of the discrepancy is due to the second effect, for which no analytical approach is evident.

In summary, it appears that the simple approach described here can estimate Z_w for hover for VTOL unshrouded propellers with only limited accuracy, tending to predict a Z_w of about twice the actual value. It is anticipated that for helicopters and low disk loading VTOLs the accuracy

should be much better due to the smaller tip vortices associated with lower disk loading.

It is suggested that a semiempirical procedure should be employed for VTOLs, calculating Z_w as indicated and applying a factor of 50 percent to allow for the tip losses.

From symmetry, X_w and M_w are zero in hover for a configuration supported solely by a single rotor or two or more side-by-side rotors. Nonzero M_w can, however, arise when the trim (tail) rotor contributes lift due to the vehicle c.g. not lying on the axis of the main rotors. In such instances M_w can be computed from the individual Z_w effects of the main and trim rotors. M_w will be zero if the main and trim rotors have the same disk loading.

4. w-Derivatives for a Ducted Fan

The presence of the duct eliminates some of the complex flows that occur for unshrouded propellers. The transition from static to forward flight conditions can be quite smooth. Figure B-10, taken from Ref. 38, illustrates C_T versus J for the Doak VZ-4 ducts; note that $\partial C_T/\partial J$ is constant from $J = 0.6$ right down to static conditions. This is in marked contrast to Fig. B-11 which shows C_T versus J for the much cruder model duct of Ref. 35. Here $\partial C_T/\partial J$ falls off as J approaches zero in much the same way as the graphs of Fig. B-9 for unshrouded propellers.

The difference between the C_T versus J graphs of Fig. B-10 and Fig. B-11 arises from the very crude nature of the duct employed in Ref. 35. As noted in Ref. 35, with the small lip radius used, inlet separations occurred at static conditions. These separations cause an effective decrease of actuator disk area and hence of thrust. At forward speeds the curvature of the flow in the vicinity of the inlet becomes less acute, and separations correspondingly smaller. We shall show that momentum theory can be used to preduct $\partial C_T/\partial J$ with fairly good accuracy provided flow separations are not significant. The development of the theory follows lines similar to those used for unshrouded propellers. The presentation given below is an extension of that given in Ref. 2, Appendix C.

For simplicity a duct with no diffusion (i.e., exit area = disk area) is considered. In practice, diffusing ducts are used to obtain the maximum

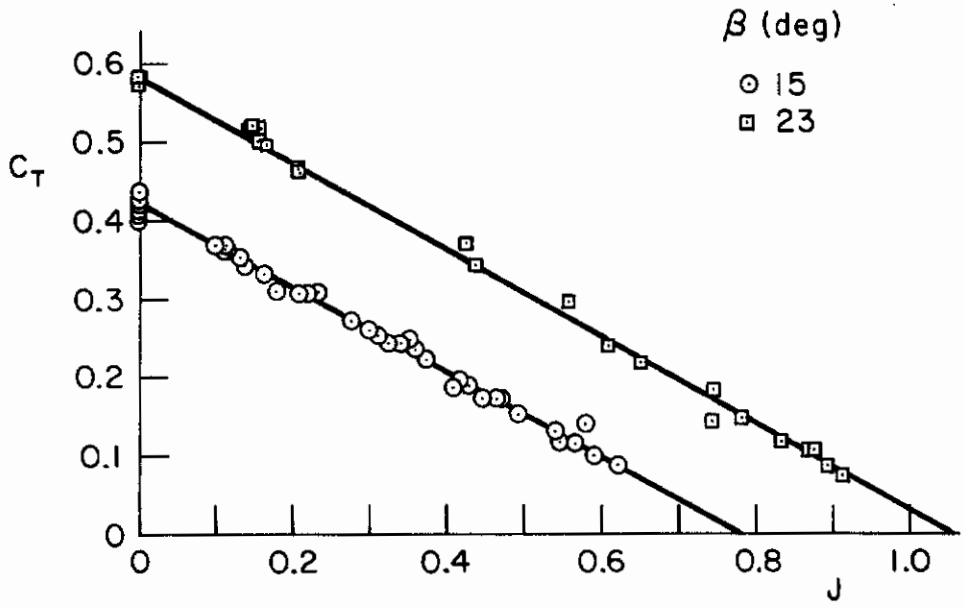

Figure B-10. C_T Versus J for Doak VZ-4 Ducted Fan in Axial Flow (Data from Ref. 47)

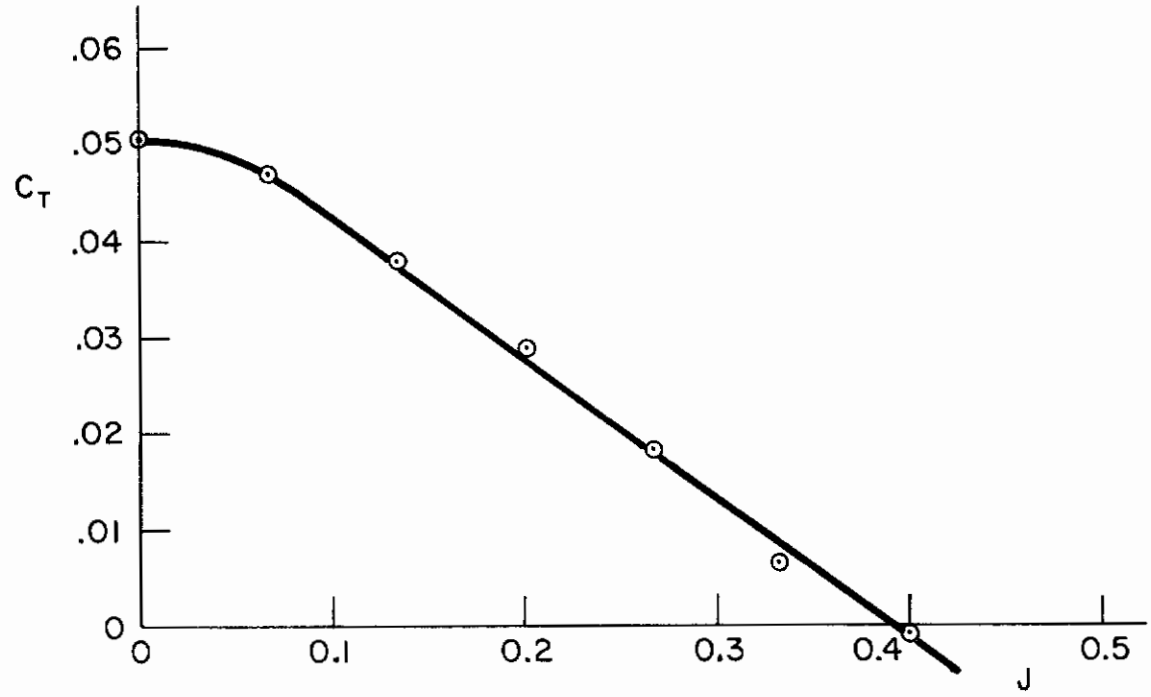

Figure B-11. C_T Versus J for Duct with a 0.5" Lip Radius in Axial Flow (Data from Ref. 35)

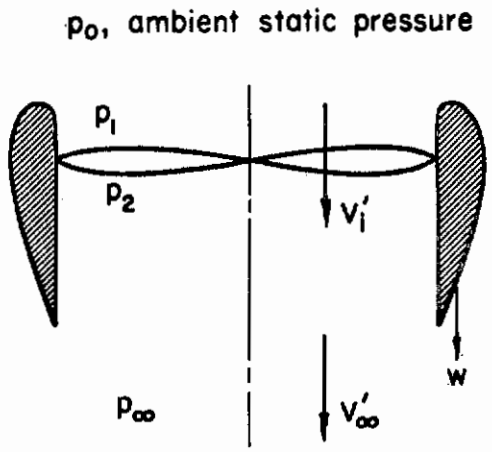

Sketch 5. Idealized Ducted Propeller

static thrust, but the diffusion is partly canceled out by boundary layer growth. For the present purpose it is sufficiently accurate to consider a duct of constant cross section. As before, the thrust of the propeller is

$$T'_{prop} = a_1 \pi\sigma \frac{1}{2} \rho\Omega^2 R^4 \left(\frac{\theta_o}{3} - \frac{V_i'}{2\Omega R}\right) \quad \text{(B-35)}$$

But this is not the total thrust. The total thrust can be calculated from momentum theory as

$$T'_{total} = \rho\pi R^2 V_i' (V_\infty' + w) \quad \text{(B-36)}$$

The thrust on the propeller can be obtained by considering the pressure jump across the actuator disk:

$$T'_{prop} = (p_2 - p_1)\pi R^2 \quad \text{(B-37)}$$

p_2 and p_1 can be eliminated by substituting in equations based on Bernoulli's principle, i.e.,

$$p_1 + \frac{1}{2}\rho V_i'^2 = p_0 + \frac{1}{2}\rho w^2 \quad \text{(B-38)}$$

$$p_\infty + \frac{1}{2}\rho V_\infty'^2 = p_2 + \frac{1}{2}\rho V_i'^2 \quad \text{(B-39)}$$

whence

$$p_2 - p_1 = (p_\infty - p_0) + \frac{1}{2}\rho(V_\infty'^2 - w^2) \quad \text{(B-40)}$$

Assuming, as is usual in momentum theory,* that $p_\infty = p_0$

$$T'_{prop} = \frac{1}{2}\rho\pi R^2 (V_\infty'^2 - w^2) \quad \text{(B-41)}$$

*For a full discussion of the significance of this assumption, see Ref. 59.

From Eqs B-36 and B-41,

$$\frac{T'_{prop}}{T'_{total}} = \frac{\frac{1}{2}\rho\pi R^2(V_\infty'^2 - w^2)}{\rho\pi R^2 V_i'(V_\infty' + w)} = \frac{1}{2}\frac{(V_\infty' - w)}{V_i'} \qquad \text{(B-42)}$$

At static conditions ($w = 0$) for a nondiffusing duct ($V_i = V_\infty$), this gives $T_{prop} = (1/2)T_{total}$. This well-known result is verified by the experimental data of Fig. 17a of Ref. 38. These data show the division of thrust between the duct and propeller of the Doak VZ-4 configuration is essentially 0.5 for small perturbations from the static condition in either w or u or both combined.

Differentiating Eq B-42 and putting $(\partial/\partial w)(T'_{prop}/T'_{total}) = 0$ for small w to match these experimental data yields, after some reduction, denoting $(\partial V_i'/\partial w)_{w=0}$ as $(\partial V_i/\partial w)$, etc.,

$$V_\infty \frac{\partial V_i}{\partial w} = V_i\left(\frac{\partial V_\infty}{\partial w} - 1\right) \qquad \text{(B-43)}$$

The primes have been dropped to indicate static conditions. For a nondiffusing duct, $V_i = V_\infty$; therefore,

$$\frac{\partial V_i}{\partial w} = \frac{\partial V_\infty}{\partial w} - 1 \qquad \text{(B-44)}$$

Differentiating Eq B-36,

$$\frac{\partial T'_{total}}{\partial w} = \rho\pi R^2\left[V_i'\left(\frac{\partial V_\infty'}{\partial w} + 1\right) + \left(V_\infty' + w\right)\frac{\partial V_i'}{\partial w}\right] \qquad \text{(B-45)}$$

Substituting from Eq B-44 into Eq B-45 for $w = 0$ and $V_i = V_\infty$,

$$\frac{\partial T_{total}}{\partial w} = 2\rho\pi R^2 V_\infty \frac{\partial V_\infty}{\partial w} \qquad \text{(B-46)}$$

Differentiating Eq B-35 and putting $w = 0$ gives

$$\frac{\partial T_{prop}}{\partial w} = -a_1 \pi \sigma \frac{1}{4} \rho \Omega R^3 \frac{\partial V_i}{\partial w} \tag{B-47}$$

$$= -a_1 \pi \sigma \frac{1}{4} \rho \Omega R^3 \left(\frac{\partial V_\infty}{\partial w} - 1 \right) \tag{B-48}$$

Equations B-46 and B-48 can be related by making use of the experimental result that $(T'_{prop}/T'_{total}) = 1/2$, for small w. Differentiating T'_{prop}/T'_{total},

$$\frac{\partial}{\partial w} \frac{T'_{prop}}{T'_{total}} = \frac{T'_{total} \frac{\partial T'_{prop}}{\partial w} - T'_{prop} \frac{\partial T'_{total}}{\partial w}}{\left(T'_{total}\right)^2} \tag{B-49}$$

But since the division of thrust does not change for small w, this can be equated to zero, giving

$$\frac{\partial T'_{prop}/\partial w}{\partial T'_{total}/\partial w} = \frac{T_{prop}}{T_{total}} = \frac{1}{2} \tag{B-50}$$

Combining Eqs B-46, B-48, and B-50,

$$-a_1 \pi \sigma \frac{1}{4} \rho \Omega R^3 \left(\frac{\partial V_\infty}{\partial w} - 1 \right) = \rho \pi R^2 V_\infty \frac{\partial V_\infty}{\partial w} \tag{B-51}$$

Put $\lambda_D = V_i/\Omega R$ $(= V_\infty/\Omega R$ for a nondiffusing duct), and Eq B-51 becomes

$$\frac{\partial V_\infty}{\partial w} - 1 = \frac{-4\lambda_D}{a_1 \sigma} \frac{\partial V_\infty}{\partial w} \tag{B-52}$$

$$\frac{\partial V_\infty}{\partial w} = \frac{1}{1 + \frac{4\lambda_D}{a_1 \sigma}} \tag{B-53}$$

Substituting Eq B-53 into Eq B-46,

$$\frac{\partial T_{total}}{\partial w} = 2\rho \pi R^2 V_\infty \left(\frac{1}{1 + \frac{4\lambda_D}{a_1 \sigma}} \right) \tag{B-54}$$

But $T = \rho\pi R^2 V_\infty^2$, hence $V_\infty = \left(\frac{\text{Disk loading}}{\rho}\right)^{1/2}$, whence Eq B-54 can be reduced to give

$$Z_w = \frac{-\rho^{1/2} g}{(\text{Disk loading})^{1/2}} \left(\frac{2}{1 + \frac{4\lambda_D}{a_1 \sigma}}\right) \qquad \text{(B-55)}$$

for the total configuration with any number of ducted fans, provided that each has the same disk loading.

To correlate the above theoretical formulas with the test data of Refs. 35 and 47, it is necessary to express Z_w in the form $\partial C_T/\partial J$ used in these references:

$$\frac{\partial C_T}{\partial J} = -\frac{\partial T}{\partial w} \cdot \frac{nD}{\rho n^2 D^4} = -\frac{\partial T}{\partial w} \cdot \frac{1}{\rho n D^3} = -\frac{2\rho\pi R^2 V_\infty}{\rho n D^3} \left(\frac{1}{1 + \frac{4\lambda_D}{a_1 \sigma}}\right) \qquad \text{(B-56)}$$

Substituting $n = \Omega/2\pi$,

$$\frac{\partial C_T}{\partial J} = -\frac{\pi^2}{2} \lambda_D \left(\frac{1}{1 + \frac{4\lambda_D}{a_1 \sigma}}\right) \qquad \text{(B-57)}$$

Note that, strictly, this formula is only valid near $J = 0$ because it assumes

$$T = \rho\pi R^2 V_i V_\infty \doteq T' = \rho\pi R^2 V_i' (V_\infty' + w)$$

For the high C_T considered here, $V_\infty \gg w$, so the formula may be used over most of the range of J tested. It is more convenient to express Eq B-57 in terms of C_T rather than λ_D. This is achieved by the following substitutions, assuming a uniform duct so that $V_i = V_\infty$.

$$C_T^{1/2} = \left(\frac{T}{\rho n^2 D^4}\right)^{1/2} = \left[\frac{\rho\pi R^2 V_\infty^2}{\rho\left(\frac{\Omega}{2\pi}\right)^2 16R^4}\right]^{1/2} = \left(\frac{\pi^3 V_\infty^2}{4\Omega^2 R^2}\right)^{1/2} = \left(\frac{\pi^3 \lambda_D^2}{4}\right)^{1/2} \qquad \text{(B-58)}$$

$$\lambda_D = \frac{2C_T^{1/2}}{\pi^{3/2}} \tag{B-59}$$

Substituting for λ_D in Eq B-57,

$$\frac{\partial C_T}{\partial J} = -(\pi C_T)^{1/2}\left(\frac{1}{1 + \frac{8C_T^{1/2}}{\pi^{3/2} a_1 \sigma}}\right) \tag{B-60}$$

For the Doak configuration of Ref. 47 the following values were assumed: $\sigma_{prop} = 0.224$, $a_1 = 2\pi$. The configuration also included nine stators, twisted 15 deg from center body to tip. These stators produce a net positive thrust through extraction of slipstream swirl. It is debatable whether or not some allowance should be made for the stators in Eq B-60, since our simple theory has neglected slipstream swirl. Arguing that the function of the stators is essentially to restore the unswirled condition, the most logical course appears to be to use Eq B-60 directly, taking σ as the solidity of the rotating blades only. With this assumption the calculated and measured $\partial C_T/\partial J$ become:

C_T	0.42	0.59
$\partial C_T/\partial J$ (theory)	−0.69	−0.76
$\partial C_T/\partial J$ (measured)	−0.55	−0.55

Considering such factors as the uncertainty regarding the stator contributions to $\partial C_T/\partial J$, the neglect of duct diffusion and blade twist, etc., the agreement is about as good as might be expected.

Repeating the calculation for the ducted fan of Ref. 35 (see Figs. B-1 and B-11) gives

$\partial C_T/\partial J$ (measured at $J = 0$)	$\doteq 0$
$\partial C_T/\partial J$ (measured at $J = 0.1$)	−0.146
$\partial C_T/\partial J$ (theory)	−0.150

Again the agreement is fairly good, considering the simplicity of the momentum theory employed and ascribing the fall-off in $\partial C_T/\partial J$ at $J = 0$ to lip separations which were noted in Ref. 35.

In summary, it appears that the simple approach described here can predict hover Z_w for ducted propellers with accuracy acceptable for stability and control calculations.

The earlier comments regarding hovering X_w and M_w apply equally to ducted configurations.

5. q-Derivatives for Ducted and Unshrouded Propellers

In many VTOL configurations the major contributions to X_q, Z_q, and M_q arise through the X_w, Z_w, X_u, and Z_u of parts located away from the c.g. For example, the X_u of a helicopter rotor produces a positive M_u, proportional to the height of the rotor hub above the c.g.; on a VTOL with a horizontal tail rotor the Z_w of this rotor produces a contribution to M_w, M_q, etc. Similarly for lateral derivatives, a single-rotor helicopter possesses a nonzero N_v in hover due to the Y_v of the tail rotor. These contributions are fairly obvious and will not be discussed further here.

For a flapping rotor with zero hinge offset, moments cannot be transmitted from the rotor to the hub, and therefore for such a rotor the sole contributions to M_q arise through the Z_w and X_u of the rotor. It should be accurate enough to assume a constant average u or w across the rotor instead of the actual u or w which is proportional to the distance from the c.g. For a flapping rotor with a finite hinge offset, the effects of pitch rate are more complicated and must be calculated by standard methods (e.g., Ref. 53).

For a shrouded or unshrouded rigid rotor, rotating about its hub, M_q arises through local changes in angle of attack of blade elements. Again this lies outside the scope of momentum theory, but we shall nevertheless discuss it to compare the magnitude of this contribution to M_q with other contributions which arise for a ducted propeller. These are:

a. Changes in momentum of the airflow at the duct inlets

b. Coriolis forces associated with mass flow

In the following analyses we make use of methods employed by Greenman and Gaffney in Ref. 64, in which stability derivatives for the Hiller stand-on ducted-fan configuration are calculated. A brief but fundamental statement of the contributions made by air and fuel flow Coriolis forces to stability derivatives is also given in Ref. 65. The discussion given below is a more general version of that given in Appendix A of Ref. 2, which was concerned only with Doak VZ-4 derivatives in hover and forward flight.

Coriolis forces — The Coriolis force associated with rotation of a system containing a translating mass is given by the vector equation

$$\overrightarrow{\text{Coriolis force}} = 2 \times \text{mass} \times \overrightarrow{\text{angular velocity}} \times \overrightarrow{\text{translational velocity}} \qquad \text{(B-61)}$$

Here the angular velocity of interest is q and the translational velocity is V_i. The appropriate mass is the mass of air contained in the duct at any given instant, i.e., $\rho A_i l_D$, where l_D is the duct length.

Resolving the Coriolis force into X- and Z-components leads to the following expressions for the derivatives X_q and Z_q in hover (duct vertical):

$$\Delta m Z_q = 0 \qquad \text{(B-62)}$$

$$\Delta m X_q = -2\rho A_i l_D V_i \qquad \text{(B-63)}$$

There may also be a contribution to M_q if the duct center is above or below the airplane c.g., but in Ref. 2 this was found to be negligible for the Doak configuration. If the duct center is a height h_{DC} above the c.g., then

$$\Delta M_q I_y = -h_{DC} \Delta m X_q = 2\rho A_i l_D h_{DC} V_i$$

Substituting the expressions for V_i at hover,

$$\Delta M_q = \frac{2\rho A_i l_D h_{DC}}{I_y} \sqrt{\frac{mg}{\rho A_i}} = \frac{2 l_D h_{DC}}{k_y^2} \sqrt{\frac{\rho g A_i}{m}} \qquad \text{(B-64)}$$

Forces and moments due to change of momentum at duct inlets — As discussed earlier, the turning of the main flow through the vertical ducts associated with u-perturbation produces a drag force. A similar drag arises when the u-perturbation is purely local and is induced by a pitch rate q. (The previous comments regarding possible additional moments due to separation on the lee side of the ducts also apply here.) The net contribution to M_q is therefore given by

$$\Delta M_q I_y = m X_u h_D^2 \tag{B-65}$$

where h_D is the height of the duct inlets above the c.g. Using the ducted-fan expression for X_u gives

$$\Delta M_q = -\frac{h_D^2}{k_y^2}\sqrt{\frac{\rho g A_i}{m}} \tag{B-66}$$

There is also a contribution to X_q:

$$\Delta X_q = -X_u h_D \tag{B-67}$$

For the Doak VZ-4, X_q was of no importance in the vehicle dynamics.

Forces and moments due to changes in blade angle of attack caused by q — In the analyses to follow we shall assume that the airplane c.g. lies on the duct axis of rotation. It will be shown that there is no contribution to X_q or Z_q due to blade angle of attack changes. Only M_q, a pure couple, results, and because the moment of a couple is the same about any point in its plane, no correction need be made for the actual c.g. position.

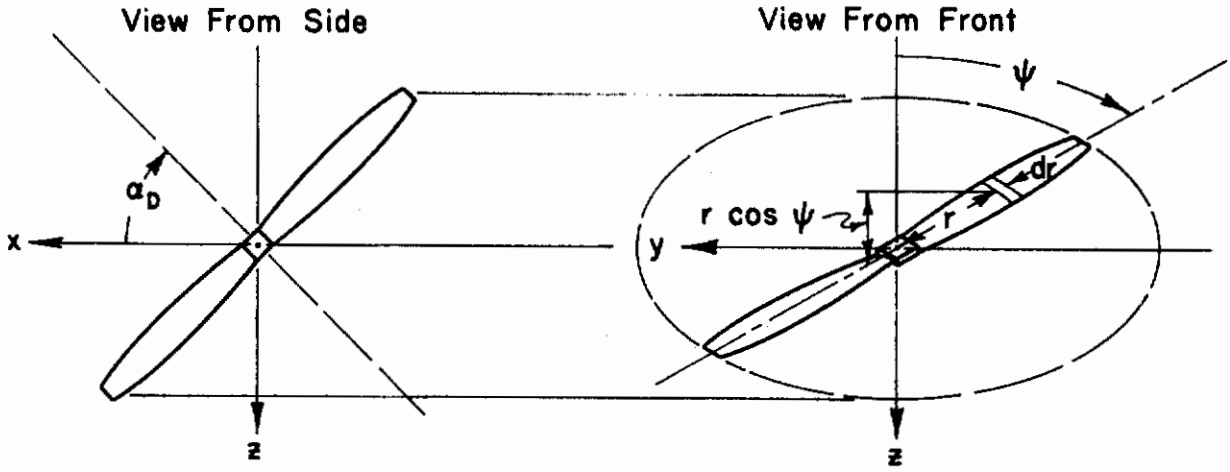

Sketch 6. Symbols for Calculating Blade Angle of Attack Effects

Consider a blade element a distance r from the hub. The change in angle of attack due to q is

$$\Delta\alpha = q \frac{r \cos\psi}{\Omega r} = \frac{q}{\Omega} \cos\psi \qquad \text{(B-68)}$$

where Ω is the blade rotational speed

Considering only lift forces on the blade element, the pitching moment on the airplane due to the local change in angle of attack at the element is

$$I_y dM = \underbrace{-c\,(\Omega^2 r^2 + V_i^2)\,\frac{1}{2}\rho\left(\frac{dC_L}{d\alpha}\right)_B dr}_{q \cdot \frac{dC_L}{d\alpha} \cdot \text{area}} \cdot \underbrace{\frac{q}{\Omega}\cos\psi}_{\Delta\alpha} \cdot \underbrace{r\cos\psi}_{\text{Moment arm}} \qquad \text{(B-69)}$$

where $(dC_L/d\alpha)_B$ is the blade section lift coefficient

Greenman and Gaffney (Ref. 64) present a similar expression, but do not include the through-flow velocity, V_i. V_i is of comparable magnitude to ΩR, and we retain it in the analysis that follows. However, it will be demonstrated a posteriori that the neglect of V_i is in fact justifiable.

Integrating Eq B-61,

$$I_y M_q = -\frac{1}{2} b\rho\left(\frac{dC_L}{d\alpha}\right)_B \cos^2\psi \left[\int_0^R \Omega r^3 c\, dr + \int_0^R \frac{V_i^2 rc}{\Omega} dr\right] \qquad \text{(B-70)}$$

The change in the thrust of the element is (neglecting drag forces)

$$dT = c\,(\Omega^2 r^2 + V_i^2)\,\frac{1}{2}\rho\left(\frac{dC_L}{d\alpha}\right)_B dr \cdot \frac{q}{\Omega}\cos\psi \qquad \text{(B-71)}$$

But this is equal and opposite on opposite blades, so there is no net change in thrust and hence no contributions to X_q and Z_q.

To evaluate Eq B-70 we first note that the average value of $\cos^2\psi$ is 1/2. Then taking $(dC_L/d\alpha)_B$ as 2π, and using $J_i = V_i\pi/\Omega R$,

$$(M_q I_y)_{\text{per prop}} = -\frac{\pi b \rho \Omega}{2}\left[\int_0^R r^3 c\,dr + \left(\frac{J_i R}{\pi}\right)^2 \int_0^R rc\,dr\right] \qquad \text{(B-72)}$$

Usually the magnitude of J_i will be such that the last term inside the bracket is negligible, i.e., the effects of V_i can be neglected. With this simplification, $M_q I_y$ due to blade angle of attack change is simply

$$(M_q I_y)_{\text{per prop}} = -\frac{\pi b \rho \Omega}{2}\int_0^R r^3 c\,dr \qquad \text{(B-73)}$$

The formula should be applicable to both unshrouded and ducted propellers, but may underestimate M_q for ducted propellers because the moment resulting from differential lift induced on the duct has not been considered. However, the inaccuracy in total M_q due to this should be small because the dominant contribution to M_q will usually come from the change of momentum at the duct lip.

Equation B-73 can also be written

$$(M_q I_y)_{\text{per prop}} = -\frac{\pi b \rho \Omega R^5}{2}\int_0^1 \left(\frac{r}{R}\right)^3 \left(\frac{c}{R}\right) d\left(\frac{r}{R}\right)$$

$$= -\frac{b \rho V_i A_i^2}{2 J_i}\int_0^1 \left(\frac{r}{R}\right)^3 \left(\frac{c}{R}\right) d\left(\frac{r}{R}\right) \qquad \text{(B-74)}$$

For geometrically similar configurations operating at the same J_i,

$$M_q \quad \text{varies as} \quad \frac{\rho V_i A_i^2}{m k_y^2}$$

Making the substitution for V_i at hover,

$$M_q \text{ varies as } \frac{\rho A_i^2}{m k_y^2}\sqrt{\frac{mg}{\rho A_i}} = \frac{A_i}{k_y^2}\sqrt{\frac{\rho A_i g}{m}}$$

The main point is that all three contributions to M_q are proportional to this same factor.

APPENDIX C

DERIVATION OF $h \rightarrow \delta_T$ METRIC

With a high gain $\theta \rightarrow \delta_e$ inner loop, the altitude-to-throttle response can be approximated by

$$\left(\frac{h}{\delta_T}\right)_{\theta \rightarrow \delta_e} \doteq \frac{-Z_{\delta_T}\left(s - X_u + \frac{X_{\delta_T}}{Z_{\delta_T}} Z_u\right)}{s\left[s^2 - (X_u + Z_w)s + X_u Z_w - X_w Z_u\right]} \qquad \text{(C-1)}$$

or

$$\left(\frac{h}{\delta_T}\right)_{\theta \rightarrow \delta_e} \doteq \frac{-Z_{\delta_T}(s + z)}{s(s + p_1)(s + p_2)} \qquad \text{(C-2)}$$

where z, p_1, and p_2 are normally all less than 1 rad/sec. If $p_1 + p_2 > z$ a pure gain closure will always be stable; however, with the inclusion of higher frequency lags the closure will go unstable at a frequency ω_o. If the higher frequency lags are approximated by the transport lag, τ_{eff}, the phase margin for the $h \rightarrow \delta_T$ closure is

$$\varphi_M = 90 \text{ deg} + \tan^{-1}\frac{\omega}{z} - \tan^{-1}\frac{\omega}{p_1} - \tan^{-1}\frac{\omega}{p_2} - \omega\tau_{eff} \qquad \text{(C-3)}$$

For frequencies greater than z, p_1, and p_2, Eq C-3 can be approximated by

$$\varphi_M \doteq -\frac{z}{\omega} + \frac{p_1}{\omega} + \frac{p_2}{\omega} - \omega\tau_{eff} = \frac{p_1 + p_2 - z}{\omega} - \omega\tau_{eff} \qquad \text{(C-4)}$$

Therefore the zero-damping frequency is approximated by

$$\omega_o \doteq \sqrt{\frac{p_1 + p_2 - z}{\tau_{eff}}} \qquad \text{(C-5)}$$

From Eqs C-1 and C-2,

$$z = -X_u + \frac{X_{\delta_T}}{Z_{\delta_T}} Z_u \qquad (C\text{-}6)$$

$$p_1 + p_2 = -X_u - Z_w$$

Therefore, combining Eqs C-5 and C-6,

$$\omega_o \doteq \sqrt{\left(-Z_w - \frac{X_{\delta_T}}{Z_{\delta_T}} Z_u\right) \frac{1}{\tau_{eff}}} \qquad (C\text{-}7)$$

APPENDIX D

GAIN IDENTITIES IN HOVER

The pilot's transport lag has been approximated by

$$e^{-\tau_e s} \doteq -\frac{\left(s - \frac{2}{\tau_e}\right)}{\left(s + \frac{2}{\tau_e}\right)} \tag{D-1}$$

Combining this approximation with Eqs 5 and 8, it is seen that the θ-loop high frequency gain is

$$\kappa_\theta = -K_{p_\theta} T_L M_{\delta_e} \tag{D-2}$$

It is also clear from Eqs 5 and 8 that the d.c. gain is

$$K_\theta = \frac{K_{p_\theta} M_{\delta_e}\left(-X_u + \frac{X_{\delta_e}}{M_{\delta_e}} M_u\right)}{\left(\frac{1}{T_{sp}}\right)\omega_p^2} \tag{D-3}$$

But from the hovering cubic, Eq 2,

$$\left(\frac{1}{T_{sp}}\right)\omega_p^2 = g M_u \tag{D-4}$$

So that

$$K_\theta = \frac{K_{p_\theta} M_{\delta_e}\left(-X_u + \frac{X_{\delta_e}}{M_{\delta_e}} M_u\right)}{g M_u} \tag{D-5}$$

The x-loop d.c. gain is readily found from Eqs 9 and 10.

$$K_x = -\frac{K_{p_x} g M_{\delta_e}\left(\frac{2}{\tau_e}\right)}{\left(\frac{1}{T_{sp}}\right)'\left(\omega_p'\right)^2\left(\frac{2}{\tau_e}\right)'} \tag{D-6}$$

From the θ-closure,

$$\left(\frac{1}{T_{sp}}\right)'\left(\omega_p'\right)^2\left(\frac{2}{\tau_e}\right)' = \left(\frac{2}{\tau_e}\right)\left[gM_u + K_{p_\theta}M_{\delta_e}\left(-X_u + \frac{X_{\delta_e}}{M_{\delta_e}}M_u\right)\right] \qquad (D\text{-}7)$$

Combining Eqs D-6 and D-7,

$$K_x = \frac{-K_{p_x}gM_{\delta_e}}{gM_u + K_{p_\theta}M_{\delta_e}\left(-X_u + \frac{X_{\delta_e}}{M_{\delta_e}}M_u\right)} \qquad (D\text{-}8)$$

A convenient expression for the x-loop d.c. gain is obtained from Eqs D-5 and D-8.

$$K_x = \frac{-K_{p_x}M_{\delta_e}}{M_u(1 + K_\theta)} \qquad (D\text{-}9)$$

Another useful expression is the one for the product of the pilot-airframe poles with both the θ- and x-loops closed. Since the x/δ_e transfer function has a free-s in the denominator, the product of the closed-loop roots equals the d.c. value of the numerator, i.e.,

$$\left(\omega_x''\right)^2\left(\omega_p''\right)^2\left(\frac{2}{\tau_e}\right)'' = -K_{p_x}gM_{\delta_e}\left(\frac{2}{\tau_e}\right) \qquad (D\text{-}10)$$